Department of Civil, Environmental & Construction Engineering

Structures Research

Thermo-mechanical Durability of Carbon Fiber Reinforced Polymer Strengthened Reinforced Concrete Beams

University of Central Florida
4000 Central Florida Blvd
Orlando, Fl 32816

Project Manager:
Marc Ansley

Principal Investigator:
Kevin R. Mackie, PhD

Research Assistants:
Zachary B. Haber & Mike Olka

Funding Agency:
Florida Department of Transportation

Project No.
BD550 - 06

FINAL REPORT

July 20th, 2009

Disclaimer

The opinions, findings, and conclusions expressed in this publication are those of the authors and not necessarily those of the State of Florida Department of Transportation.

Unit Conversion Table

SYMBOL	WHEN YOU KNOW	MULTIPLY BY	TO FIND	SYMBOL
LENGTH				
in	inches	25.4	millimeters	mm
ft	feet	0.305	meters	m
yd	yards	0.914	meters	m
mi	miles	1.61	kilometers	km

SYMBOL	WHEN YOU KNOW	MULTIPLY BY	TO FIND	SYMBOL
AREA				
in^2	squareinches	645.2	square millimeters	mm^2
ft^2	squarefeet	0.093	square meters	m^2
yd^2	square yard	0.836	square meters	m^2
ac	acres	0.405	hectares	ha
mi^2	square miles	2.59	square kilometers	km^2

SYMBOL	WHEN YOU KNOW	MULTIPLY BY	TO FIND	SYMBOL
VOLUME				
fl oz	fluid ounces	29.57	milliliters	mL
gal	gallons	3.785	liters	L
ft^3	cubic feet	0.028	cubic meters	m^3
yd^3	cubic yards	0.765	cubic meters	m^3
NOTE: volumes greater than 1000 L shall be shown in m^3				

SYMBOL	WHEN YOU KNOW	MULTIPLY BY	TO FIND	SYMBOL
MASS				
oz	ounces	28.35	grams	g
lb	pounds	0.454	kilograms	kg
T	short tons (2000 lb)	0.907	megagrams (or "metric ton")	Mg (or "t")

SYMBOL	WHEN YOU KNOW	MULTIPLY BY	TO FIND	SYMBOL
TEMPERATURE (exact degrees)				
^oF	Fahrenheit	5 (F-32)/9 or (F-32)/1.8	Celsius	^oC

SYMBOL	WHEN YOU KNOW	MULTIPLY BY	TO FIND	SYMBOL
FORCE and PRESSURE or STRESS				
lbf	poundforce	4.45	newtons	N
lbf/in^2	poundforce per square inch	6.89	kilopascals	kPa

Technical Report Documentation

1. Report No.	2. Government Accession No.	3. Recipient's Catalog No.
4. Title and Subtitle Thermo-mechanical Durability of CFRP-Strengthened RC Beams		5. Report Date 7/18/2009
		6. Performing Organization Code
7. Author(s) Zachary B. Haber, Kevin R. Mackie, Lei Zhao, & Mike Olka		8. Performing Organization Report No.
9. Performing Organization Name and Address **University or Central Florida** 4000 Central Florida Blvd Orlando, Fl 32816		10. Work Unit No. (TRAIS)
		11. Contract or Grant No. BD550-06
12. Sponsoring Agency Name and Address **Florida Department of Transportation** 605 Suwannee Street, MS 30 Tallahassee, Fl 32399		13. Type of Report and Period Covered FINAL 12/3/2004 – 7/18/2009
		14. Sponsoring Agency Code
15. Supplementary Notes		

16. Abstract

In recent years the Federal Highway Administration (FHWA) has identified a critical need to upgrade the transportation infrastructure in the United States. Of the nearly 600,000 bridges in the FHWA's bridge inventory, upwards of 90,000 bridges have been deemed structural deficient and are in need of rehabilitation to increase member capacity. Research has shown that externally-bonded fiber-reinforced polymer (FRP) composite materials can provide an effective means to upgrade deficient structures. Yet, there exists a question as to the long-term durability of this type of retrofit technology. The study presented discusses the results from a large-scale experimental study focused on the effects of mechanical and thermal fatigue on reinforced concrete (RC) beams strengthened with externally-bonded carbon fiber-reinforced polymer (CFRP) sheets. Three different resin matrix systems were investigated: two epoxy systems and one pre-impregnated polyurethane system. Specimens were subjected to 2 million loading cycles and/or one year of thermal/humidity cycling previous to monotonic loading until failure. Results indicate that the polyurethane system is promising; however, such a system has not been heavily researched in the infrastructure sector.

17. Key Word CFRP, Durability, Debonding, Strengthening, Fatigue, Polyurethane Matrix Composites	18. Distribution Statement No Restrictions		
19. Security Classif. (of this report) Unclassified	20. Security Classif. (of this page) Unclassified	21. No. of Pages 113	22. Price N/A

Acknowledgements

The authors must extend great thanks to Dr. Lei Zhao for he was the individual that developed the main ideas that made this project possible. Thanks must also be given to Mike Olka, Steve Eudy, William Potter, and the staff at the FDOT Structures Research Center for their technical assistance. Franz Worth from the Air Logistics Corporation provided a significant amount of technical assistance during the duration of this project. Finally, to the undergraduate research assistants, Robert Slade and Jasna Tomasevic, for their contributions to the content of this document.

Executive Summary

Background

Increasing service loads, extreme loading events, and constant exposure to an ever-changing ambient environment are just a few reasons why civil structures, over extended service periods, degrade and ultimately become structural deficient. In many cases, it is economically more feasible to repair/strengthen the damaged structure than full demolition and re-construction. Traditional methods of strengthening include steel jacketing/plating, addition of concrete, and near surface mounting additional steel. Although these methods have been proven effective, they can be cumbersome, time inefficient, and susceptible to corrosion. The 1980s saw the advent of more cost effective means to manufacture advanced fiber-reinforced polymer (FRP) composite materials; making the use of such materials more suitable for construction purposes. By the late 1980's, numerous researchers began investigating the possibilities of using FRPs to strengthen reinforced concrete structures. With excellent corrosion resistance, high strength-to-weight ratio, and stiffness-to-weight ratio, externally bonded FRP composites provided a time and strength efficient means to strengthen reinforced concrete (RC) structures.

Since its beginnings in the late 1980s, the use of FRP for civil strengthening applications has been heavily researched over the past 20 years. Although much progress has been made, there still exists hesitation from engineers and the construction industry to implement such technology in the field. This hesitation stems from the lack of concise design provisions and uncertainty in the long-term field durability of the technology.

Although design guidelines have been compiled by a number of countries, many design guides do not sufficiently address the issue of durability and life expectancy of strengthened members. The reasoning being that there has not been a significant amount of data available on the subject.

In Florida, research on the use of carbon fiber reinforced polymer (CFRP) composites for external strengthening of reinforced concrete structures began in the early 1990s (Florida Department of Transportation); followed by field implementations as early as 1994. Currently, there are a number of CFRP strengthened bridges in the state of Florida. A majority of these strengthened bridges have not shown signs of degradation or damage. However, there have been cases where visual inspections have revealed noticeable damage and deterioration to the CFRP material and its bond to the concrete substrate. Figure 1 shows photos taken of beams that were removed from a bridge in the State of Florida. Nearing the conclusion of the beams' service life, they had been retrofitted with externally bonded CFRP/epoxy laminate. Upon removal, the beams were inspected. There were numerous locations where damage to the CFRP was found. It was concluded that the damage found occurred from two main causes; vehicle impact and/or exposure to service loads and the ambient environment. Due to the number of uncertainties associated with FRP-to-concrete bond behavior and the lack of data on the durability of the FRP/concrete interface, it is difficult to make predictions regarding how long a given CFRP retrofit will extend a member's service life. The inability to accurately predict the service life of strengthened member in the service environment poses an important question to bridge owners; is external CFRP strengthening a short-term fix or a long-term solution? It was this question that the FDOT was facing regarding its CFRP strengthened bridges.

Figure 1: Beams Removed from 1-95 Bridge

Objectives and Scope

The objective of this study is to investigate the ability of externally bonded CFRP composite systems for strengthening civil infrastructure to resist service environments similar to that of the State of Florida. Combined effects of cyclic thermal and fatigue loads where investigated through accelerated large-scale laboratory testing. The effect of conditioning on the CFRP and its interface with the concrete substrate were determined by visual inspection, bond tests, ultimate load-deflection behavior, and strain data recorded during tests. The results of the tests will provide FDOT with evidence of the field durability of CFRP strengthening on concrete beams, which is critical for establishing design and implementation guidelines.

This study is primarily an experimental investigation into the thermo-mechanical durability of CFRP strengthened RC. Three different CFRP systems where considered; two commercially available epoxy systems and a new pre-impregnated polyurethane system. The scale of specimens is representative of those found currently in the field. Furthermore, unlike previous studies, the thermo-mechanical exposure applied to specimens is not extreme but representative of field conditions.

Findings

The most significant finding in this study is related to the performance of the polyurethane base CFRP system. The ultimate load bearing capacity, strain at failure, ductility, and load-deflection behavior of this composite system was virtually independent of the type of applied conditioning. Furthermore, unlike the epoxy-based composite systems, the urethane-based system displayed consistent failure modes. It is believed the inconsistent results observed with the epoxy-based cannot be fully attributed to bond degradation, but also to poor surface preparation and premature matrix gelling.

Based on results found, the use of externally bonded CFRPs are suitable for short-term rehabilitation efforts. No definitive conclusion can be made on the feasibility of externally bonded CFRP as a long-term or permanent strengthening option. Bond degradation appears to occur initially from fatigue but seems to stabilize over time. Thermal/humidity cycling had no apparent effect on bond or flexural performance.

Recommendations

Based on the findings of this study, it is recommended that further investigation be completed on the use of polyurethane matrix composites for structural applications. It is advised that untested matrix resin/hardener combinations not be considered for field use. Thorough surface preparation must be completed to ensure that good FRP-to-concrete adhesion is developed. It is recommended that additional laminate-end anchorage (either bonded or mechanical) be provided to prevent premature debonding.

This study did not incorporate a sufficient number of specimens nor was a sufficient quantity of data collected to develop a mechanics or chemistry-based model to describe the service life of concrete members strengthened with CFRP. Yet, Investigating service-level fatigue in existing FDOT retrofitted bridges could be investigated using load testing and ADT data; a possible correlation with this study could be developed.

Table of Contents

List of Figures

List of Tables

Chapter 1: Introduction

1.1 Problem Statement

In recent years the Federal Highway Administration (FHWA) has identified a critical need to upgrade the transportation infrastructure in the United States. Of the nearly 600,000 bridges in the FHWA's bridge inventory, upwards of 90,000 bridges have been deemed structural deficient and are in need of rehabilitation to increase member capacity. Research has shown that externally-bonded fiber-reinforced polymer (FRP) composite materials can provide an effective means to upgrade deficient structures. Moreover, In Florida, research on the use of carbon fiber reinforced polymer (CFRP) composite for external strengthening of reinforced concrete beams started in the early 1990s, followed by field implementations as early as 1994. A majority of these strengthened bridges have not shown signs of degradation or damage. However, there have been cases where visual inspections have revealed noticeable damage and deterioration to the CFRP material and its bond to the concrete substrate. The durability and expected service life of the girders strengthen with CFRP, beyond the years they already experienced, is not well understood. The FDOT is now facing the question of whether to treat the CFRP strengthening as a permanent (>50 years) repair or a short-term (~10 years) fix. If the technology is proven to be only a short-term fix, additional strengthening will have to be done to those structures soon. This project investigates the combined effects of cyclic thermal and fatigue loads on the CFRP and its interface with the concrete substrate through accelerated large-scale laboratory testing. The results of the tests will provide FDOT with evidence of the field durability of CFRP strengthening on concrete beams, which is critical for establishing design and implementation guidelines.

1.2 Research Objectives

The main objectives of this study were to provide the FDOT the following:

1. A brief review of current design guidelines for RC structures externally strengthened with CFRP; provisions for materials and durability being the primary focus.

2. Make recommendations on the following inquiries:

    a. Should CFRP composite strengthening of bridge girders be used as a permanent repair (>50+ years) or a short-term solution (~10 years)?

    b. If not permanent, what is the expected service lifespan of the repair?

3. Investigate the performance durability of two CFRP/matrix systems not used previously by the FDOT

    a. A epoxy matrix CFRP composite system employing a generic epoxy resin.

    b. A CFRP composite system utilizing a pre-impregnated carbon fabric with a water activated polyurethane resin

1.3 Report Outline

This research report is presented in the following format:

1) *Literature Review*: The literature presented is a comprehensive overview of background, materials, and previous work integral to the motivation and understanding of the study being presented. The following topics are addressed:

    a. Basic overview of reinforcing fibers and resin matrices used in infrastructure applications

    b. A comprehensive survey of existing work related to durability of RC beams strengthened with externally bonded FRP composite material

    c. A brief overview of FRP strengthening guidelines currently available

        i. ACI-440 (USA)
        ii. TR-55 (UK)

2) *Materials, Material Models, & Moment-Curvature Analysis*: This portion of the report discusses all materials used in this research study; from mechanical behavior to analytical modeling

3) *Design of Experimental Procedure*: All key elements involved with the design, development, and execution of the experimental program are discussed.

4) *Presentation and Discussion of Results*: Here all key results are presented on a specimen-by-specimen basis. Specimens are presented in the following respective groups:

    a. Baseline specimens
    b. Fatigued specimens
    c. Thermally conditioned specimens
    d. Specimens exposed to both fatigue and thermal conditioning

    After the discussion of each specimen group, a comparative discussed is presented in regard to resin system.

5) *Conclusions & Recommendations*: Conclusions will be drawn on observed experimental results. Based on the conclusions drawn, recommendations will be made in regard to durability and resin system.

Chapter 2: Literature Review

The following section discusses the literature survey that was conducted in conjunction with this research project. In order to provide a thorough and orderly treatment of past work the following review will be presented first at the composite component level and will proceed to the strengthened member level. The composite constituents that will be covered are only those that have been used in civil infrastructure applications.

2.1 Fiber Reinforced Polymers Composites: Mechanical Performance & Durability

Fiber Reinforced Polymer (FRP) composites consist of two main constituents: a reinforcing fiber, which is the main load-carrying component, and a polymeric matrix which is used as a stress transferring mechanism, binder, and to protect the reinforcing fibers from the ambient environment. The matrix material also ensures that reinforcing fibers maintain their designed orientation in the structural component.

2.1.1 Reinforcing Fibers

There are a number of different types of reinforcing fibers. This portion of the report will focus on carbon, glass, and aramid reinforcing fibers. Research has shown that these are the best suited for infrastructure applications. Table 1 contains a good representation of commercially available fibers and their mechanical and physical properties.

Table 1: Typical Reinforcing Fiber Material Properties†

Fiber Type	Fiber Identification	Density (g/cm^3)	Tensile Modulus GPa (MSi)	Tensile Strength GPa (ksi)	Failure Strain (%)	Coefficient of Thermal Expansion (longitudinal)		Poisson's Ratio
						S.I. (10^{-6}/ºC)	U.S. (10^{-6}/ºF)	
Glass	*E-glass*	2.54	72.4 (10.5)	3.45 (500)	4.8	5	8.99	0.2
	S-glass	2.49	86.9 (12.6)	4.30 (625)	5	2.9	5.22	0.22
Carbon	*T-300*	1.76	231 (33.5)	3.65 (530)	1.4	-0.6	-1.08	0.2
	P-100	2.15	785 (110)	2.41 (350)	0.32	-1.45	-2.61	0.2
	AS-4	1.8	248 (36)	4.07 (590)	1.65	-0.6	-1.08	0.2
	IM-7	1.78	301 (43.5)	5.31 (770)	1.81	-0.75	-1.35	0.2
Aramid	*Kevlar 49*	1.45	131 (19)	3.62 (525)	2.8	-2	-3.60	0.35
	Techora	1.39	70 (10.1)	3.0 (435)	4.6	-6	-10.79	0.35

†All Values taken from (Mallick, 2008)

2.1.1.1 Glass Fibers

Glass fibers are one of the most common and popular types of reinforcing fibers. Glass fibers are low cost compared to carbon or aramid fiber and have a high commercial availability. Some of the notable advantages of glass fibers are high ultimate strength, relatively high elongation until failure compared to other fiber types, non-conductive, good resistance to chemicals. The disadvantages of glass fibers are low tensile modulus, high specific gravity compared to carbon and aramid fibers, and surface abrasion sensitivity. Glass fibers also have some critical durability issues with mechanical fatigue (both static and cyclic), prolonged exposure to hydro-thermal loads, and alkali or acidic environments.

2.1.1.2 Carbon Fibers

As seen in Table 1, carbon fibers can be found with various mechanical properties. Yet, generally speaking, carbon fibers have high strength-to-weight ratios, stiffness-to-weight ratios, chemical resistivity, and excellent resistance to mechanical fatigue. Also, carbon fibers have negative coefficients of thermal expansion (CTE) which means that combine with the correct resin matrix system can yield a composite with a zero CTE. Some of the disadvantages of carbon fibers are poor impact resistance, high cost compared to other fibers, limited availability, low strain-to-failure, and high electric and thermal conductivity.

Tavakkolizadeh, et al., 2001 discusses the issue of carbon-to-steel galvanic corrosion. It was found that the corrosion rate was primarily dependent on the matrix thickness, direct carbon-to-steel contact area, and presence of salt solutions.

2.1.1.3 Aramid Fibers

Aramid fiber technology saw its first commercial appearance in the 1960s under the DuPont Company. Aramid fibers have the highest tensile strength-to-weight ratio amount the popular reinforcing fibers. Some advantages of aramid fibers are high resistance to extreme heat, high tensile strength, a negative CTE, excellent resistance to impact damage, and good chemical resistance. The disadvantages of aramids are difficult to machine, low compressive strength, and have durability issues with UV light and prolonged exposure to moisture (Mallick, 2008).

2.1.2 Polymeric Matrix Materials and Composites

There exists a wide variety of matrix material materials used in the manufacturing of FRP composites. Matrices can be organic or inorganic and can come from different material families i.e. ceramic, metallic, or polymeric. The matrices that will be of focus in this section are epoxy and polyurethane.

2.1.2.1 Epoxy Resins

Epoxy resin is one of the most popular matrix types used with carbon, glass, and aramid fibers in infrastructure applications. This is due to the number of advantageous chemical and mechanical properties that epoxy resins possess. Table 2 displays some general material properties of epoxy resin. Of these properties, the two worth mentioning are the Poisson ratio and the cure shrinkage. With a Poisson value in the range of 0.2-0.33, cured epoxy resins have a similar Poisson values to steel and concrete which are normally the bonding substrates in civil applications. The low cure shrinkage for epoxies, which is in the low range for polymeric matrices, means that cure-induced residual strains at the substrate level are low.

Table 2: Generic Cast Epoxy Resin Properties

Density (g/cm^3)	**Tensile Strength, MPa (psi)**	**Tensile Modulus, GPa (10^6 psi)**	**Poisson Ratio**	**CTE, 10^{-6} m/m/C (10^{-6} in/in/F)**	**Cure Shrinkage (%)**
1.2 - 1.3	55-130 (8,000-19,000)	2.75-4.10 (0.4-0.595)	0.2-0.33	50-80 (28-44)	1-5

†All Values taken from (Mallick, 2008)

Epoxy resins also have a number of attractive chemical properties such as absence of volatile matter during cure, excellent resistance to chemicals, and excellent adhesion properties. The disadvantages of epoxy matrices are high cost and prolonged cure time (Mallick, 2008)

2.1.2.2 Polyurethane Adhesives

Polyurethane is generic name used more for convenience than accuracy. Polyurethanes are not produced by polymerizing urethane monomers and do not consist solely of urethane groups; they can contain a number of different chemical groups. The development of polyurethane based adhesives began in the late 1930's with the first structural use introduced in 1968 by Goodyear (Szycher, 1999). Urethane adhesives have vast range of attractive properties making them a good candidate for a variety of substrate applications:

- Effectively wet the surface of most substrates.
- Have small molecular size that allows the adhesive to permeate porous substrates.
- Rapid cure time that is adjustable with catalyst.
- Cost effective.
- Excellent at low temperature.

Some of the disadvantages of polyurethane adhesives are as follows:

- Limited thermal stability due to molecular constituents.
- Issues with hydrolytic stability.
- Sensitive to moisture in bulk.
- Conditions under which application/curing occurs are critical.
- Some substrates require the use of primers.

2.1.2.3 Polyurethane Matrix Composites

There does not exist, to the authors' knowledge, a significant amount of research available on the use of polyurethanes as matrix materials for FRPs. The majority of early work published on the subject is related to fiber reinforced elastomeric polyurethanes (Andreopoulos, et al.1989) and thermoplastic polyurethane composites (Kutty, et al. 1991 and Kutty, et al. 1991) which do not exhibit mechanical performance suitable for infrastructure load-bearing applications.

Setiadi, et al. (2005) conducted a study on random fiber reinforced polymer composites and the damage sequence induced onto the composite by cyclic loading. Two different types of polymeric matrices were considered for the study; a modifed polyester employing a methyl ethyl ketone peroxide (MEKP) initiator and a thermosetting polyurethane. Test specimens (of dogbone geometery per ASTM D 628-01) were reinforced with 5 layers of random oriented E-glass mat and manufacured via resin tranfer molding (RTM). The approximate fiber fractions for each matrix type where 25 to 28% for the polyester-based FRP and 23 to 25% for the urethane-based FRP. Fatigue testing was conducted at 0.3 Hz within a stress range of 0 to 50% of the ultimate stress of the respective specimen types.

Results from static loading show that the urethane matrix composite had significantly higher strain at failure, ultimate strength, and energy absorption at failure than the polyester composite at the cost of lower tensile stiffness. Furthermore, the fracture plane and the observed post-failure cracking was more localized for that of the urethane composite.

Results from fatigue loading indicate that both matrix types show increased strains with cycle number. Yet, the strain increases in the urethane composite were smaller than those observed in the polyester composite. Furthermore, a decrease in elastic modulus was observed for both specimen types but was less significant in the urethane composite. The urethane matrix composite also exhibited a lower amount of matrix cracking at 1000 cycles. Moreover, cracks in the urethane matrix were observed to originate from micro-voids caused by CO_2 during cure.

It was concluded that urethane matrix composite performed better, under the inposed conditions, than of the polyester matrix composite.

2.2 Component Level Review

Although extensive research has been conducted on strengthening RC members with externally bonded FRP sheets and plates (Ritchie, et al. 1991, Meier & Kaiser 1991, Norris, et al. 1997, and Spadea, et al. 1998) there still exists a question as to the long-term performance and durability of the technology. Karbhari, et al. (2003) conducted a study focused on identifying the current state of durability knowledge for FRP composites in civil infrastructure. The conclusions regarding the importance and availability of data can be found in Table 3 where Table 4 gives explanation of ranking. Note that the information given below reflects only durability gap information for external strengthening.

Table 3: Importance and Availability of Data Measures

Exposure Environment	Importance of Data	Availability of Data
Moisture/Solution	5	3
Alkaline	5	3
Temperature	5	3
Mechanical Fatigue	3	3
Fire	5	5
UV	1	5
Creep/Relaxation	3	3
Combination	5	5

Compiled from Karbhari et al. 2003

Table 4: Rank Descriptions

Importance of Data		Availability of Data	
Rank	***Rank Description***	***Rank***	***Rank Description***
5	Critical, cannot go forward without it	5	Not Available
3	Important to have	3	Sparse and /or questionable
1	Good to have, but not essential	1	Widely available and validated

Compiled from Karbhari et al. 2003

Since the publication of the study by Karbhari, et al. (2003), there have been a number of durability related studies conducted and published. In the following sections available literature on the durability of RC beams externally strengthened with FRP composite materials will be discussed. The literature survey is focused on the following topics of durability:

- Mechanical fatigue
- Exposure to NaCl solution/vapor
- Humidity and/or moisture exposure
- Exposure to temperature baths/cycling

2.2.1 Fatigue

A critical factor effecting the long-term performance and durability of RC members strengthened with externally bonded FRP systems is repeated or fatigue loading. There only exist a limited number of available studies that have investigated the fatigue response of FRP strengthened members.

One of the earliest studies conducted was by Meier, et al. (1992) at EMPA (The Swiss Laboratories for Material Testing and Research at Dubendorf). In this study an RC beam with length 2000mm, depth 250mm, and wide 300mm, was strengthened in flexure with a glass/carbon hybrid sheet that was bonded to the tension face of the beam. The member was loaded in 4-point bending at a frequency of 4 Hz with a loading range of 1 to 19 kN (stress in the tension reinforcement was in the order of 400 MPa). Ultimate failure of the member occurred at 805,000 cycles.

Two more fatigue tests were conducted by Meier at EMPA. In these tests other test parameters were investigated such as slight increase in temperature and humidity during fatigue loading and pre-stress of the composite plate. Complete failure occurred at 14 and 30 million cycles. It must be noted that stress range for the second and third tests was not as intense as the initial test.

Barne, et al. (1999) conducted a similar fatigue study on CFRP strengthened RC beams. In their study, 5 RC beam specimens were constructed with the following dimensions and reinforcement: a span length 2.3m, depth 230mm, width 130mm, and 3 T12 rebars as tension reinforcement. Of the 5 beams, 3 beams were strengthened with pultruded CFRP composite plates. The plates were bonded to the tension face of the beams using SikaDur 31 two part structural epoxy. Moreover, all of the strengthened specimens incorporated plate-end anchorage consisting of two steel anchor bolts and a steel plate. The remaining two beams were used as control specimens.

Fatigue loading was conducted at 1 Hz in a 4-point bending configuration. The maximum load range considered for fatigue testing was between 25.9% and 39% of the predicted ultimate capacity of the beams (stress in the tension steel between 198 and 303 MPa). All strengthened specimens failed via fatigue rupture of the tension steel reinforcement.

The results of this study concluded that the fatigue stress range and the amount of tension steel were the most critical parameters when considering fatigue life of a CFRP strengthened member.

Ferrier, et al. (2005) conducted a study that employed the use of small-scale single and double lap shear test specimens. The purpose of the study was to determine the allowable shear bond strength and FRP strength as a function of number of load cycles. The test parameters considered in this study were epoxy type and stress range.

The results from this study concluded that as the number of fatigue cycles increase there is a proportional decrease in failure strength and composite elastic modulus. Moreover, it could also be observed that the stress range applied during fatigue loading had a significant impact on fatigue life. Recall, this result was noted by Barnes and Mays (1999) as well.

Ferrier et al. also describes the syntax of progressive failure during the fatigue life of the specimen as follows:

- *10% - 15% of fatigue life:* Debonding begins to occur near the loaded end of the specimen.

- *50% - 75% of fatigue life:* Epoxy adhesive begins to undergo softening and fatigue induced degradation.

- 75% - *100% of fatigue life:* Crack propagation at the concrete/FRP interface leading to failure.

The fatigue and monotonic strength of RC beams strengthened with externally bonded CFRP was investigated by Gheorghiu, et al. (2006). Fifteen RC beam specimens were constructed with dimensions: length 1215mm, width 100mm, and depth 150mm. All beams were strengthened with one layer of Sika CarboDur (50mm width). A 260mm portion of the composite laminate was left unbounded at the mid-span of all beams to ensure that specimen failure would occur via debonding.

Thirteen beams were subjected to cyclic loading and then to monotonic loading until failure. The two beams not subjected to cyclic loading were used as reference specimens and only subjected to monotonic loading.

Cyclically loaded beams were subjected to 400,000 to 2,000,000 load cycles at one of two load intensities. A low-range load intensity that varied from 15-35% of specimen yield strength and a high-range load intensity that varied from 35-75% of specimen yield strength. Beams were tested at 2 Hz (10 beams) or 3 Hz (3 beams).

The study concluded that the number of fatigue cycles at the low-range load intensity did not have a significant effect on the strengthened beams. Yet, the converse was true for the beams fatigued at the higher load intensity range. After about 200 cycles there was a significant increase in laminate strain and crack presence. Although the higher load range had an effect on observed strain and cracking, it was concluded that fatigue loading did not have a significant effect on member ultimate load (monotonic to failure).

Toutanji, et al. (2006) investigated the cyclic behavior of RC beams strengthened with CFRP sheets impregnated and bonded with an inorganic matrix. The main objective of the study was to investigate the relationship between fatigue strength, crack width, and number of fatigue cycles. Seventeen beam specimens were cast for the experiment. Thirteen beams were strengthened with three layers of externally bonded CFRP fabric. Strengthened specimens also incorporated externally bonded 45 degree shear strengthening CFRP strips.

The fatigue load applied ranged between 50% and 80% (strengthened specimens) of the ultimate static load capacity. The study concluded that member deflections and laminate strains do not vary significantly after the fatigue rupture of tension steel. It was also concluded that due to CFRP's higher ultimate strength compared to that of steel that the application of CFRP can increase the fatigue load capacity of a strengthened RC member. Finally it was concluded that crack initiation and propagation occurs during that first few hundred fatigue cycles.

Grace, et al. (2005) conducted an experimental study investigating the effect of repeated loading on the flexural response of CFRP strengthened RC beams. Twelve beam specimens with the following dimensions were used: length 2740mm, length 254mm, and width 152mm. Beams were strengthened with either externally bonded CFRP plates or sheets. Specimens were loaded in a 4-point bending configuration at 3.25 Hz for 2 million cycles. The loading ranges were 15%, 25%, or 40% of the ultimate flexural capacity. The study concluded that fatigue had no adverse effect on the ultimate load carrying capacity of the strengthened beam. It was noted that for the 40% of ultimate load range that specimens for both CFRP plate and fabric experienced softening without increase in applied load.

A study by Aidoo, et al. (2004) investigated the fatigue performance of large-scale RC bridge girders retrofitted with CFRP materials. Particular attention was paided to the bond between CFRP and concrete and fatigue life of strengthened specimens. Test parameters taken into consideration were CFRP system (plates and sheets) and fatigue stress range (60% and 80% of tension steel yeild stress). Eight 6.1m (20') reinforced concrete T-beams were prepared for the study. The construction details of the specimens prepared represented a 62% scaling of beams removed from an interstate bridge constructed in 1961. Fatigue loading was applied with a servo-controlled MTS hydraulic actuator under load control at 1Hz.

It was observed that strengthened specimens for both stress ranges failed in the following manner:

- Initial failure was caused by fatigue rupture of the extreme tension layer of reinforcing steel. In some specimens, multiple tension bars experienced fatigue rupture.

- Shear cracking/deformation near mid-span initiated CFRP debonding.

- Complete CFRP delamination from concrete. In some cases delamination was induced by steel rupture.

It was concluded that the addition of externally bonded CFRP can increase the fatigue life of RC beams. The increase in fatigue life is limited by the CFRP-to-concrete bond quality and ability to resist fatigue induced bond degradation. It was also found that the preformed CFRP strip preformed better than the fabric retrofit.

The following general conclusions can be drawn from past research on the fatigue durability of CFRP strengthened RC beams:

- Fatigue stress range seems to play an important role in the fatigue performance of CFRP strengthened members.

- The majority of studies reported softening in strengthened members due to fatigue induced degradation of the FRP-to-concrete interface.

- Studies report mixed results in regard to post-fatigue monotonic ultimate flexural capacity.

2.2.2 NaCl Solution

There are numerous situations in externally strengthening applications where the FRP composite system could be subjected to salt exposure i.e. road de-icing salts and sea water. Although FRP composites have a high tolerance against corrosion, the FRP-to-concrete interface could be compromised due to such exposure. There have been a few studies conducted on the effects of salt exposure on RC members externally strengthened with FRP materials.

One of the earliest studies to investigate exposure to chlorides was done by Karbhari, et al. (1996). The study focused on the FRP-to-concrete bond behavior under short term exposure to various environments. Two different commercially available epoxy resin systems were investigated with glass and carbon reinforcing fibers. Small-scale mortar (1:3 – cement:sand) beam specimens were used with dimensions of 13”(length) x 2”(width) x 1”(height). Three layers of epoxy impregnated reinforcing fiber were applied to each strengthened specimen. After a one week cure period specimens were subjected to 60 days (1440 hours) of immersion in a 5% NaCl solution. Upon completion of environmental conditioning specimens were subjected to 4-pt monotonic loading until failure.

All four composite systems tested experienced decreased flexural performance in terms of ultimate load bearing capacity, deflection capacity, and flexural stiffness (*EI*). The decreases in performance were reported as follows: 13-47%, 15-53%, and 7-31% for ultimate load, deflection, and flexural stiffness respectively. It must be noted that the epoxy systems with the lower glass transition temperature experienced the most severe degradation for both glass and carbon fibers. Furthermore, it was determined that the epoxy system was more critical to the post-conditioned behavior than the reinforcing fiber.

The effect of immersion in NaCl solution was investigated as a portion of the study conducted by Grace, et al. (2005). 12 beam specimens, with dimensions 9’(length) x 6”(width) x 10”(height) and ρ=1.15%,were exposed to immersion in a NaCl solution for 1000, 3000, or 10,000 hours at 73°F ± 3°F. Beams were strengthened with either CFRP plates or fabric sheets. The CFRP systems were adhered to the concrete surface using one of two types of structural epoxy. Both epoxy systems had similar material properties. Ultimate load testing was conducted under 4-point bending in three stages.

Results from load tests show no significant decrease in ultimate load bearing capacity for either CFRP strengthening system. The system employing CFRP plates actually showed an increase in ductility for all exposure periods. The system employing CFRP sheets showed a 16.6% decrease in ultimate deflection capacity. Ultimate strains values for both systems at all exposure periods experienced slight or no reductions from baseline values. In conclusion there did exist any type of definitive relationship between time of exposure and mechanical response.

An experimental study on the durability characterization of wet lay-up carbon/epoxy composites was conducted by Abanilla, et al. (2006). A portion of the study was focused on the effect of a salt solution on CFRP at the material level. The carbon fabric used had the following properties: ρ = 1.80 g/cm^3, E = 230 GPa, and f_{frp} = 4900 MPa. Specimens exposed to saline solution immersion consisted of either 2 or 6 layers of carbon fabric. After curing, a standard ASTM D3171 acid digestion test was conducted and it was determined that specimen volume fractions ranged from 34 to 43%.

Specimens where subjected to 100 weeks of immersion in a 5% NaCl solution at 23 °C. The effect of saline immersion was quantified via uniaxial tension (ASTM D3039), 3-point flexure (ASTM D790), glass transition temperature T_g (ASTM E1640), and moisture uptake testing. Specimens were tested throughout the 100 week period of exposure (5 specimens per time interval).

It was concluded that the presence of NaCl in solution had a negligible effect on the rate of moisture uptake and T_g. Tensile test (2-layer specimens) results showed an 18 and 12% decrease in tensile strength and modulus respectively after 100 weeks of exposure. 3-point bending test (6-layer specimens) results showed a 25 and 9.4% decrease in flexural strength and modulus respectively after 100 weeks of exposure. It must be noted that the respective strength and modulus decreases seen over the 100 week period for both tests were progressive and had a tendency to stabilize over time.

Soudki, et al. (2007) conducted an experimental study which examined the ability of externally bonded CFRP plates (Sika CarboDur) and sheets (Forca-Tow) to prevent chloride intrusion of concrete. A total of 11 RC beams (2400mm-length x 150mm-width x 250mm-height and ρ=0.6%) were cast. Of which 8 beams were cracked and strengthened with CFRP and 3 beams remained uncracked. There were two strengthening schemes employed: beams strengthened with CarboDur plates incorporated U-wrap plate-end anchorage and beams strengthened with Forca-Tow sheets employed lateral CFRP anchorage strip throughout the length of the beam shear span. It must be noted that both the sides and tension face of the beams strengthened with Forca-Tow were covered with saturating epoxy.

Beams were subjected to 0, 100, 200, or 300 wet/dry cycles in the presence of 3% NaCl solution. Each wet/dry cycle took 2 days to complete (1 day for the wet cycle and 1 day for the dry cycle). Upon completion of the wet/dry conditioning beams were loaded monotonically to failure in a 4-point bending configuration.

Results of the study showed that beams strengthened with CarboDur plates yielded 19, 25, and 28% reduction in load bearing capacity for 100, 200, 300 wet/dry cycles respectively. Beams strengthened with the Forca-Tow system showed 2, 6, and 11% reductions in ultimate capacity for 100, 200, and 300 wet/dry cycles respectively. The performance of the Forca-Tow system verses the CarboDur system was attributed to the epoxy coverage of the beam. It is also concluded by the authors that the Forca-Tow system was not greatly affected by the applied conditioning. It must be noted that the authors of this document believe that the performance of the Forca-Tow system can be attributed to the amount of additional transverse anchorage that was used.

2.2.3 Moisture & Humidity

Karbhari, et al. 2003 identified exposure to moisture and humidity to be a critical area in need of investigation for externally strengthening. This is due to the susceptibility of the resin matrix to be infiltrated by moisture. Moisture intrusion of the matrix can lead to a number of negative effects. On the matrix level, this can cause hydrolysis, plasticization, and saponification. At the fiber/matrix interface level, moisture intrusion can cause both chemical and mechanical fiber/matrix bond degradation. If moisture is allowed to reach the reinforcing fibers, in the cases of aramid and glass fiber, can cause deterioration of the fiber and a higher possibility of premature fiber rupture.

Although significant work has been completed on the investigation of humidity and moisture effects of FRP composites (Marom and Broutman 1981, Apicella et al. 1983, Zheng and Morgan 1993, and Schutte 1994) the same is untrue for externally reinforced RC members. The following section discusses some of the available studies conducted on moisture/humidity effects on FRP strengthened RC members

The study conducted by Karbhari, et al. (1996), as discussed earlier, was one of the earliest experimental investigations on environmental effects on FRP strengthened concrete. A portion of this study focused on the immersion of specimens in water at 68°F (20°C) for 60 days (1440 hours).

Results showed that of the four composite systems tested there were 15-35% and 15-52% reductions ultimate load and deflection at failure respectively. It was also found that immersion in water did not have an effect on the glass transition temperature for all systems. It was concluded that the resin matrix system used in creating the externally bonded composite had the greatest effect on the post-immersion load deflection behavior of the specimens.

The study conducted by Grace, et al. (2005), previously discussed, included a portion of the experimental program that exposed specimens to 100% humidity for periods of 1000, 3000, and 10,000 hours at 100±3°F (38±2°C) per ASTM D 2247. Recall that both CFRP plates and sheets were used to strengthen beam specimens.

Results of the study showed that beams strengthened with CFRP sheets exhibited more stable post-humidity performance than those strengthened with CFRP plates. Of the various exposure environments used in the study (dry heat, humidity, NaCl solution, freeze-thaw, alkali solution, and fatigue) it was found that the beams strengthened with CFRP plates showed a greater tendency to experience decreased flexural performance in terms of ultimate load bearing capacity and maximum flexural strain due to humidity exposure (at 10,000 hours); decrease of 31.9% and 54% from baseline ultimate capacity and maximum strain respectively. The post-exposure behavior of the specimens strengthened with CFRP sheets was not nearly as critical for 10,000 hours of exposure; 9.67% , 11.4%, and 19.9% decreases from baseline results in terms of ultimate load, deflection, and mid-span strain respectively. All specimens failed via CFRP debonding and/or concrete cover delamination.

2.2.4 Temperature Effects

In infrastructure service environments, variations in ambient temperature are to expected. Therefore, the effect of temperature variation on the FRP-to-concrete interface is of importance when considering the long-term durability of strengthened members. There have been three types of temperature oriented tests conducted in relation to infrastructure applications:

1) Exposure to a constant temperature (either elevated or decreased).

2) Cyclic temperature exposure (such as freeze/thaw or heat/cool).

3) Steady-state or transient temperature exposure during the loading (both experimental and analytical conducted).

The study conducted by Grace, et al. (2005), previously discussed, included portions of the experimental program that exposed specimens to constant elevated temperatures and freeze/thaw cycles. Twelve RC (4 per exposure period) beam specimens were exposed to 1000, 3000, or 10,000 hours of 60°C (140°F) dry heat in a specially design chamber. Eight (4 per exposure period) beam specimens were exposed to 350 or 700 freeze/thaw cycles where temperature cycled between -17.8°C and 4°C (0°F and 40°F). Air was used to freeze beams while water was used for thawing. After the conditioning period, specimens were loaded monotonically until failure.

Results revealed that freeze/thaw conditioning resulted in reduced loading bearing capacity of RC member strengthened with FRP plates and sheets by 3.3-9.5% and 6-13% respectively. There was no significant decrease in flexural performance observed in specimens subjected to dry heat conditioning. All specimens failed via CFRP debonding.

Gamage, et al. (2006) investigated, via analytical means, the bond properties of CFRP to concrete under elevated temperatures. More specifically, the study focused on bond performance under transiant thermal loads like those associated with structural fires. 13 single-lap shear specimens (2 of which were coated with an insulating material) were prepared to calibrate a non-linear heat transfer finite element model (FEM). Test specimens were loaded using displacement control. During testing, non-insulated specimens were subjected to a constant rate applied temperature of 10°C/min (50°F/min). Parameters investigated via FEM were bond length, bond slip, failure load, temperature rate, fire resistance level, and insulation thickness.

Based on both experimental and analytical results, the study by Gamage, et al. concluded the following:

- The epoxy adhesives currently being used for construction applications are extremely sensitive to temperature variations.

- A maximum service temperature of 70°C (158°F) is recommended to maintain force transfer between concrete and CFRP.

- Bond strength, under elevated temperatures, is not dependent on bond length.

- Un-insulated concrete-CFRP composites will reach the point of bond failure in the standard fire within 5-6min.

Karbhari, et al. (2003) suggested that for civil infrastructure applications freeze/thaw conditons are to be considered the most critical temperature related service environment.

2.3 Survey of Current Design Guidelines

Within the last 15 years a number of countries have developed design guidelines for strengthening RC structures with FRP composite materials. These design guidelines were developed to answer the growing needs of designers and owners reluctant to adopt the use FRP technologies for strengthening due to lack of standardized design practices. The following section will review current design guidelines from the United States and United Kingdom. The key areas of focus within each guideline will be:

- Material Design Properties
- Reduction Factors
- Provisions for Fatigue
- Provisions for Durability

Although the guidelines have provisions for flexural, shear, and column strengthening, this document will only review design provision for flexure.

2.3.1 United States – ACI-440.2R-08

Committee 440 of the American Concrete Institute (ACI) was organized in 1991 in order to report on FRP material, research, current industry practices, and most importantly develop design guidelines, specifications, and standard for FRP in construction (ACI-440.2R-08, 2008). Published in 2008, ACI-440.2R-02 *Guide for the Design and Construction of Externally Bonded FRP Systems for Strengthening Concrete Structures* provides a good basis to applications, limitations, design recommendations, and construction detailing of externally bonded FRP systems for RC infrastructure. The following section will review the basis, terms of use, and design provisions discussed in ACI-440.2R-08. The contents of ACI-440 are as follows:

1) Background
2) Material Properties, Behavior, and Durability
3) Recommended Construction Requirements
4) Inspection, Evaluation, and Maintenance Methodologies
5) Design of Flexural, Shear, and Confined Members
6) Detailing Recommendations
7) Design Examples

2.3.1.1 General Information

The ACI-440 design guideline is based on approximately 20 years of experimental, analytical, and field studies. Although much research has been conducted, there still exist a number of uncertainties associated with the use of FRP materials in civil infrastructure. Of those uncertainties, the most critical are those related to the integrity of the FRP-to-concrete interface. Research has shown that debonding of the FRP plate/sheet from the concrete substrate is the most dominate failure mode of RC members externally strengthened (Bonacci & Maalaj, 2001). Since such uncertainties exist, ACI-440 design provisions are very conservative for all points in the design procedure i.e. material properties, reduction factors, and design flexural strain limits. Moreover, the design procedures outlined have not, in many cases, been thoroughly developed/proven and are based heavily on design philosophies presented in ACI-318 *Building Code Requirements for Structural Concrete.* Furthermore, the research based design equations and factors are based on specimens of moderate size and portion. ACI-440 is a guide to the design of FRP externally strengthened RC member and not a code. Therefore, engineering judgment must be used when interpreting recommendations made.

2.3.1.2 FRP Material Properties

The material properties for an FRP system (here system refers to the combination of the selected type of reinforcing fiber(s) and the selected resin matrix) should be determined one of two ways; from first hand experimental result or obtain from the manufacturer. In either case, the FRP system is to be characterized as a composite in accordance with ASTM D3039. If material properties are obtained from a manufacturer they should be reported in the following fashion:

$$f_{fu}^{*} = \overline{f}_{fu} - 3\sigma \qquad \textbf{Equation 1}$$

$$\varepsilon_{fu}^{*} = \overline{\varepsilon}_{fu} - 3\sigma \qquad \textbf{Equation 2}$$

Where Equation 1 and Equation 2 represent ultimate strength and strain respectively (where $\overline{f}_{fu}$ and $\overline{\varepsilon}_{fu}$ are defined as the ultimate strength and strain respectively). Using such values yields a 99.87% probability that the values indicated will be exceeded

Table 5: ACI-440 Environmental Reduction Coefficients

Exposure Conditions	Fiber & Resin Type	Environmental Reduction Factor C_E
Interior Exposure	Carbon/Epoxy	0.95
	Glass/Epoxy	0.75
	Aramid/Epoxy	0.85
Exterior Exposure	Carbon/Epoxy	0.85
	Glass/Epoxy	0.65
	Aramid/Epoxy	0.75
Aggressive Environments	Carbon/Epoxy	0.85
	Glass/Epoxy	0.5
	Aramid/Epoxy	0.7

Adapted from Table 8.1 ACI 440.2R-02

$$f_{fu} = C_E f_{fu}^{*} \qquad \textbf{Equation 3}$$

$$\varepsilon_{fu} = C_E \varepsilon_{fu}^{*} \qquad \textbf{Equation 4}$$

$$E_f = \frac{f_{fu}}{\varepsilon_{fu}} \qquad \textbf{Equation 5}$$

Equation 3, Equation 4, and Equation 5 are used to determine the design material properties values. C_E is defined to be the environmental reduced factor which is based on the FRP system and the exposure environment (See Table 5). It should be mentioned that ACI 440 assumes the FRP composite does not undergo any type of softening (reduction of E_f) due to long-term environmental exposure.

2.3.1.3 Flexural Strengthening

ACI-440 recommends that the factored M_u of a section be calculated according to the load factors described in ACI-318-05. The nominal flexural capacity of an FRP strengthened member (utilizing mild steel or bonded pre-stressing tendon) can be determined based on the following:

- Strain Compatibility
- Internal Force Equilibrium
- Governing Failure Mode

It is suggested that the following failure modes be investigated during the design procedure:

- Crushing of concrete in compression before yielding of steel
- Yielding of steel in tension followed by rupture of the FRP laminate
- Yielding of steel in tension followed by concrete crushing
- Shear / Tension delamination of the concrete cover
- Debonding of the FRP from the concrete substrate

It is recommended that if the strengthened member be exposed to sustained or cyclic loading (this is the case with virtually all civil structures) that stress limitations be imposed on the strengthening material. These limits are based on previous investigations with different composite material and loading conditions. The suggested limits are shown in Table 6.

Table 6: Sustained and Cyclic Stress Limits

	Fiber Type		
Stress Type	***GFRP***	***AFRP***	***CFRP***
Sustained plus Cyclic Stress Limits	$0.20f_{fu}$	$0.30f_{fu}$	$0.55f_{fu}$

2.3.1.4 Durability

The ACI 440 design guideline for externally bonded FRP strengthening does not have explicit and well defined (other than material reduction factors) details regarding how to handle durability issues.

2.3.2 United Kingdom – TR-55

In 2000, the Concrete Society of the United Kingdom published *Technical Report No. 55 – Design Guidance for Strengthening Concrete Structures using Fibre Composite Materials.* The main contents of this guideline are as follows:

1) Background, Material Types & Properties
2) Review of Applications
3) Design of Members Strengthened for Flexure
4) Design of Members Strengthened for Shear
5) Design of Strengthened Columns
6) Installation and Long-term Inspection

2.3.2.1 FRP Material Properties

TR-55 specifies that the FRP composite material properties be obtained via the manufacturer of the composite. If the composite plate is manufactured in the field i.e. wet lay-up, material properties are to be determined from experimental result of representative samples. From which the ultimate tensile strength of the FRP composite is to be determined from Equation 6.

$$f_{fk} = f_{fm} - 2\sigma \qquad \textbf{Equation 6}$$

It is also specified that a sufficient number of samples be tested to ensure that 2 standard deviations be realistic (a more detailed description of test methods, test provisions, and material quality requirements can be found in Appendix C of the TR-55 guideline).

The designs values for FRP composite ultimate strength and elastic modulus are to be determined by adjusting the assumed value (Equation 6) with a combination of appropriate safety factors. Equation 7 depicts the expression used to determine the design ultimate strength of FRP f_{fu}.

$$f_{fd} = \frac{f_{fk}}{\gamma_{mF} \cdot \gamma_{mE}} \qquad \textbf{Equation 7}$$

Where

$$\gamma_{mF} = \gamma_{mf} \times \gamma_{mm} \qquad \textbf{Equation 8}$$

The constants γ_{mF}, γ_{mE}, γ_{mf}, and γ_{mm} are define as the partial safety factors for the FRP composite, the composite elastic modulus, the reinforcing fiber, and method of application/manufacturing respectively. The numerical values for γ_{mE}, γ_{mf}, and γ_{mm} can be found in Table 7, Table 8, and Table 9 respectively. These values are used to take into account various uncertainties associated with the fiber type, manufacturing method, and time-dependant changes in composite elastic modulus.

Table 7: TR-55 Partial Safety Factors for Strength

Material	Partial Safety Factor (γ_{mf})
Carbon FRP	1.4
Aramid FRP	1.5
Glass FRP	3.5

Taken form TR-55 (Table 5.2)

Table 8: TR-55 Recommended Partial Safety Factors (Based Manufacturing Type)

Type of System	Manufacturing Process	Additional Partial Safety Factor (γ_{mm})
Plates	Pultruded	1.1
	Pre-preg	1.1
	Preformed	1.2
Sheets or Tapes	Machine-controlled Application	1.1
	Vacuum Infusion	1.2
	Wet Lay-up	1.4
Prefabricated (Factory Made) Shell	Filament Winding	1.1
	Resin Transfer Molding	1.2
	Hand Lay-up	1.4
	Hand-held Spray Application	2.2

Adapted from EUROCOMP Design Code (Clarke 1996)

Table 9: TR-55 Partial Safety Factors for FRP Elastic Modulus

Material	Factor of Safety (γ_{mE})
Carbon FRP	1.1
Aramid FRP	1.1
Glass FRP	1.8

Taken form TR-55 (Table 5.4)

2.3.2.2 Performance Limitations

TR-55 suggests the following performance limitations be followed for flexural strengthening in regard to fatigue stress range and sustained maximum stress within the composite plate (see Table 10 and Table 11 respectively)

Table 10: TR-55 Fatigue Stress Range Limits (% of Design Strength)

Material	Stress Range (%)
Carbon FRP	80
Aramid FRP	70
Glass FRP	30

Taken form TR-55 (Table 6.1)

Table 11: Maximum Sustained Stress to Avoid Stress Rupture (% of Design Strength)

Material	Maximum Stress (%)
Carbon FRP	65
Aramid FRP	40
Glass FRP	55

Taken form TR-55 (Table 6.2)

Not shown here is a factor of safety for the structural adhesive (γ_{mA}) used to bond the FRP composite to the structural member. TR-55 specifies that in general the ultimate strength of a section will be governed by the strength of concrete not by the strength of the bonding adhesive. Yet, it is specified that the design engineer of the strengthening system ensure that the selected adhesive perform adequately with the structure and the surrounding environment. TR-55 suggests the following criteria for selecting the adhesive factor of safety:

- A 10% reduction of the fully cured material be applied if the strengthened member experiences cyclic strains during the cure period.

- The sustained stress in the adhesive should be maintained below 25% of the short-term strength. This equates to a partial material safety factor of 4.0.

Chapter 3: Materials

3.1 Concrete

The concrete beams used in this study were cast at the FDOT Structural Research Center (SRC) in Tallahassee, FL. Beams were poured in eight separate batches with two beams per batch. After each beam was poured a number was inscribed on the beams to aid in the beam's identification. Standard 6" x 12" (152.4mm x 304.8mm) compression cylinders were created and tested according to ASTM Standard C39 for each batch. See Table 12 for details about the concrete mix design.

Table 12: Concrete Mix Design

Cement Type:	Class II
Target Slump:	3in (76.2 mm)
Minimum f '$_c$:	4,500 psi (31 MPa)
Max Water to Cement Ratio:	0.44
Minimum Cementitious Mat.:	611lb/yd^3 (362.5kg/m^3)
Air Content Range:	1% - 6%

Consecutive batches were poured a minimum of seven days apart, this allowed all beams to cure undisturbed in the molds. Refer to Table 13 for the pour dates, batch numbers, and the compressive strength results for the seven and twenty-eight day tests of the cylinders. After seven days of curing, beams were removed from the forms and stored outdoors at the SRC for further curing. As noted in Table 13, two of the beams had been cast with under-strength concrete and were therefore excluded from the experiment. The two under-strength beams and one of the full strength beams were damaged during handling of the beams. The damage to the full strength beam was some minor tensile cracking in the compressive face of the beam but this would not pose a problem therefore the beam was still utilized for the experiment.

Table 13: Concrete Details

Batch No.	Pour Date	Beam ID	Compressive Strength			
			MPa		*psi*	
			7 Day	28 Day	7 Day	28 Day
1	5/11/2005	1 & 2	22.1	35.5	3205	5149
2	5/18/2005	3 & 4	33.3	51	4830	7397
3	6/1/2005	5 & 6	35.2	49.1	5105	7121
4	6/8/2005	7 & 8	32.1	46.7	4656	6773
5	6/15/2005	9 & 10	29.3	44.1	4249	6396
6	6/22/2005	11 & 12	34.6	51.3	5018	7440
7	6/29/2005	13[1,2,3] & 14[1,2,3]	16.1	26.7	2335	3872
8	8/31/2005	15[2] & 16	31.7	51.7	4598	7498

[1]Under Strength [2]Damaged [3]Excluded

3.2 Reinforcing Steel

The rebar used in this study were standard grade 60 deformed bars. Samples of the rebar were tensile tested at UCF to obtain stress-strain relations to be used later in analytical models. The results from these tests can be found in Figure 2.

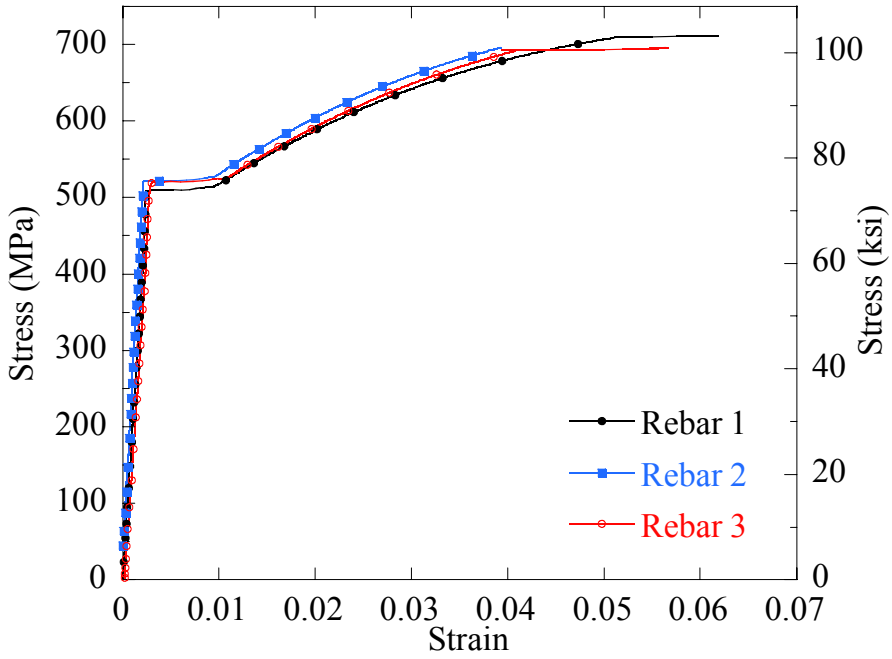

Figure 2: Reinforcing Steel Tensile Behavior

3.3 CFRP

The CFRP systems used in this study consisted of three fabric-resin systems. The first two CFRP composite systems utilized an epoxy matrix with unidirectional carbon fabric produced by the Hexcel Corporation (product identification GA130). The first system, denoted as the GE system, consisted of commercially available products produced by DOW and Huntsman. The second system, denoted as the EP system, employed a structural epoxy produced by PTM&W Company (commercially known as Aeropoxy) that has been used previous by the FDOT in prior FRP research and field applications. The constituent materials used for the epoxy matrices can found in Table 14.

Table 14: Epoxy Matrix Constituents

System ID	*Resin Type*	*Hardener*	*Additive*
GE	D.E.R.™ 383 (DOW)	Jeffamine® D-230 (Huntsman)	399 Accelerator (Huntsman)
Mix proportions (by Weight)	1Part	0.329 Parts	Unknown
EP	PR2032 (Aeropoxy)	PH3660 (Aeropoxy)	None
Mix proportions (by Weight)	1Part	0.333 Parts	-

The third system used was a carbon/polyurethane pre-preg system (known as Aquawrap®) commercially available through the Air-Logistics company. System three, denoted "PU", employed a unidirectional pre-impregnated carbon fabric. Unlike the GE and EP systems which employ the use of a resin hardener, the PU system initializes its cure sequence when misted with water. The PU system used in this study was researched previously by Bazinet, et. al (2003) and Sen & Mullins (2007). Specification on the three systems can be found in Table 15.

Table 15: CFRP System Physical Properties

Resin System		Fabric Weight		Fabric Thickness		Filaments/Tow
ID	***Resin Type***	***g/m²***	***oz/yd²***	***mm***	***in***	
GE	Epoxy	447.6	13.2	0.508	0.02	12,000
EP	Epoxy	447.6	13.2	0.508	0.02	12,000
PU	Polyurethane	440.8	13	0.454	0.18	12,000

The EP and PU composite systems were tested for mechanical properties. Tensile test coupons were prepared according to ASTM D3039. For each system, a 12" x 12" (304.8mm x 304.8mm) composite plate was created using the wet lay-up manufacturing process. Each plate consisted of two layers of CFRP fabric. Plates were allowed to cure for 48 hours and were then cut into 1" (25.4mm) strips. 24 hour previous to testing G10 fiberglass gripping tabs were adhered to the ends of each specimen using a structural epoxy adhesive.

Tensile testing took place at the University of Central Florida's Structure's Lab on a Satec 200kip universal testing machine. During tensile testing an Instron extensometer was used to record strain values. The extensometer was removed previous to rupture of the specimen to ensure that no damaged would be induced on the measurement device. Both EP and PU systems were tested for elastic modulus; the EP system was also tested for ultimate strength and strain at rupture. It must be noted that no material testing was conducted on the GE system. This was due to an unavailability of GE resin during the time period in which material testing was being conducted

The tested stress-strain relations for the EP and PU systems can be seen in Figure 3 and Figure 4 respectively. Tabulated results for the elastic modulus and ultimate stress/strain for the EP system can be found in Table 16 and Table 17 respectively. Finally, results for the PU system elastic modulus can be found in Table 18.

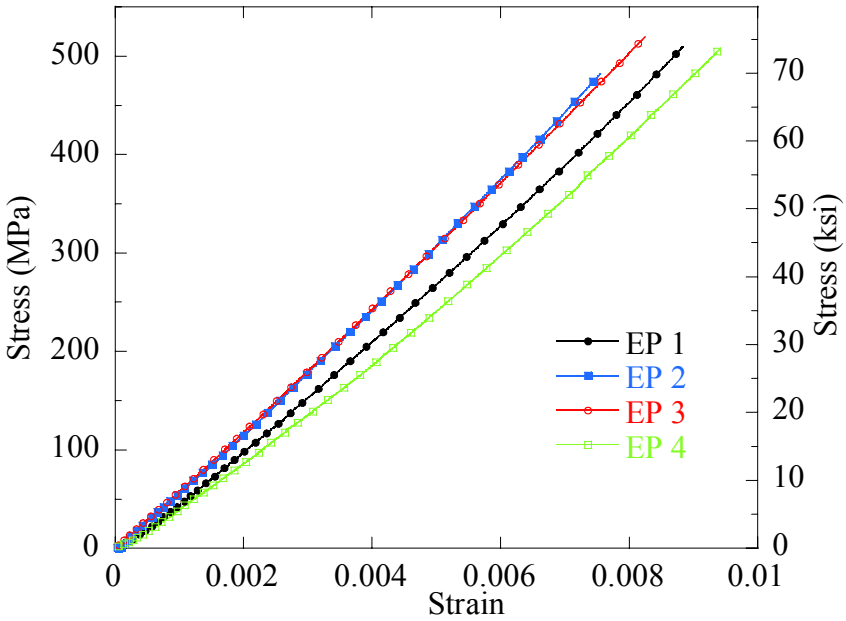

Figure 3: EP-System Tensile Behavior

Table 16: EP-System Elastic Modulus Results

Specimen	Modulus of Elasticity	
	GPa	***ksi***
EP 1	62.63	9084
EP 2	67.58	9801
EP 3	62.44	9055
EP 4	61.49	8918
Average	63.54	9215
Standard Dev.	2.74	398

Table 17: EP-System Ultimate Strength & Strain at Rupture

Specimen	Ultimate Strength		Strain at Rupture
	MPa	***ksi***	
EP R1	714.3	103.6	0.01124
EP R2	697.8	101.2	0.01099
EP R3	697.1	101.1	0.01097
EP R4	611.5	88.69	0.00962
EP R5	663.9	96.28	0.01045
Average	680.2	98.65	0.01065
Standard Dev.	46.46	6.74	0.000642

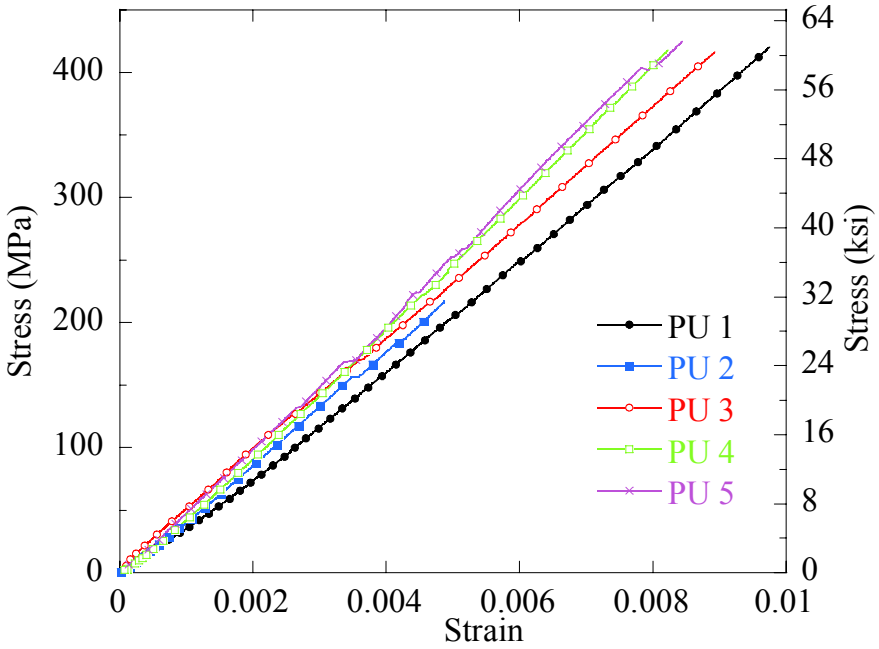

Figure 4: PU-System Stress-Strain Behavior

Table 18: PU-System Elastic Modulus Results

Specimen	Modulus of Elasticity	
	GPa	***ksi***
PU 1	44.54	6459
PU 2	47.31	6861
PU 3	45.65	6621
PU 4	52.48	7611
PU 5	52.25	7578
Average	48.45	7026
Standard Dev.	3.71	538

It should be noted that the tested elastic modulus for the PU system varied significantly from the mechanical data provided by the system manufacturer. The manufacturer material properties are listed in Table 19.

Table 19: PU-System Manufacturer Mechanical Properties

Units	Tensile Strength	Tensile Modulus	Compressive Strength	Interlaminar Shear
ksi (MPa)	123 (848)	11,400 (78,600)	20 (138)	2.8 (19.3)

Chapter 4: Analytical Modeling

Analytical moment-curvature (M-Φ) models were created for the four baseline beams (strengthened and unstrengthened) in order to determine the perfect theoretical flexural behavior. The main assumption used in creation of the models was that plane sections of the unloaded beam remain plane after the application of pure bending. Moreover, this assumption requires that there is no relative slip or debonding in the adhesive layer or at adhesive/substrate interface. It must noted that this assumption becomes less valid as loading increases for research shown that relative slip and debonding does indeed occur at the FRP-to-concrete interface (Lu, et al. 2005). Yet, a fairly good prediction of flexural behavior can still be generated.

The behavior of materials were either defined directly from experimental results or defined with an existing (and accepted) empirical model. The following sections discuss the development of the material models used and any additional assumptions that were considered. The model used was created by Olka (2009)

4.1 Concrete

The material constitutive model used for concrete was developed using both the Modified Hognestad Model and Hordijk Model. The combination of the two models yielded complete material model that incorporates the linear and nonlinear tension and compression behavior of concrete. The Modified Hognestad Model was used to model the compression behavior of concrete. While the Hordijk model was used to model the tension behavior of concrete. Both models were calibrated according to experimental compression test results. Figure 5: Material Model for Concrete represents the constructed stress-strain behavior for concrete with f'_c = 6.7ksi.

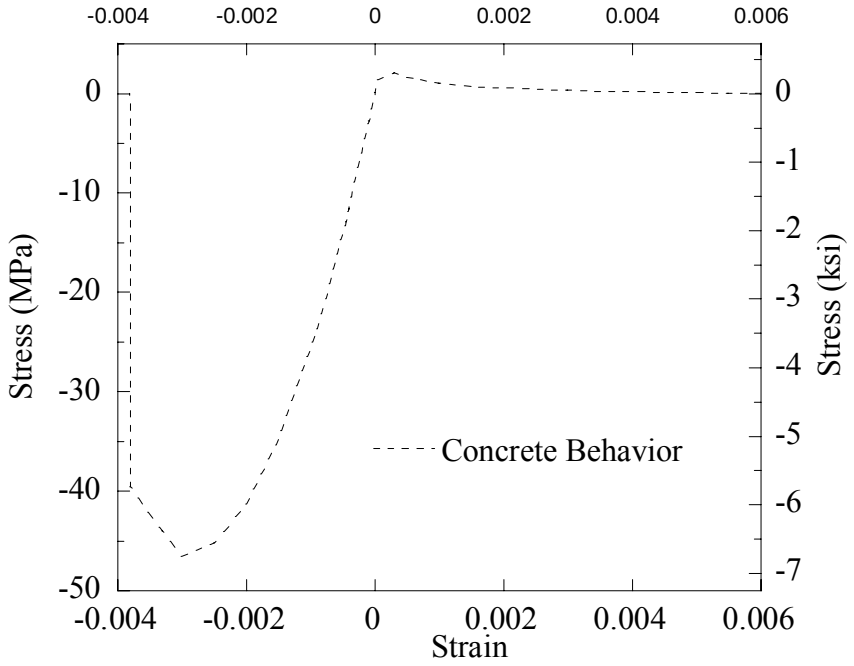

Figure 5: Material Model for Concrete

4.2 Steel

The material model for the reinforcing steel used was derived directly from the tensile test results described in Chapter 3 of this document. Figure 6 depicts the tensile stress-strain behavior for the reinforcing steel used in creating the analytical models for this study.

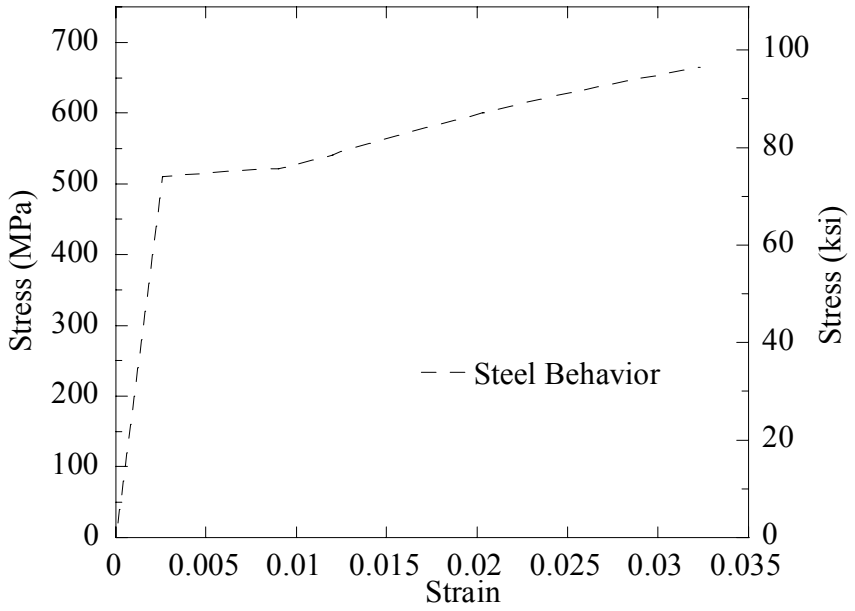

Figure 6: Material Model for Reinforcing Steel

4.3 CFRP

The material models for the externally bonded CFRP composite sheets were also defined through the use of experimental tensile test results. It was assumed that the CFRP materials behave perfectly linear until failure. Hence, the only two parameters needed to define the tensile behavior were the elastic modulus and the tensile rupture strain. The material models for the PU and EP systems can be seen below in Figure 7. It should be noted that due to lack of experimental and/or manufacture data for the GE system, the EP system material model was used to model the GE system as well.

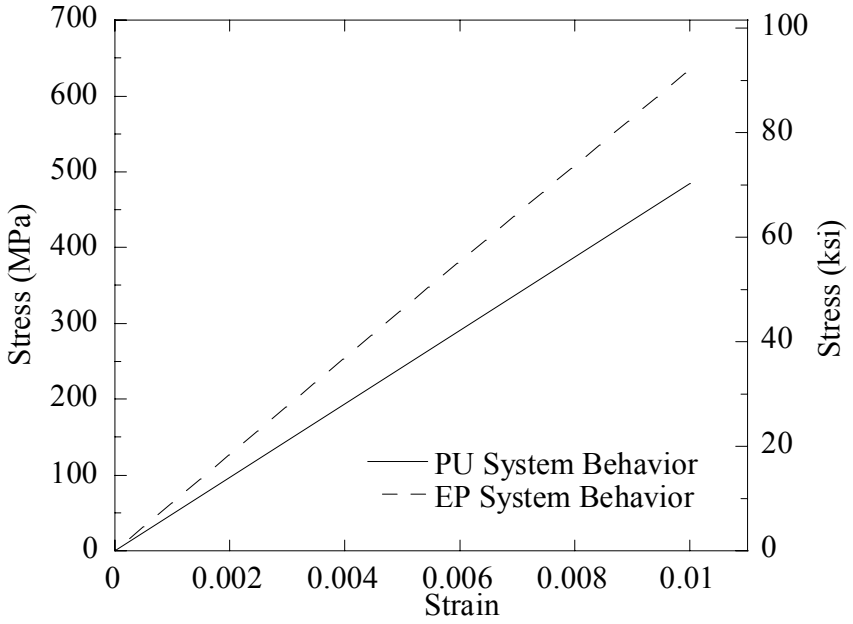

Figure 7: Material Model for CFRP

4.4 M-Φ Model

Based on the material models discussed earlier, a moment-curvature analysis was performed on the mid-span section of the designed tested specimen. See Appendix A for a flowchart describing how the analytical moment-curvature procedure was performed. Figure 8 depicts the analytical moment-curvature results.

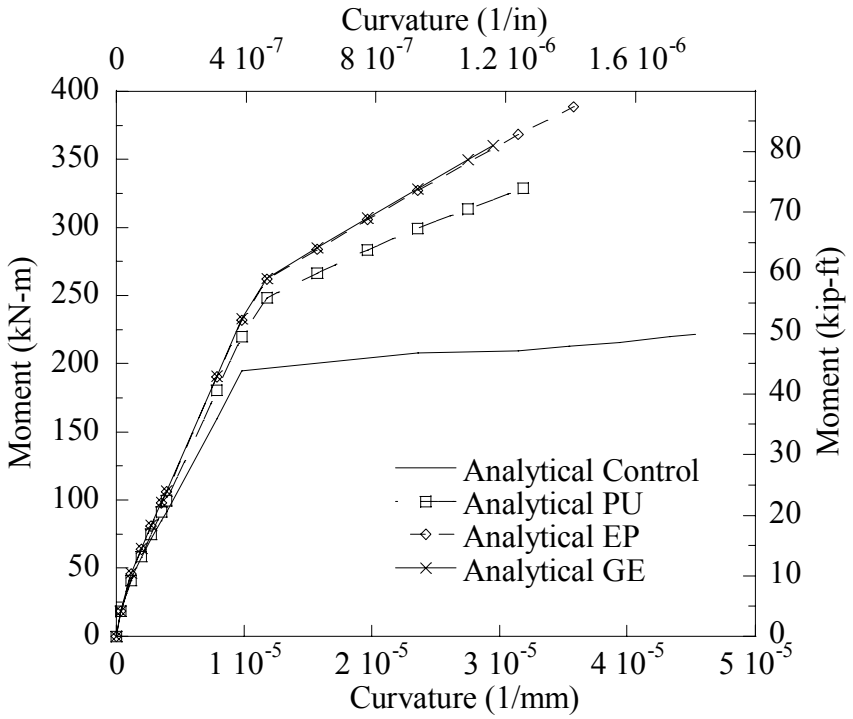

Figure 8: Moment-Curvature Model

4.5 P-Δ Model

The load-deflection models were derived from the corresponding moment-curvature models for each respective fabric-matrix systems. For all models, the ultimate capacity of the beams was limited to a compressive strain of 0.003 and a tensile strain of 0.0001 for the concrete. In an effort to more accurately predict the capacity of the beams, the 28 day compressive strength from the test cylinders was entered into the corresponding MathCAD models. For all of the MathCAD models, the same reinforcement behavior curve used in the control was utilized as well as the same concrete behavior curve. See Figure 9 for the load-deflection curves for each fabric-resin system.

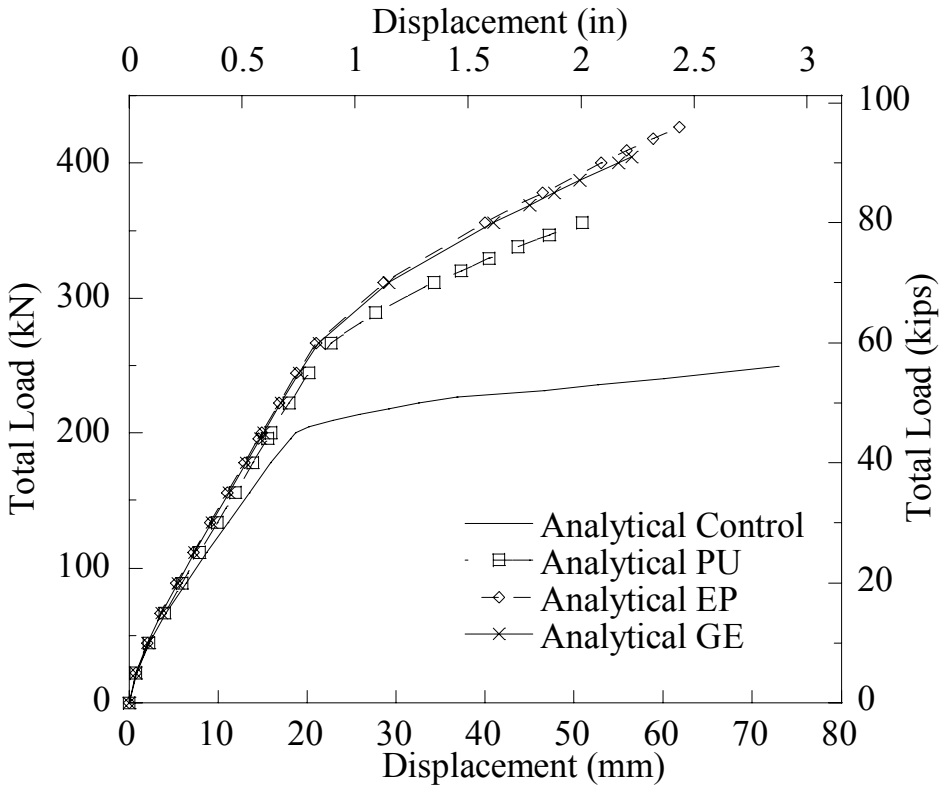

Figure 9: Load-Deflection Behavior

Chapter 5: Experimental Design & Set-up

The experimental program for this study was developed to determine the durability of CFRP strengthened RC beam; a secondary focus being the investigation of three different CFRP systems. The testing program for this study was composed of three distinct phases: ultimate testing, fatigue testing, and thermal/humidity conditioning. Table 20 displays the type of exposure that each specimen was scheduled to receive. As shown in the Table 20, a specimen from each of the fabric-resin systems was exposed to all three of the testing phases. The specimens that were exposed to all three of the testing phases would allow for the combined effects of fatigue and thermal conditioning to be studied.

Table 20: Experimental Testing Matrix

Beam Identification No.	Specimen Identification	Fatigue	Thermal	Ultimate
1	PU			•
2	PU-F	•		•
3	PU-T		•	•
4	PU-F-T	•	•	•
5	EP			•
6	EP-F	•		•
7	EP-T		•	•
8	EP-F-T	•	•	•
9	Pull Off Tests		•	
10	GE			•
11	GE-F	•		•
12	GE-F-T	•	•	•
13 [1,2,3]	-			
14 [1,2,3]	-			
15 [2]	GE-T		•	•
16	Control			•

[1] Under Strength [2] Damaged [3] Excluded

5.1 Specimen Design

As mentioned in the Chapter 3, 16 RC beams were poured for this study. The RC beams designed and constructed for this study were to be large scale and representative of those found in the field. Beam dimensions and reinforcement schedule can be seen in Figure 10. The tensile reinforcement for each specimen was 3 No. 7 grade 60 deformed bars (ρ=1.0%). Steel shown in the compression zone (2 No. 3 bars) was not intended to provide compressive reinforcement during loading, but to aid rebar cage construction and to prevent crack during the installation of CFRP sheet (beams were flipped tension-side up for CFRP application).

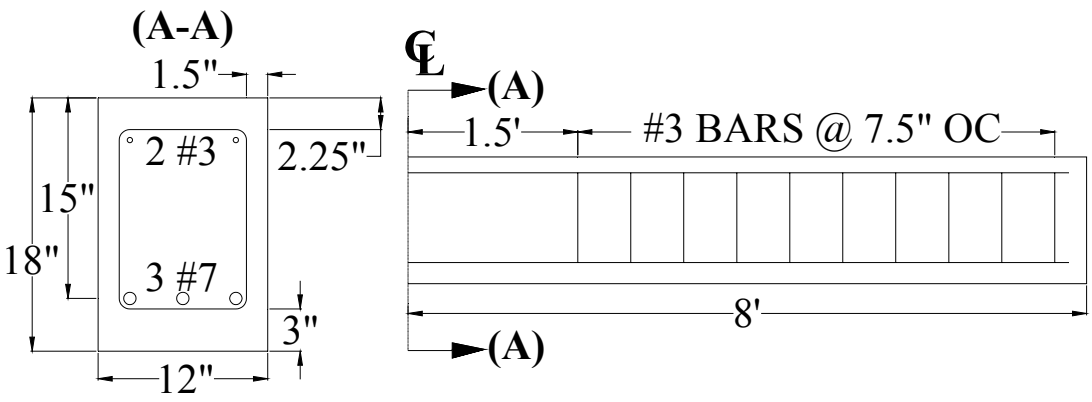

Figure 10: Specimen Dimensions and Reinforcement Schedule

5.2 Installation of CFRP

Two layers of CFRP were bonded to the tension face of each strengthened beam. The first layer of CFRP spanned 14'-4" (4368.8mm) and the second spanned 13'-10" (4216.4mm). The CFRP sheets were the full width of the beams 304.8mm (12"). Figure 11 illustrates the layout of the CFRP on the bottom of the specimens.

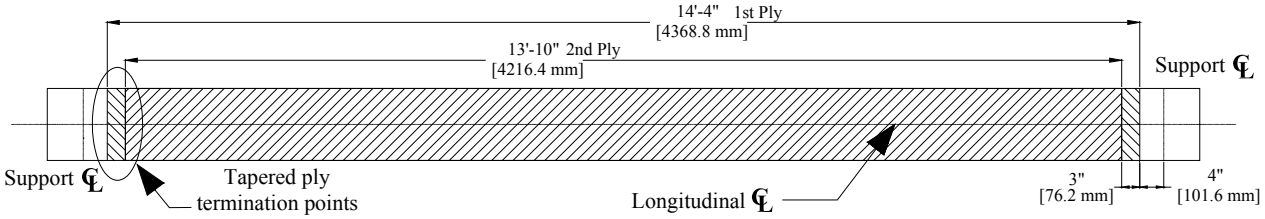

Figure 11: CFRP Layout

Previous to installing the EP and GE systems, the components for each resin systems were mixed according to their perspective ratios and then applied to the bottom of the beam. The first layer fabric was then hand lain onto the resin and a metal roller was used to press the fabric into the resin. Once the first layer had been completely pressed into the resin, a second coating of the resin was applied. After the second coating of resin was applied, the second layer of fabric was installed. Once the second layer had been completely pressed a final coating of resin was then applied. It should be noted that the GE resin system had several difficulties due to a premature gelling of the resin prior to finishing the CFRP installation. In one case the fabric was not fully saturated prior to the hardening of the resin. When the GE system hardened prior to completing installation, more of the resin was mixed and the fabric was re-saturated.

The PU system came pre-impregnated with resin, and was delivered hermetically sealed packages ready to use. Installation of the PU system consisted of applying a primer (BP1 systems) to the beam then laying the first layer of pre-impregnated fiber. The layer is lightly misted with water to activate the resin and then the fabric was rolled with a metal roller to work out the air pockets that form due to the resin curing. After rolling the air pockets out of the first layer the second layer of pre-impregnated fabric was laid on top of the first. Then the second layer was misted with water and the air pockets were rolled out. See Figure 12 for photos from the lay-up of the PU system.

(a) (b)

Figure 12: Installation of PU-System

After all of the CFRP sheets for all three systems had been installed on the beams, all of the specimens received a FDOT Class 5 finish which is a standard finish applied to all exposed surfaces of bridges in Florida. After being coated the specimens were stored outdoors at the SRC.

5.3 Loading Procedure

5.3.1 Ultimate Loading

The ultimate testing phase consisted of loading the specimen until failure. Failure was defined as a drop of at least 10% to 15% from the maximum load carried by the specimen. Load was applied in displacement control at a constant rate of 0.1in/min (2.54mm/min). Pauses were taken at specific load increments to visually inspect and mark the specimen for cracks. Once the inspection and marking of the specimen was completed the loading procedure would be resumed. The specific loads that corresponded to the pauses during the loading of the specimens were 50% of the theoretical yielding, 75% of the theoretical yielding, at theoretical yielding, and 90% of the theoretical ultimate load. It should be noted that for all of the CFRP strengthened specimens once the theoretical yielding load was obtained the visual inspection of the beam was done from afar, with no marking of the cracks. The reason for not marking the cracks was that it was deemed an unacceptable risk for anyone to get close to the loaded CFRP-strengthened specimens. Thus all cracks that formed after the theoretical yield were marked once testing was completed.

5.3.2 Fatigue Loading

The fatigue phase of the experiment consisted of subjecting the appropriate specimens to two million cycles of cyclic loading at a frequency of two hertz. The loading used for fatigue testing ranged from 0.5kip (2.2kN) up to 19.2kip (85.4kN). At this load range, a calculated change in stress of 23ksi (158.6MPa) would be imposed on the tensile reinforcement of the beam. The fatigue load range was selected such that yielding of the tension steel would not occur and that the stress range achieved in the reinforcement was within AASHTO 5.5.3.2 limitations, which was calculated to be 23.4ksi (161.3MPa). This stress range would allow for an unlimited fatigue life for the steel reinforcement. During the fatigue loading the beam displacement and CFRP strain were measured. The strain gauges were calibrated to compensate for the temperature changes that occurred in the lab during the two million cycles. During the fatigue tests the data was recorded on cycles 1, 1000, 20,000, 100,000 and every 100,000 thereafter until cycle 2 million. The data that was recorded was the maximum and minimum of load, displacement, beam temperature, and axial CFRP strains.

5.4 Environmental Chamber Design & Thermal Conditioning Procedure

The thermal conditioning phase of the experiment consisted of exposing the selected beams to heating and cooling cycles inside of an environmental conditioning chamber (ECC). Inside of the environmental chamber the beams were also exposed to cycling levels of humidity. The purpose of the temperature and humidity cycles was to simulate exposure to climate conditions similar to that of Florida. Hence the intended temperature and humidity ranges were to be typical for a Florida service environment.

A design schematic of the ECC can be seen in Figure 13. The ECC utilized three main components to produce the desired environment:

1) *Temperature Conditioning Unit* – Temperature conditioning was provided by a 2 ton Goodman AC/Heating Unit (PCK 024-1 HK 50-1); A commercially available packaged unit capable of producing 24,000 Btuh.

2) *Humidifier* – A Honeywell HE160A By-Pass Disk Humidifier was used to provide humidification (commercially available).

3) *Cycle Controller* – A Watlow SD Series controller was used to control the environmental cycles for the chamber. (See Appendix B for programming chart.)

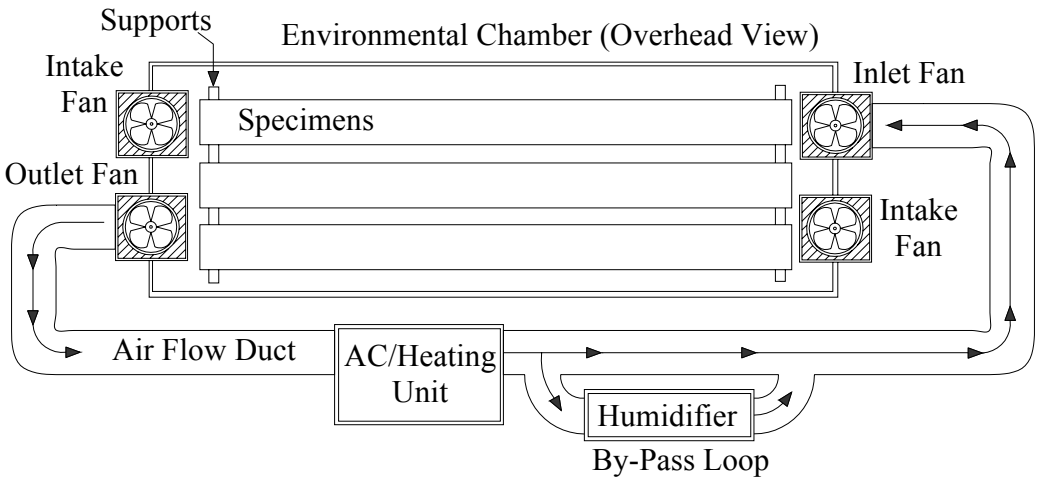

Figure 13: Environmental Chamber Schematic

(a) Interior View **(b) Exterior View**

Figure 14: Environmental Chamber As-built

The thermal conditioning procedure entailed 4 main steps in order to complete a single heat-cool cycle:

1) *Heating/Humidity Ramp-up Period* – The first step in the full cycle was heating and humidification. During this cycle, both the AC unit (heat) and humidifier would be engaged and flow would be introduced into the chamber through the input fan. It was determined that the average input air temperature was approximately 126 °F. The duration of the ramp-up heating cycle was 18hr.

2) *Heat Soak Period* – The second step was a heat soak process. During this phase, it was attempted to maintain the chamber temperature for a duration of 6hr. Exhaust fan were engaged at the conclusion of the heat soak period, expelling air volume, and beginning the cool ramp period.

3) *Cooling Ramp-up Period* – The cooling ramp-up period is similar to the heating/humidity but the AC unit is engaged to provide cold air. It was determined that average input air temperature, for this period, was approximately 39 °F. The cooling ramp-up period lasted for 18hr.

4) *Cool Soak Period* – During this phase, it was attempted to maintain the chamber temperature for a duration of 6hr. Exhaust fan were engaged at the conclusion of the cool soak period, expelling air volume, and beginning the heat/humidity ramp period and completing the full conditioning cycle.

A full heat-cool cycle would take 2 full days to reach completion. It must be mentioned that during the time frame in which specimens were being conditioned, the ECC had intermittent malfunctions with critical components. Therefore, controlled environmental conditioning was not continuous throughout the conditioning portion of this study.

In order to measure the thermal performance of the ECC, thermocouples were installed on each beam specimen during conditioning, on the top and bottom of the ECC, and outside the ECC (ambient). Thermocouple and specimen locations within the chamber are shown explicitly in Figure 15: Specimen & Thermocouple Locations within ECC Figure 15. Temperature data was acquired continuously during the conditioning period. A multi-day sample of this data can be found in Figure 16. It can be seen that the ECC produced internal ambient temperatures between 40 – 115 °F and beam surface temperatures between 55 – 100 °F. Hence the desired conditioning environment was achieved by the chamber constructed.

Humidity measurements were also recorded during the conditioning period. A multi-day sample of this data can be seen in Figure 17. The humidity range achieved by the ECC was within the range of 19 – 89%. This was considered to be acceptable for a simulated "Florida-like" environment.

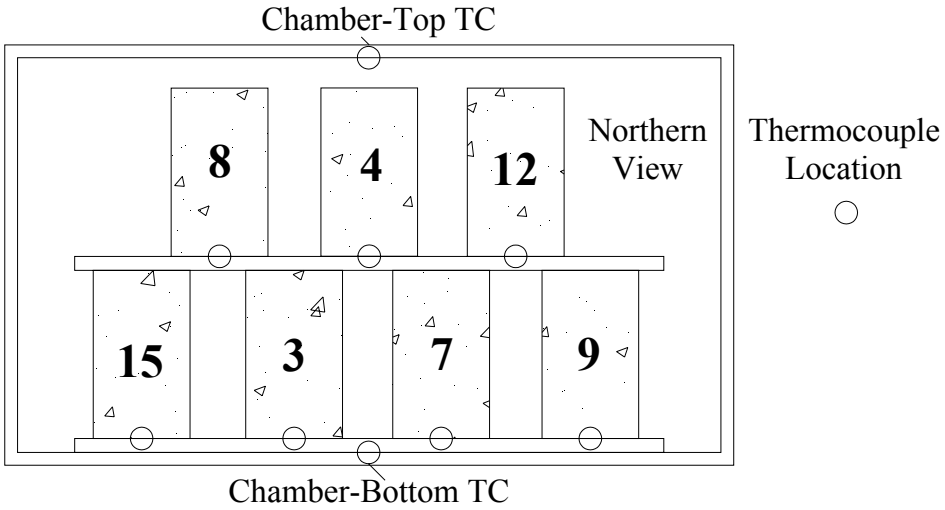

Figure 15: Specimen & Thermocouple Locations within ECC

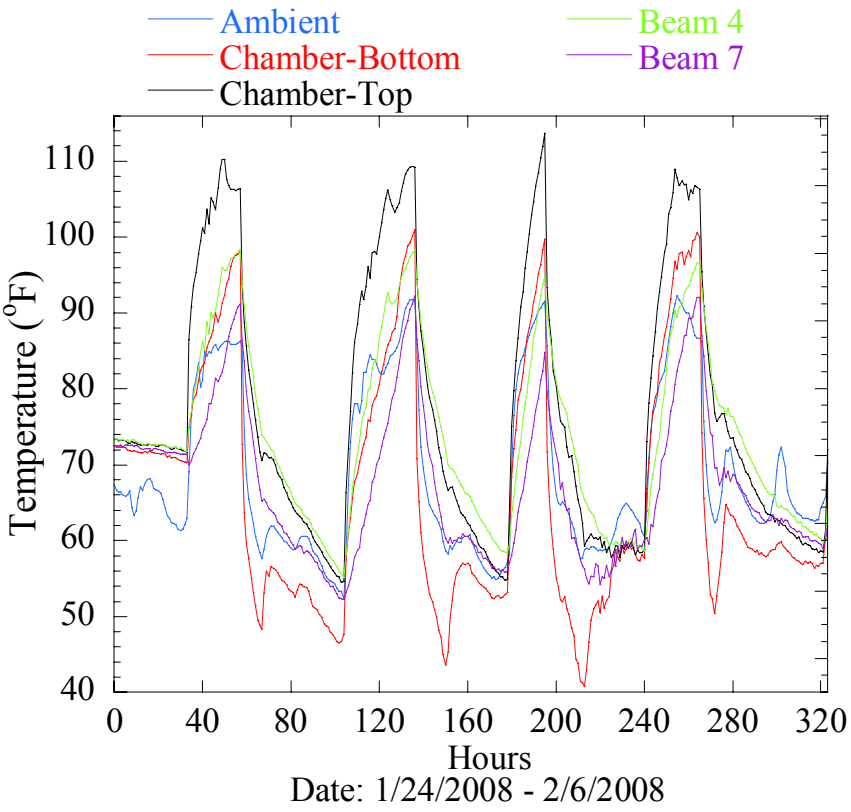

Figure 16: Conditioning Chamber Temperature Variation

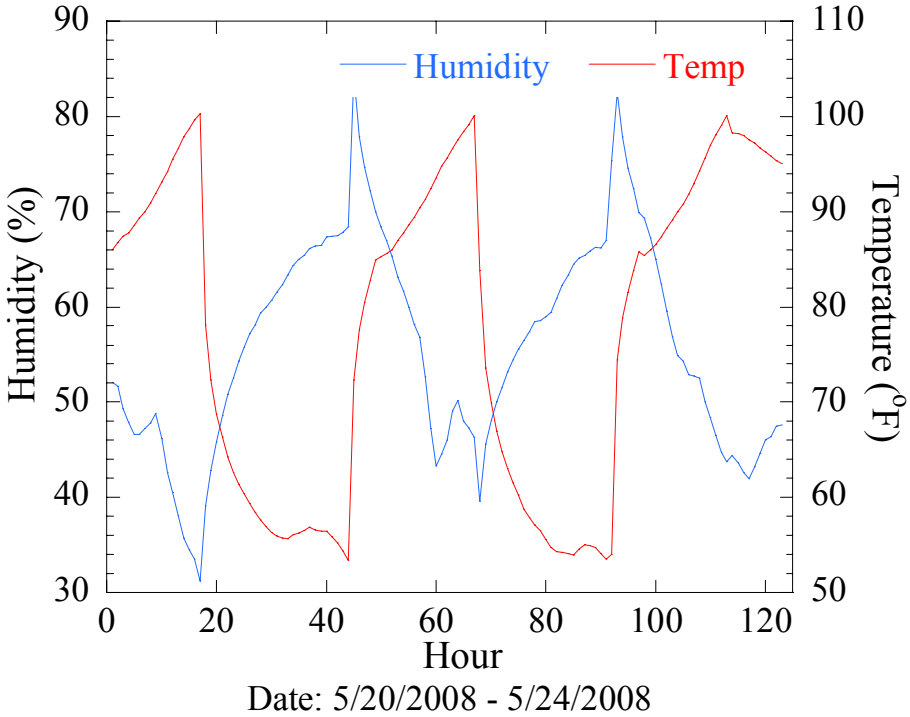

Figure 17: Humidity Variation within Chamber

5.5 Non-controlled Environmental Conditioning

It should be noted that all of the beams received some environmental conditioning due to outdoor storage at the FDOT SRC, as shown in Figure 18. See Figure 19 for the average monthly air temperatures for the duration the specimens were stored. See Figure 20 for the monthly precipitation for during the storage duration. The temperature and precipitation data was taken from the National Oceanic and Atmospheric Administration (NOAA) archives for the Tallahassee Regional Airport. The beams also received some thermal conditioning when inside of the SRC due to the fact that the facility does not have a climate control system for the testing area.

Although there is a relatively accurate record of the environmental conditions that occurred during that length of this study, there is no way to full quantify the effect that the ambient environment had on test specimens. Furthermore, the exact time specimens were place outside, duration of time outside, and which specimens were outside is also unknown. Therefore this "non-controlled" conditioning will not be discussed further in this report.

Figure 18: Specimens during Storage Time

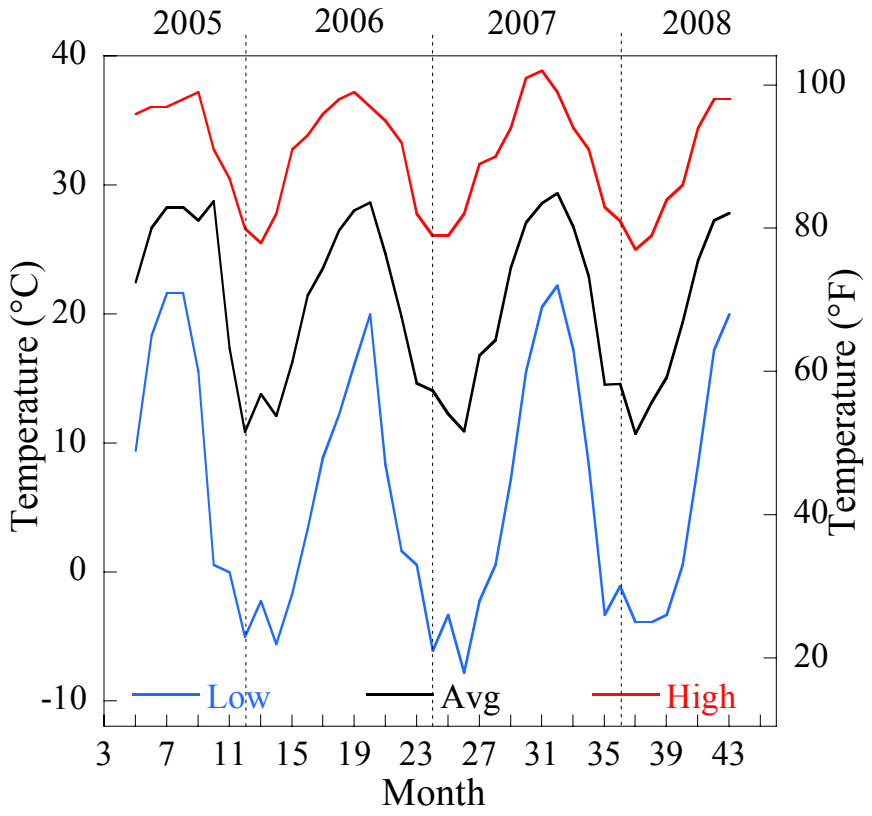

Figure 19: Monthly Temperature (Low-Average-High)

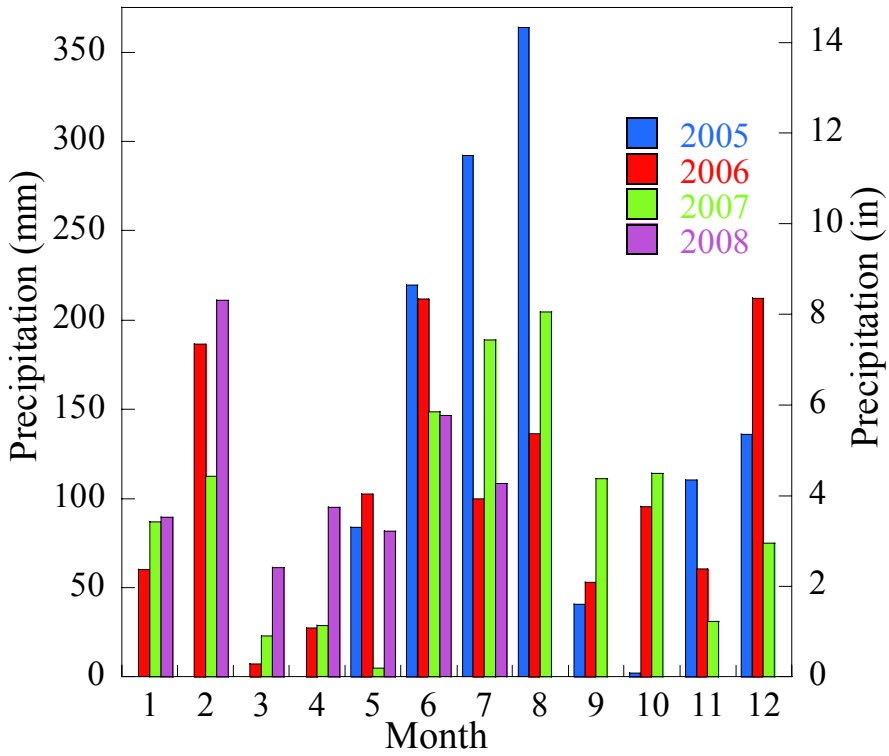

Figure 20: 2005-2008 Monthly Precipitation

5.6 Test Setup and Data Acquisition (DAQ)

The following section describes the experimental testing configuration for all beams loaded in fatigue and/or ultimate failure. Refer to Figure 22 for all diagrams related to the following discussion.

All specimens were loaded using a four-point bending configuration. This configuration was used for both ultimate and fatigue tests that were performed. The simply supported length for all specimens was 15’ (4572mm). All loading was applied using a 3’ (915mm) spreader beam. During the fatigue loading procedures, a MTS servo-controlled actuator was used to apply load. The ultimate loading procedures employed either an MTS servo-controlled actuator or an Enerpac hydraulic jack to provide load. During load testing (fatigue or ultimate), steel reinforced neoprene bearing pad or steel plates were used between load bearing surfaces.

The instrumentation of the specimens was done using two main groups of sensors; one for measuring deflection of the specimen and the other for measuring uniaxial strains within the CFRP composite plate. The displacement gauges used were either linearly variable displacement transducers (LVDT) or laser displacement gauges. LVDTs were placed at the mid-span and support positions during testing. It must be noted that Figure 22 does show the location of the laser displacement gauge during testing for this sensor type was only used during the fatigue testing of the PU-F specimen. The use of the laser gauges was discontinued for it was found that a significant amount of sensor drift was occurring. Yet for the sake of completeness, the laser displacement gauge during this test was placed at mid-span slightly offset from the longitudinal centerline.

Strain measurements were also recorded during both fatigue and ultimate loading procedures. The strain gauges used were conventional foil-backed uniaxial resistance gauges. Gauge positions can be seen in Figure 22 and are relative to the datum shown at the left-hand support. After surface preparation, gauges were attached to the CFRP surface using a cyanoacrylate adhesive. After attachment, all gauges were covered with a protective coating to prevent interaction with moisture and to shield the gauges from damage. A photograph of the actual testing configuration can be seen in Figure 21.

Figure 21: Specimen in Test Configuration

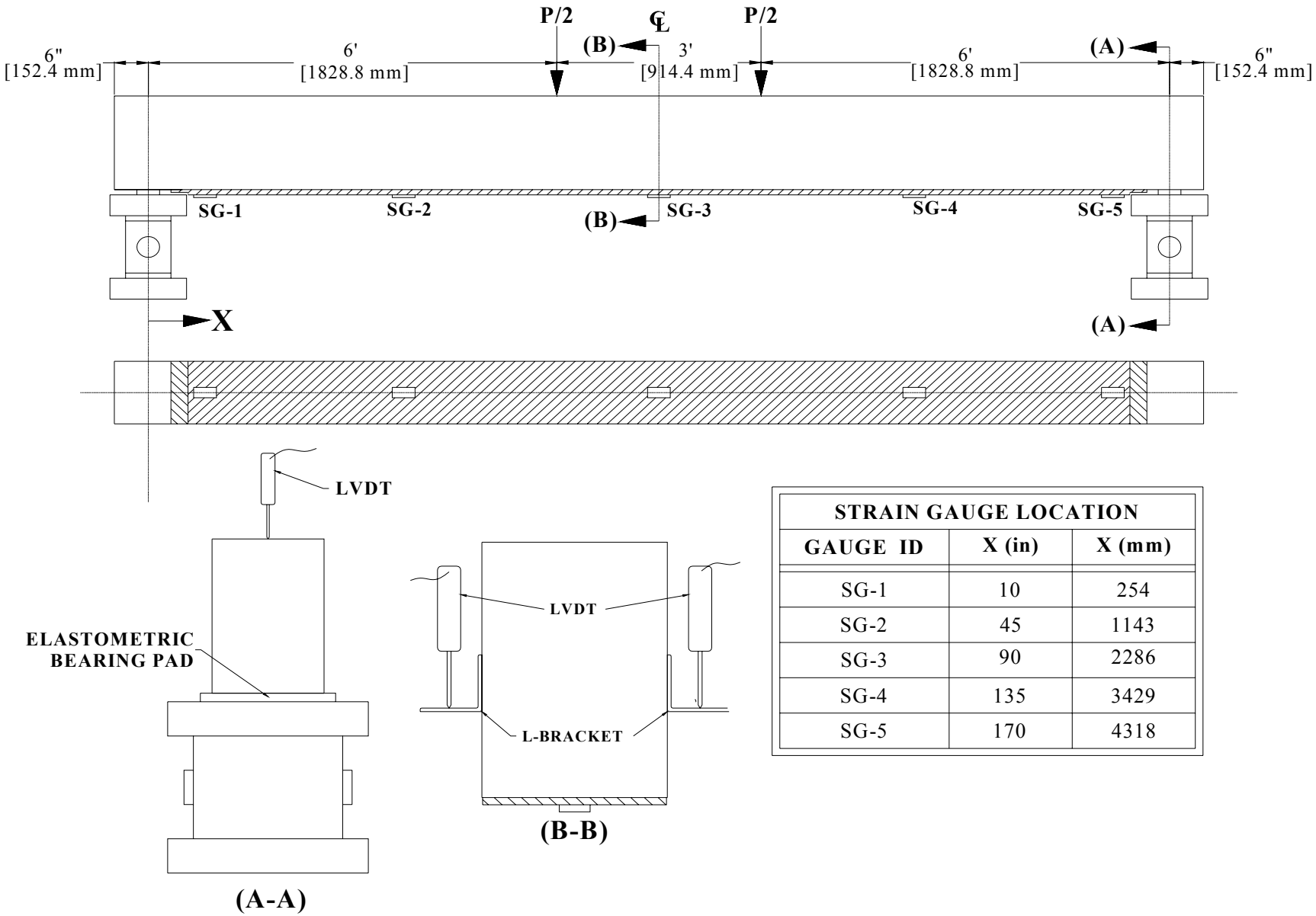

STRAIN GAUGE LOCATION		
GAUGE ID	X (in)	X (mm)
SG-1	10	254
SG-2	45	1143
SG-3	90	2286
SG-4	135	3429
SG-5	170	4318

Figure 22: Loading ad Sensor Configuration

Chapter 6: Results and Discussion

The following chapter discusses the experimental results found in this study. Individual specimen results will be presented in the following groups:

1) Baseline Specimens
2) Fatigue Specimens
3) Thermally Conditioned Specimens
4) Fatigue + Thermally Conditioned Specimens

Once a group of specimens has been discussed, quantitative results for the group will be presented for comparative purposes. Once all groups have been discussed, a results summary will be presented to examine the effect of the applied conditioning on the individual CFRP systems

Table 21 and Table 22 show important information regarding test date, specimen cure time, and day-of-test concrete strength for each specimen tested.

Table 21: Specimen Test Dates

Beam No.	Specimen ID	Test Day	Beam No.	Specimen ID	Test Day
1	*PU*	2/6/2007	9	*Pull-Off*	N/A
2	*PU-F*	5/30/2008	10	*GE*	2/6/2007
3	*PU-T*	10/23/2008	11	*GE-F*	5/30/2008
4	*PU-F-T*	10/22/2008	12	*GE-F-T*	10/22/2008
5	*EP*	2/6/2007	13	-	N/A
6	*EP-F*	5/30/2008	14	-	N/A
7	*EP-T*	10/22/2008	15	*GE-T*	10/23/2008
8	*EP-F-T*	10/22/2008	16	*Control*	2/6/2007

Table 22: Test Date Cylinder Data

Batch No.	Pour Date	Test Date	Cure Time (days)	Beam ID	Compressive Strength	
					MPa	*psi*
1	5/11/2005	5/30/2008	1115	1 & 2	56.6	8203
2	5/18/2005	11/7/2008	1269	3 & 4	65.7	9530
3	6/1/2005	5/30/2008	1094	5 & 6	66.8	9684
4	6/8/2005	11/7/2008	1248	7 & 8	56.8	8237
5	6/15/2005	11/7/2008	1241	9 & 10	59.2	8589
6	6/22/2005	5/30/2008	1073	11	67.8	9836
	6/22/2005	11/7/2008	1234	12	64.5	9356
7	6/29/2005	N/A	N/A	13[1,2,3] & 14[1,2,3]	N/A	
8	8/31/2005	11/7/2008	1164	15[2] & 16	66.7	9668

[1]Under Strength [2]Damaged [3]Excluded

6.1 Baseline Specimen Results

6.1.1 Control: Beam 16

The control beam for this project was tested to failure on 2/6/2007. Loading was paused at 20.3, 30.5, and 40.6kip to mark cracks. Crack patterns observed at failure can be seen in Figure 23 and Figure 24. The control beam failed in a progressive manner; first with concrete cracking, steel yielding, and finally concrete crushing. The ultimate load obtained by the control beam was 52.2kip (Δ=2.63").

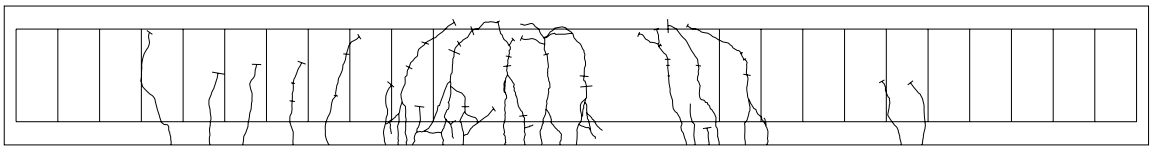

Figure 23: Control Eastern Face Crack Pattern

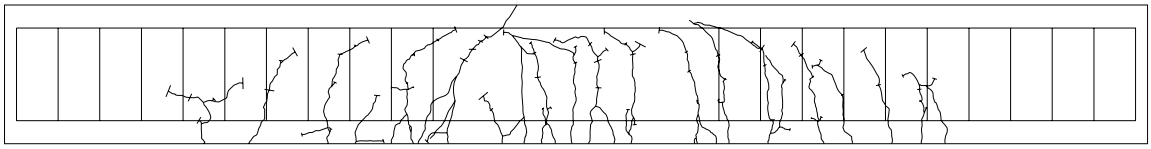

Figure 24: Control Western Face Crack Pattern

6.1.2 PU Baseline: Beam 1

The PU baseline specimen was tested to failure on 2/6/2007. During the load testing, there were no observed problems with DAQ or the test set-up. Therefore the load test was completed in a single run. Loading was paused at 26.3, 39.5, and 52.6 kips for cracks to be marked. Refer to Figure 25 and Figure 26 for the observed crack patterns at failure. The strain recorded, at various percentages of the ultimate recorded load, during the test can be found in Figure 27.

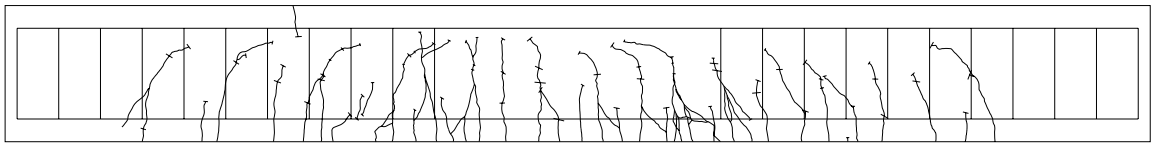

Figure 25: PU Baseline Eastern Face Crack Pattern

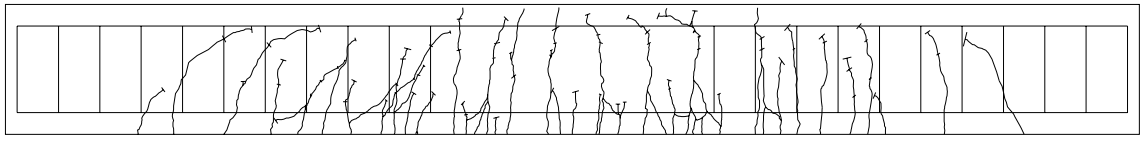

Figure 26: PU Baseline Western Face Crack Pattern

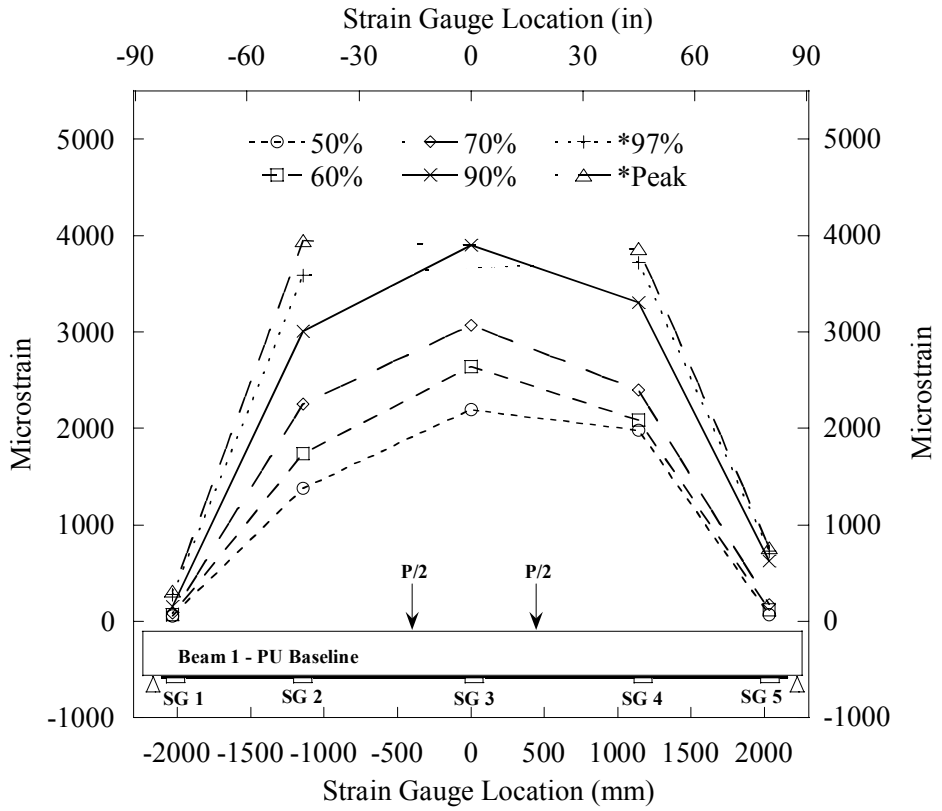

Figure 27: PU-Baseline Strain Distribution

Failure of the PU baseline specimen ultimately occurred at 74.3 kips (Δ=1.82"). The failure mode was determined to be CFRP rupture followed by laminate debonding. During the final three minutes of the load test, a video was recorded to capture the beam's failure. Figure 28 shows two frames from the video taken. Figure 28-a shows the first frame where failure was evident (initial CFRP rupture). This frame is denoted to have a time interval of *t = 0sec* for reference. The initial ruptured occurred approximately 50" from the north support (between SG2 and SG3). Immediately after the CFRP rupture, laminate debonding occurred (see Figure 28-b). Furthermore, the debonding portion of failure can be justified by the load-strain plot depicted in Figure 30. Strain gauges 1, 2, 3, and 4, which are all located in or near the region of debonding, all indicate softening (flattening of the load-strain curve) near failure. Softening would if indicate a loss of concrete-to-CFRP composite action (or debonding). It should be noted that debonding failure occurred within the urethane adhesive layer. Figure 29 shows a close-up picture of the debonding surface. It can be observed that a whitish colored layer of material (urethane) remains on the concrete substrate, supporting the conclusion of cohesive failure within the adhesive layer

(a) Initial CFRP Rupture (b) Debonding

Figure 28: PU Baseline at Failure: Video Frame Shots

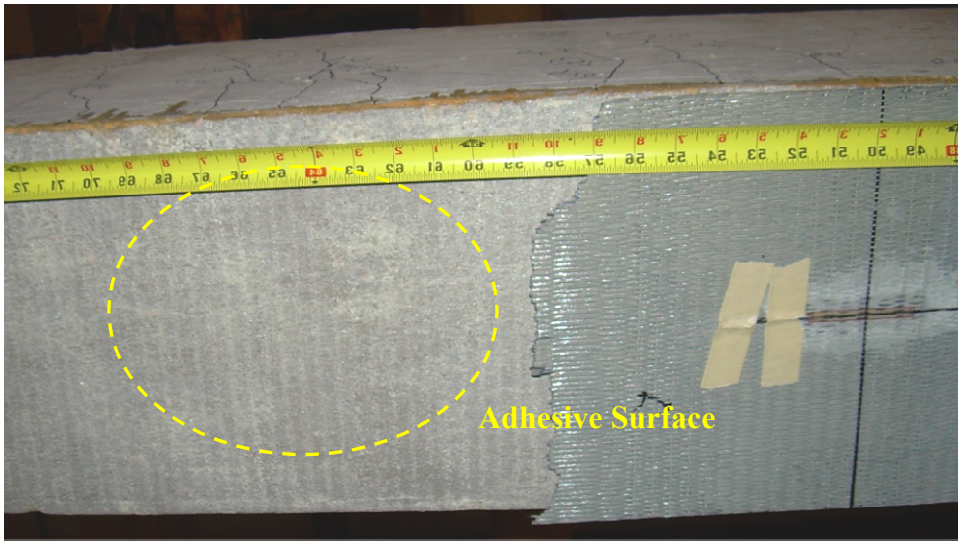

Figure 29: PU Baseline CFRP Rupture Plane

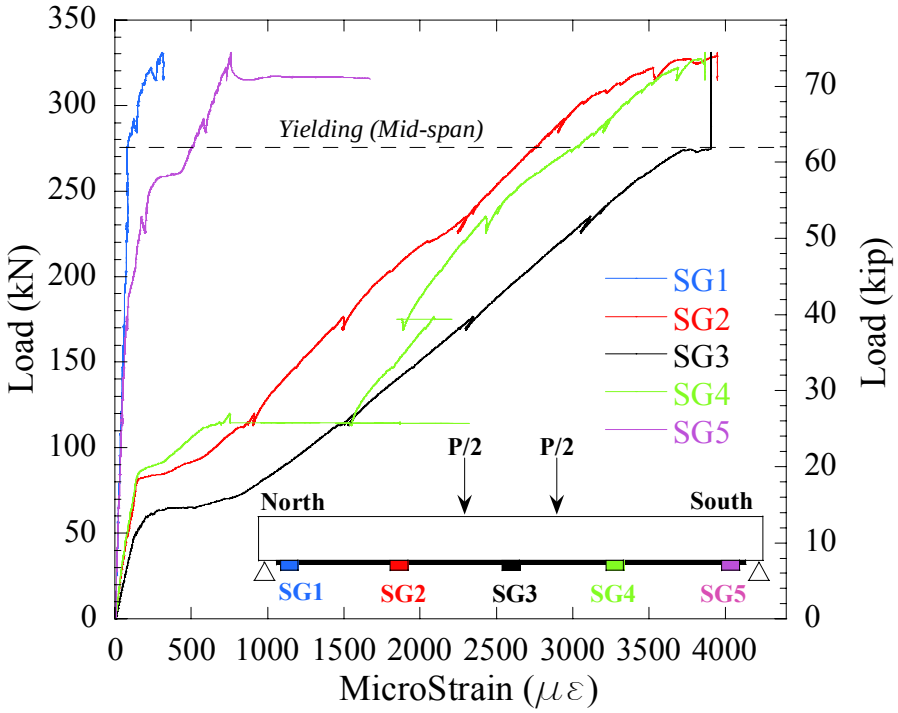

Figure 30: PU-Baseline Load vs. Strain Plot

6.1.3 EP Baseline: Beam 5

The EP baseline specimen was tested to failure on 2/6/2007. During the load testing, there were no observed problems with DAQ or the test set-up. Loading was paused at 25.5, 38.3, and 51.1 kips for cracks to be marked. Refer to Figure 31 and Figure 32 for the observed crack patterns at failure. The strain recorded, at various percentages of the ultimate recorded load, during the test can be found in Figure 33.

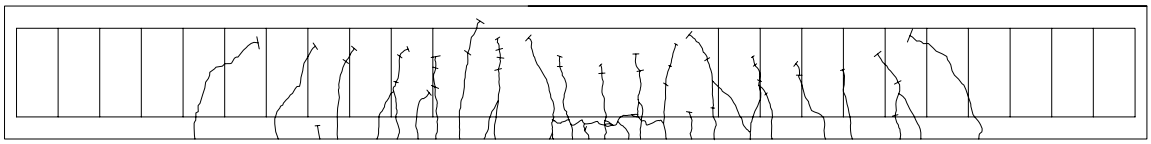

Figure 31: EP-Baseline Eastern Face Crack Pattern

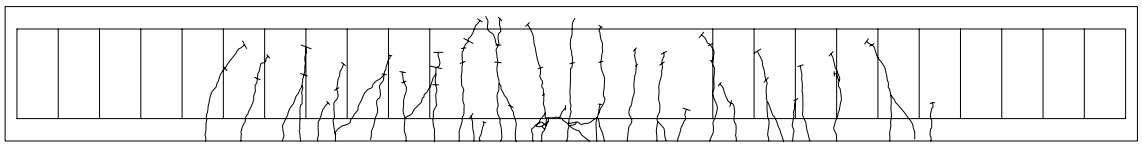

Figure 32: EP-Baseline Western Face Crack Pattern

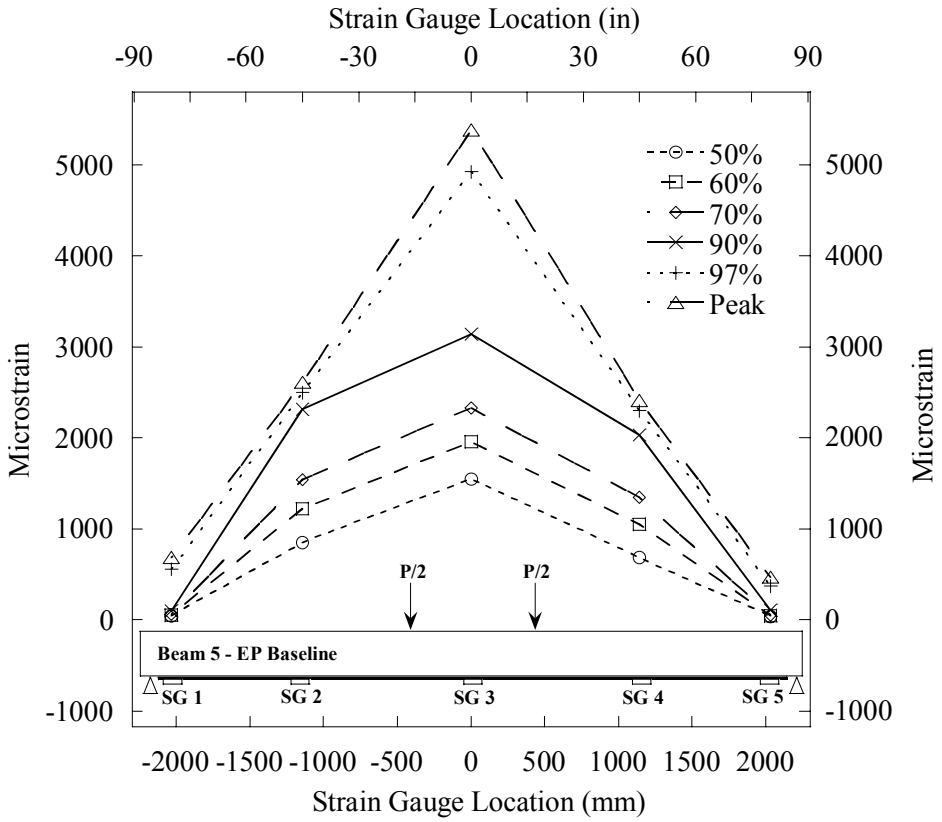

Figure 33: EP-Baseline Strain Distribution

The EP baseline specimen failed at a load of 70.3kip (Δ=1.56”). The dominate mode of failure was CFRP debonding. Figure 34-a was taken from a video, taken during the time of testing, that shows the initiation of CFRP debonding occurring the North end of the specimen. It was observed that during the debonding failure longitudinal splitting of the CFRP composite and concrete cover separation occurred. Figure 34-b shows a photo taken after failure occurred. It can be observed that both light and dark colored portions exist on the concrete tensile face. The lighter colored areas indicate the removal of concrete substrate during debonding; this implies a sound interface between CFRP and concrete. The darker colored areas indicate that debonding occurred at the CFRP-to-concrete interface; this could indicate poor wetting of the fiber surface. Figure 35 depicts the load vs. strain behavior for the EP baseline specimen. A Significant reduction in stiffness can be observed, as the load approaches ultimate (post mid-span yield), in gauge 3. Additionally, the softening behavior at the SG1/5 location can be attributed to slip of the CFRP laminate; the calculated load for steel yielding at the SG2/4 positions was approximately 100kip. This is concurrent with observed results.

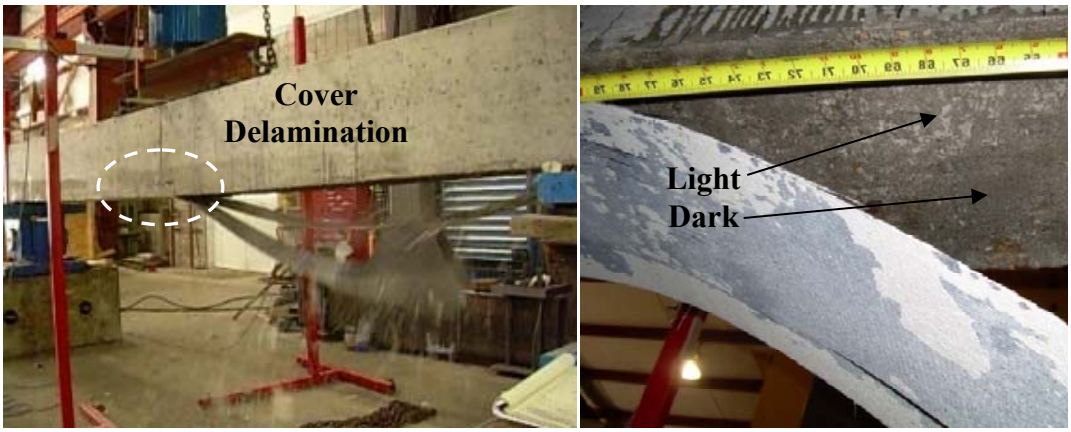

(a) During Fail (b) Post-fail

Figure 34: EP-Baseline Failure

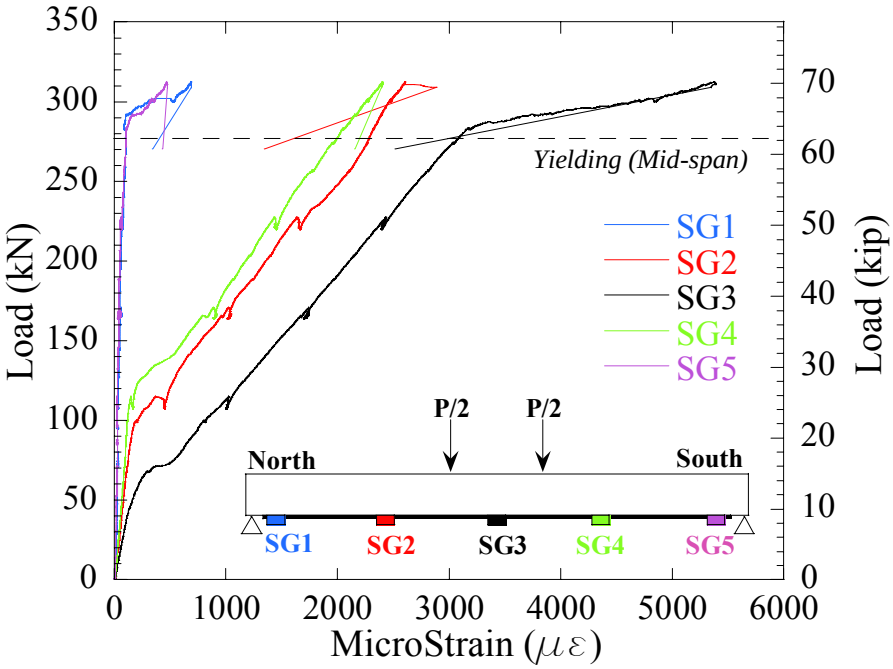

Figure 35: EP-Baseline Load vs. Strain Plot

6.1.4 GE Baseline: Beam 10

GE baseline specimen was tested on 2/6/2007. During the load testing, there were no observed problems with DAQ or the test set-up. Loading was paused at 25.5, 38.3, and 51.1 kips for cracks to be marked. Refer to and Figure 36 and Figure 37 for the observed crack patterns at failure. The strain recorded, at various percentages of the ultimate recorded load, during the test can be found in Figure 38. Recall that during the application of the CFRP sheets to the GE baseline specimen, there were problems with premature gelling of the epoxy resin. A number of the following results shown are more than likely a result of this issue.

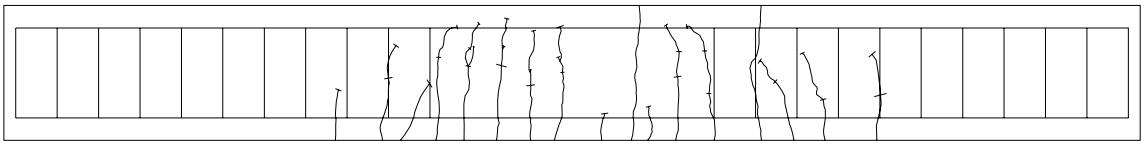

Figure 36: GE-Baseline Eastern Face Crack Pattern

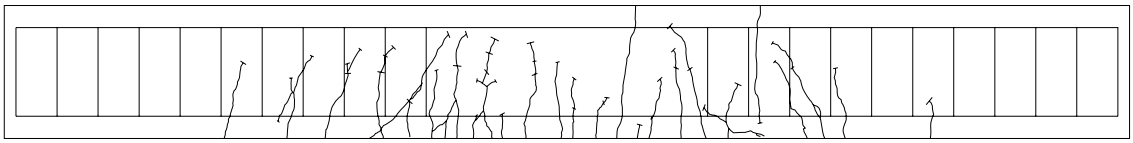

Figure 37: GE-Baseline Western Face Crack Pattern

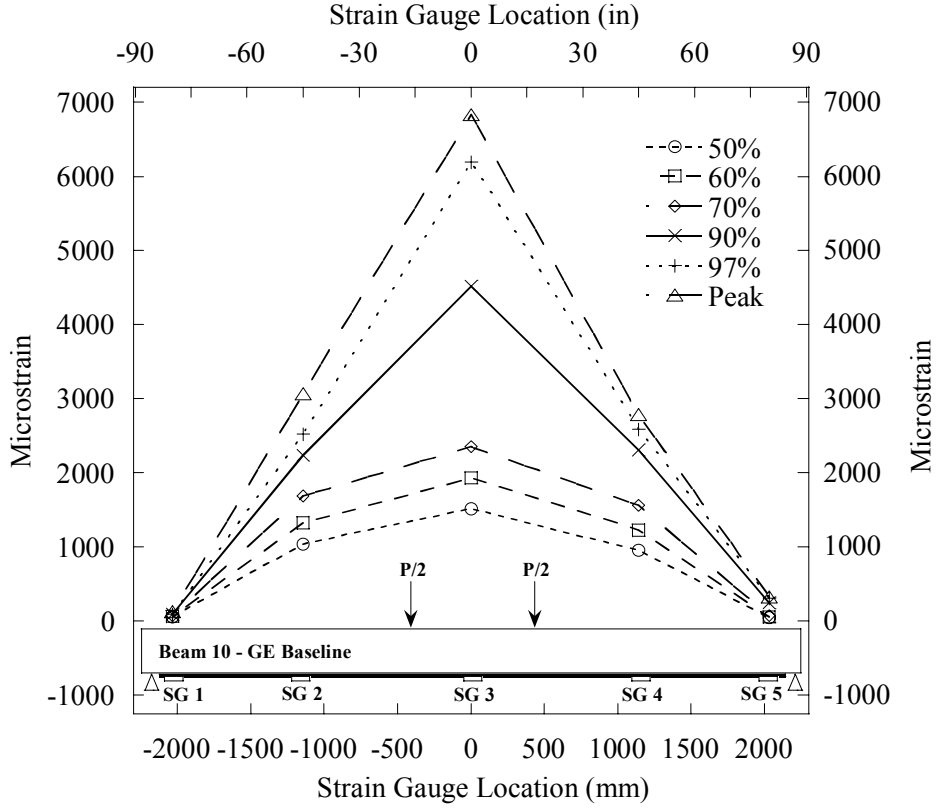

Figure 38: GE-Baseline Strain Distribution

The GE baseline specimen failed at a load of 71.5 kip (Δ=1.61”). The dominating mode of failure was debonding originating from the north end of the specimen; the sudden increase in strain at the SG2 location (refer to Figure 41) confirms this observation. When debonding failure occurred, only one half of the laminate separated from concrete (refer to Figure 39-a). During debonding, the north plate-end of the CFRP also ruptured via interlaminar shear (refer to Figure 39-a). The most interesting result to be seen was in the post-fail inspection of the debonded CFRP and respective concrete surface. If was found that a significant number of areas on the debonded plate did have adequate or any matrix saturation of the reinforcing fiber. Moreover, these areas showed signs of little or no adhesion to the concrete substrate (see Figure 39-b). Figure 40 depicts a close-up picture of the post-fail tensile concrete surface. Three distinct regions can be identified:

1) Region 1 (R1): Area where plate debonding occurred within the concrete substrate indicting sound FRP-to-concrete bonding.

2) Region 2 (R2): Area where plate debonding occurred at the FRP-to-concrete interface indicting poor bonding.

3) Region 3 (R3): Area of poor fiber saturation/wetting. R3 areas could have resulted from, as mentioned earlier, premature gelling of the resin.

It should be noted that the small area shown in Figure 40 was typical for the debonding surface found on the GE specimen.

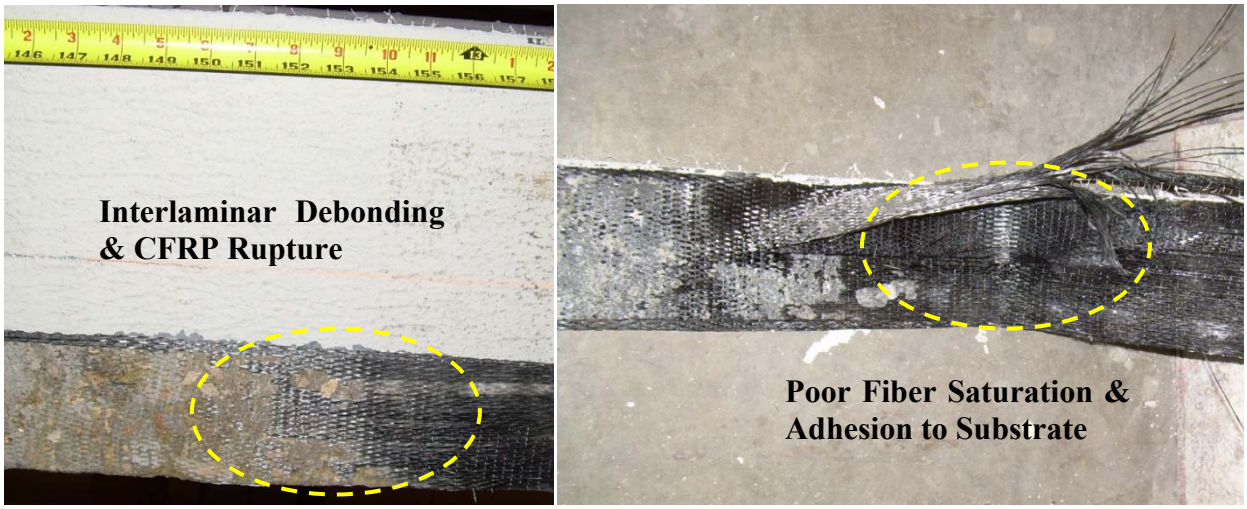

Figure 39: GE-Baseline at Failure

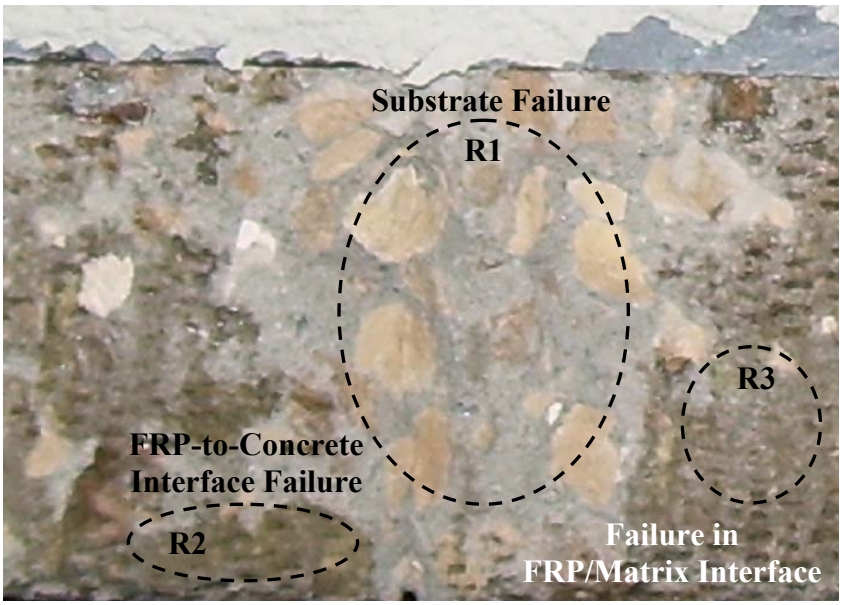

Figure 40: GE Baseline Concrete Substrate Post-fail

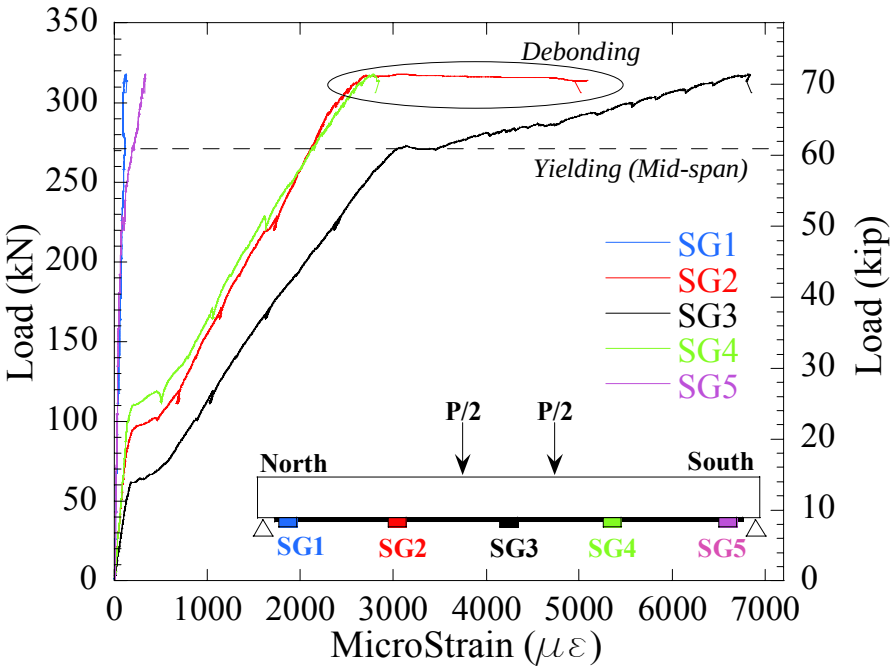

Figure 41: GE-Baseline Load vs. Strain Plot

6.1.5 Baseline Specimen Comparative Results

Now that the individual test results and failure modes of the baseline specimens have been discussed, they will be discussed in a comparative fashion in the following section.

Figure 42-a shows the load-deflection behavior of all strengthened baseline specimens along with the control beam. This figure shows that all strengthened specimens significantly increase (34.7-42.3%) the load bearing capacity of the control member. Yet, this increase in capacity comes at the cost of decreased ductility (losses of 48-60%).

It can be observed that the all specimens show no significant stiffness increases in the pre- and post-cracking stages of loading. This is more than likely due to the initial steel reinforcement ratio (ρ=0.01) and the small amount of CFRP added to the member. Yet, there is a noticeable post-yield stiffness increase with all strengthened specimens compared to the control

Figure 42-b, Figure 42-c, and Figure 42-d display comparisons between the experimental and analytical results for the PU, EP, and GE specimens respectively.

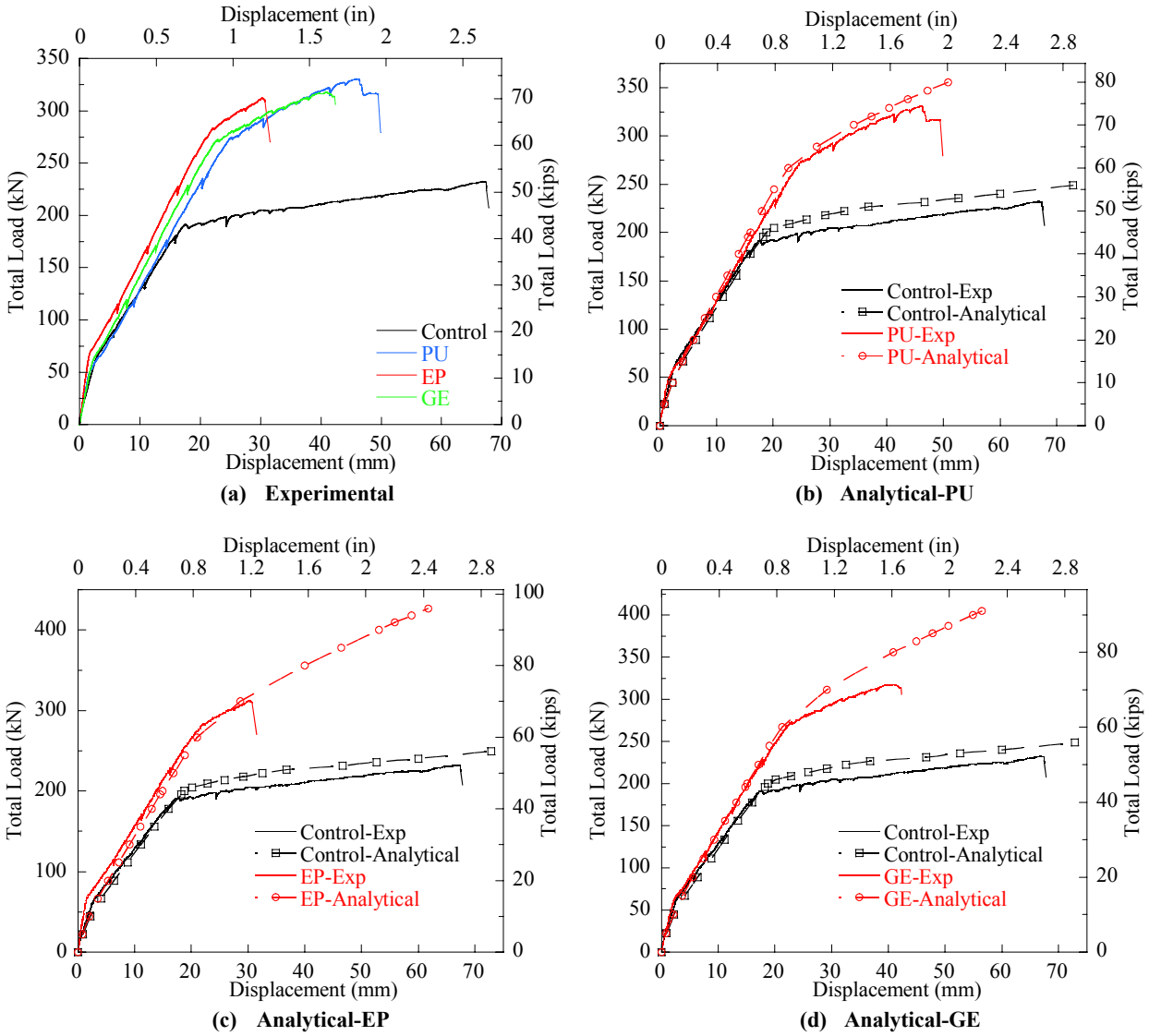

Figure 42: Baseline Load-deflection Results

Table 23: Baseline Load, Deflection, and Strain Results

Specimen ID	Beam No.	Yielding Load		Yielding Deflection		Ultimate Load		Ultimate Deflection		Maximum Strain (με)
		kN	*kip*	*mm*	*in*	*kN*	*kip*	*mm*	*in*	
Control	16	190.8	42.9	19.1	0.75	232.2	52.2	66.8	2.63	N/A
PU	1	275.8	62	116.5	26.2	330.5	74.3	46.2	1.82	3904
EP	5	275.8	62	94.7	21.3	312.7	70.3	30.2	1.19	5382
GE	10	270.9	60.9	100.5	22.6	318.0	71.5	40.9	1.61	6829

6.2 Fatigue Results

The following section presents results from specimens that received 2 millions cycles of fatigue loading. The results will be presented for individual specimens and then comparatively.

6.2.1 PU-F: Beam 2

During the fatigue loading procedure for the PU-F specimen, an error occurred in the DAQ system and the associated strain values during this loading cycle were not recorded. Deflection results will be presented in a later section

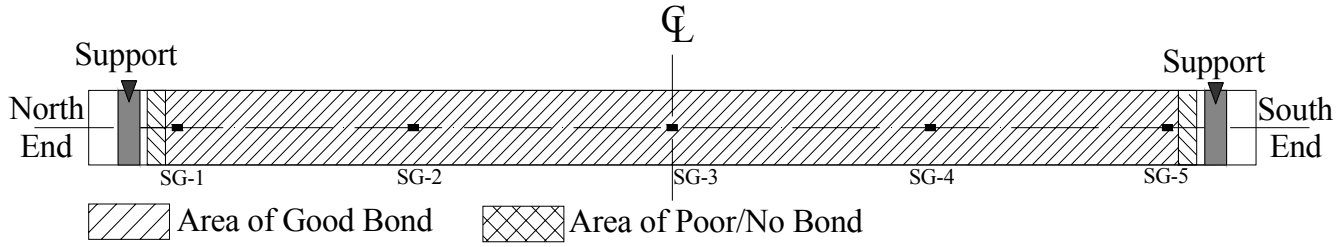

Figure 43: PU-F Post-Fatigue Bond Inspection Result

Previous to ultimate load testing, the PU-F specimen was inspected to assess the post-fatigue bond integrity. This inspection was conducted by tapping the composite surface with a coin or pen and marking void locations. The results from this bond inspection can be seen in Figure 43. The PU-F specimen indicated no post-fatigue regions of debonding.

The PU baseline specimen was tested to failure on 5/30/2008. During the load testing, there were no observed problems with DAQ or the test set-up. Therefore the load test was completed in a single run. Loading was paused at 26.3, 39.5, and 52.6 kips for cracks to be marked. Refer to Figure 44 and Figure 45 for the observed crack patterns at failure. The strain recorded, at various percentages of the ultimate recorded load, during the test can be found in Figure 46.

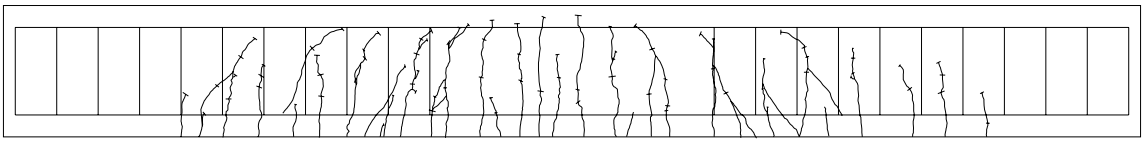

Figure 44: PU-F Eastern Face Crack Pattern

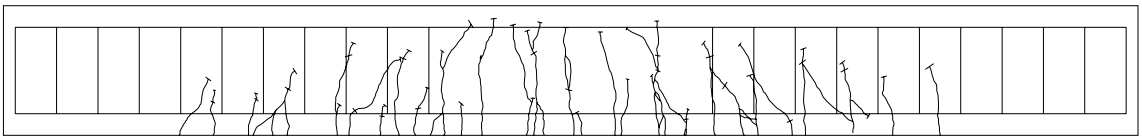

Figure 45: PU-F Western Face Crack Pattern

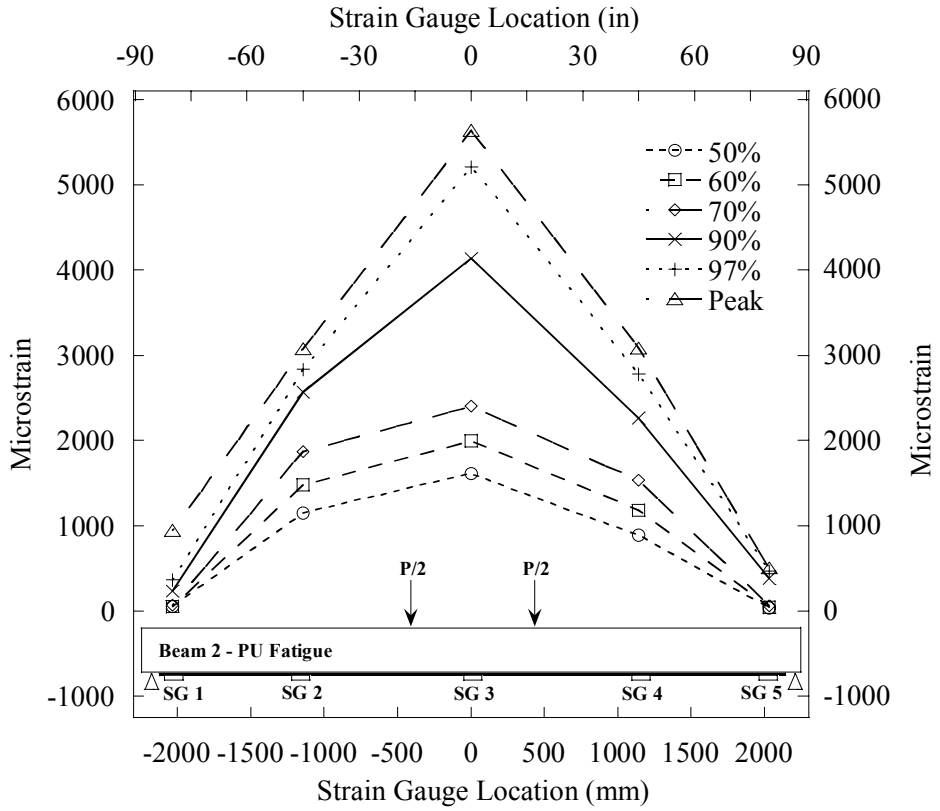

Figure 46: PU-F Strain Distribution

The PU-F specimen failed at 71.0kip (Δ=1.56"). Failure occurred in a sudden manner with the rupture of CFRP at mid-span (refer to Figure 47-a). Longitudinal splitting of CFRP also occurred (refer to Figure 47-b). The sudden nature of specimen PU-F's failure can be seen in the load vs. strain plot seen below (Figure 48). It can be observed that, prior to failure, softening occurs at the SG3 (due to yielding of steel) and at the SG 4 and 5 locations (debonding). Therefore it can be concluded that although debonding was not the ultimate mode of failure, it did occur during the loading process.

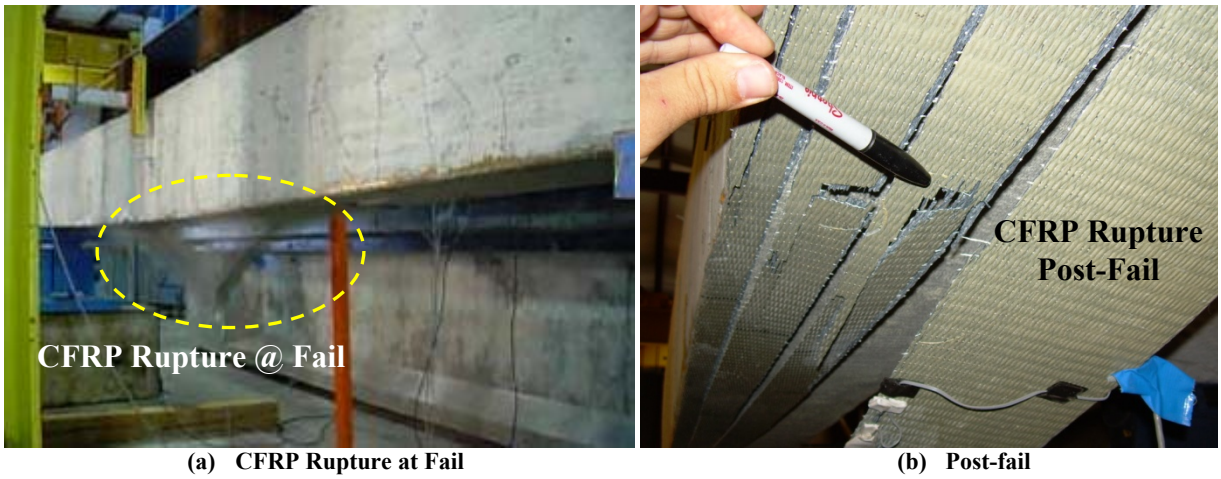

(a) CFRP Rupture at Fail **(b) Post-fail**

Figure 47: PU-F at Fail and Post-Fail

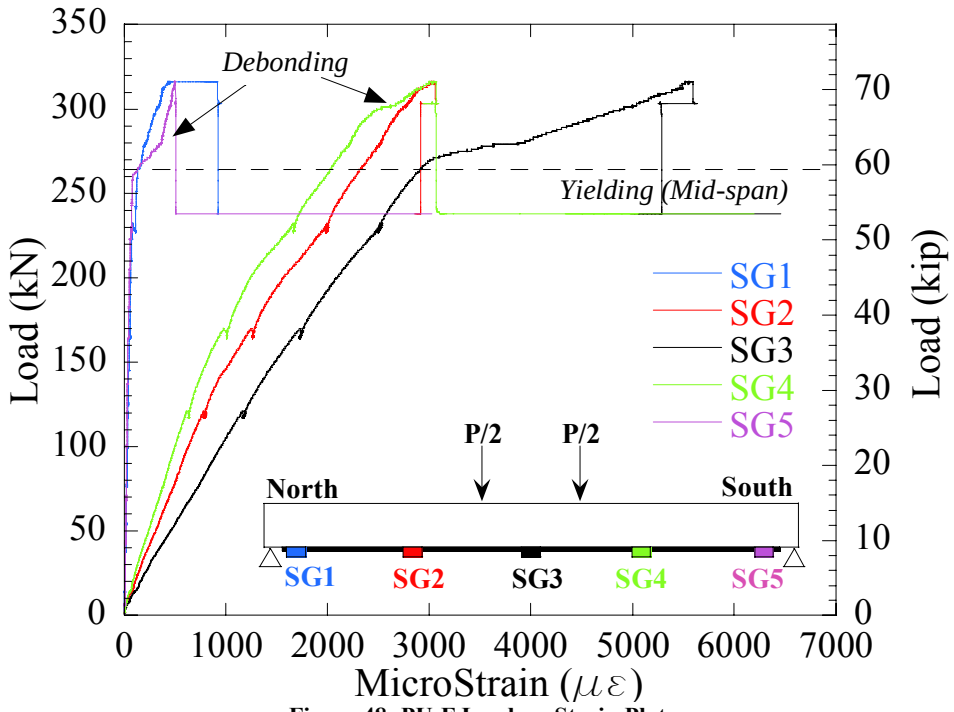

Figure 48: PU-F Load vs. Strain Plot

6.2.2 EP-F: Beam 6

During the fatigue loading of the EP-F specimen, strain measurements were recorded to capture the beam's response. Figure 49 shows the mean recorded strain plotted against the cycle number. Gauge 3 shows a gradual level of softening during the fatigue loading period. A calculated strain, at the gauge 3 position, is also shown. This value was generated using the measured deflection at the n^{th} cycle and the analytical models discussed in chapter 4. The purpose of this calculated value was to determine whether sensor drift was occurring during the test. Although the actual and calculated values are not exact, they are within a reasonable range of one another and both display the same shape. Differences could be attributed to loss of composite action at the FRP-to-concrete interface. Unlike the gradual softening seen in SG3, strain gauges 2 and 4 show a sudden increase in mean recorded strain between cycles 1,000 and 10,000. This sudden increase in mean strain is most evident in gauge 4 where there is approximately a 170% increase in mean strain.

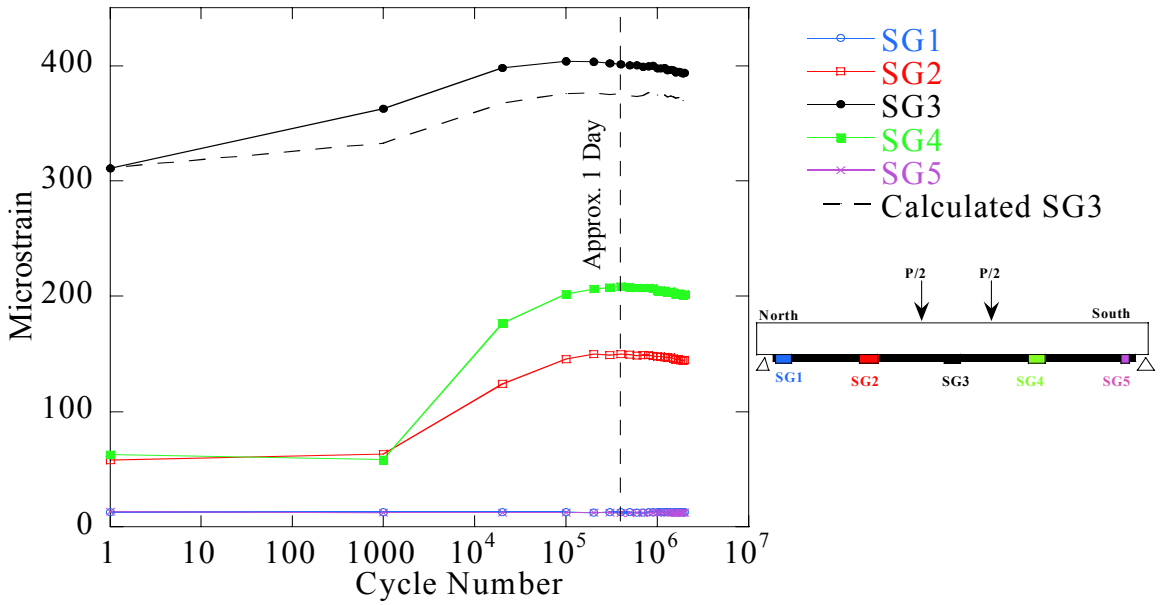

Figure 49: EP-F Mean Strain Fatigue Response

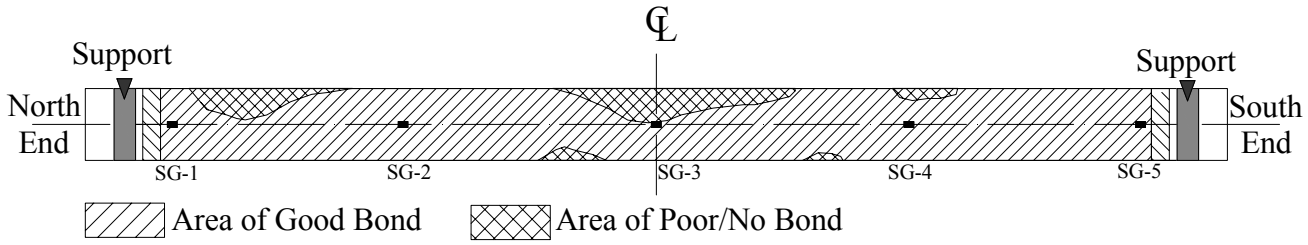

Figure 50: EP-F Post-fatigue Bond Inspection Result

Previous to ultimate testing, the CFRP-to-concrete bond was inspected to assess the degradation caused by fatigue loading. The approximate result of this inspection can be seen in Figure 50. It can be observed that a significant amount of bond degradation occurred from fatigue loading. Moreover, there could exist locations of bond degradation not detected by the tap inspection.

The ultimate load testing for specimen EP-F was conducted on 5/30/2008. There were no problems encountered during testing with DAQ or the test set-up. During loading, pauses were taken to mark cracks at 25.5, 38.3, and 51.1kip. The observed crack patterns at failure can been seen Figure 51 and Figure 52. The strain recorded, at various percentages of the ultimate recorded load, during the test can be found in Figure 53.

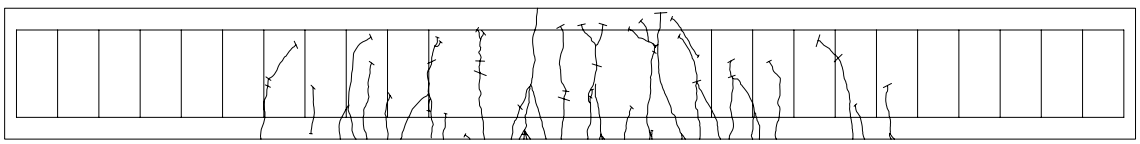

Figure 51: EP-F Eastern Face Crack Pattern

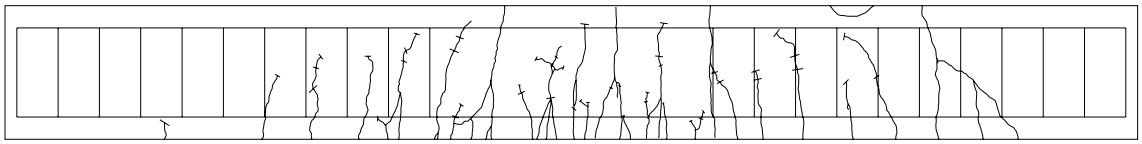

Figure 52: EP-F Western Face Crack Pattern

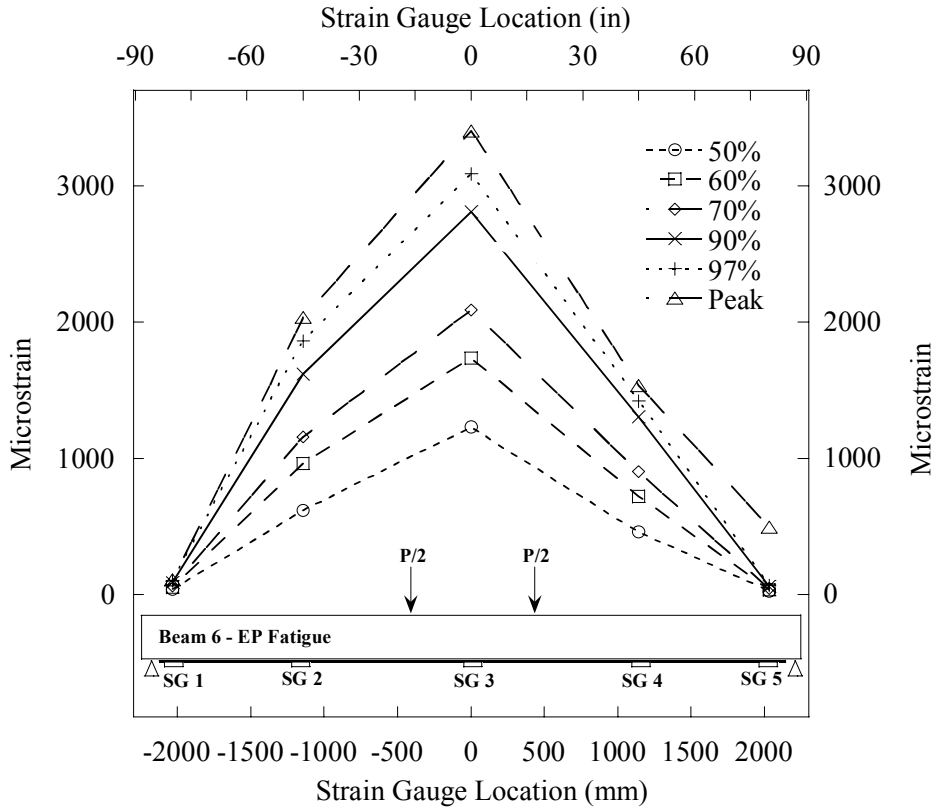

Figure 53: EP-F Strain Distribution

The failure of the EP-F specimen occurred initially at 63.5kip (Δ=0.86”). The initial failure occurred by partial (approximately one half of the sheet width) debonding of the CFRP sheet from the north end of the specimen. This can be observed in photo shown in Figure 54-a. The load vs. strain plot (Figure 55) for the EP-F specimen shows softening in strain gauges located in the northern region of the specimen previous to failure. The initial debonding caused a 10.2% drop in applied load. The load test continued until the second portion of the north end CFRP debonded from concrete. This occurred at the load of 60kip. There was a significant amount of longitudinal splitting that occurred in the CFRP sheet during failure (refer to Figure 54-b).

(a) Initial Failure via Debonding (b) Post-fail

Figure 54: EP-F Specimen at Fail and Post-fail

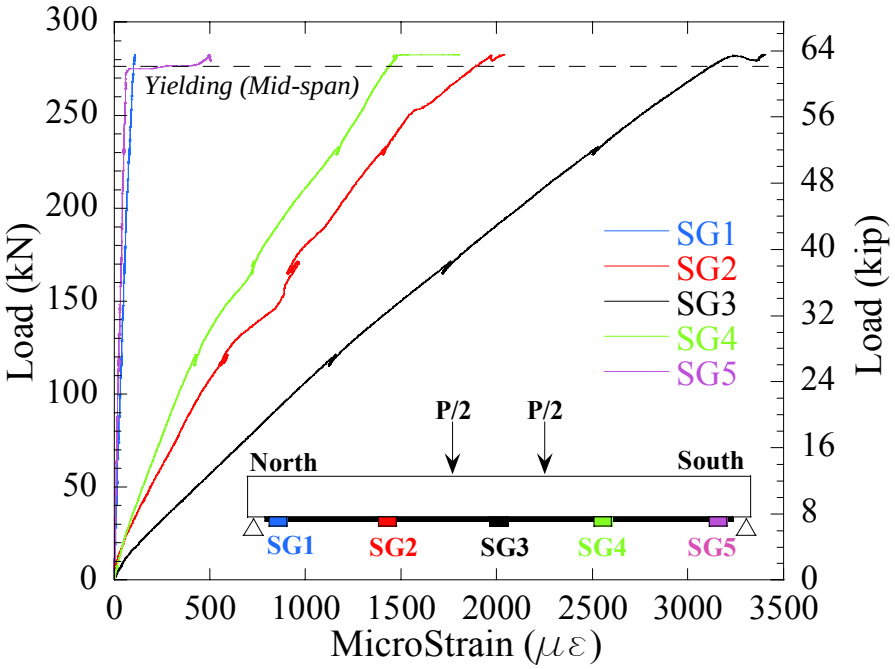

Figure 55: EP-F Load vs. Strain Plot

It should be noted that the load vs. strain plot (Figure 55) indicates a few key conclusions that can be drawn from the fatigue and ultimate loading of specimen EP-F:

- There is no indication that cracking at mid-span occurred during the ultimate test. This implies that cracking must have occurred during the fatigue loading procedure.

- There was a slight softening in the SG2 and SG4 regions. This could indicate a combination of cracking and loss of FRP/concrete composite action.

6.2.3 GE-F: Beam 11

During fatigue loading strain measurements were recorded. The results from those measurements can be seen in Figure 56. It can be observed that the recorded and calculated mean strain values, at the gauge 3 position, differ by approximately 100 microstrains. This value is somewhat significant given the relatively small mean strain values recorded. One explanation for such a discrepancy could be poor composite action between the RC beam and the CFRP laminate. Recall that during CFRP lay-up there were issues with premature gelling of the GE resin system. The other explanation for such a discrepancy would be sensor error. Yet, since both SG3 and $SG3_{CALC}$ curves display similar shape, the earlier explanation would seem more fitting rather than the latter. A significant amount softening is seen to occur in gauges 2 and 4. This loss of stiffness with increase in cycle number could be attributed to a combination of cracking, fatigue softening and/or creep of concrete, and/or CFRP debonding. Further discussion regarding the mechanisms that caused member stiffness reduced will be discussed in section 6.2.4.

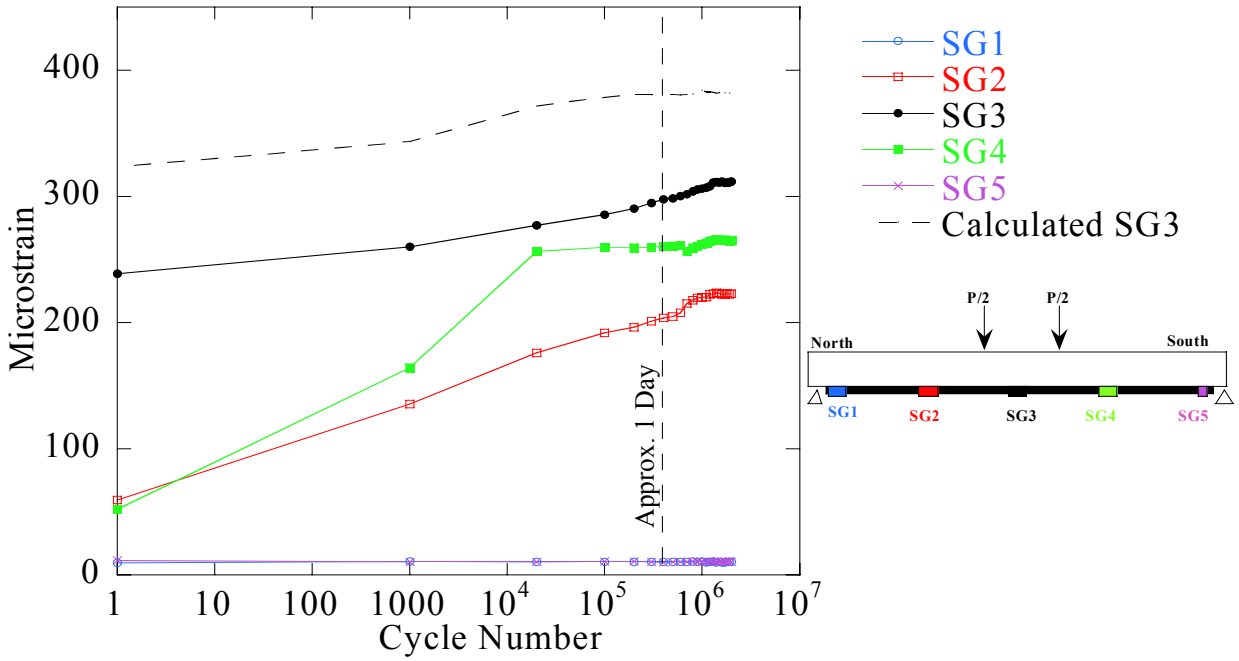

Figure 56: GE-F Mean Strain Fatigue Response

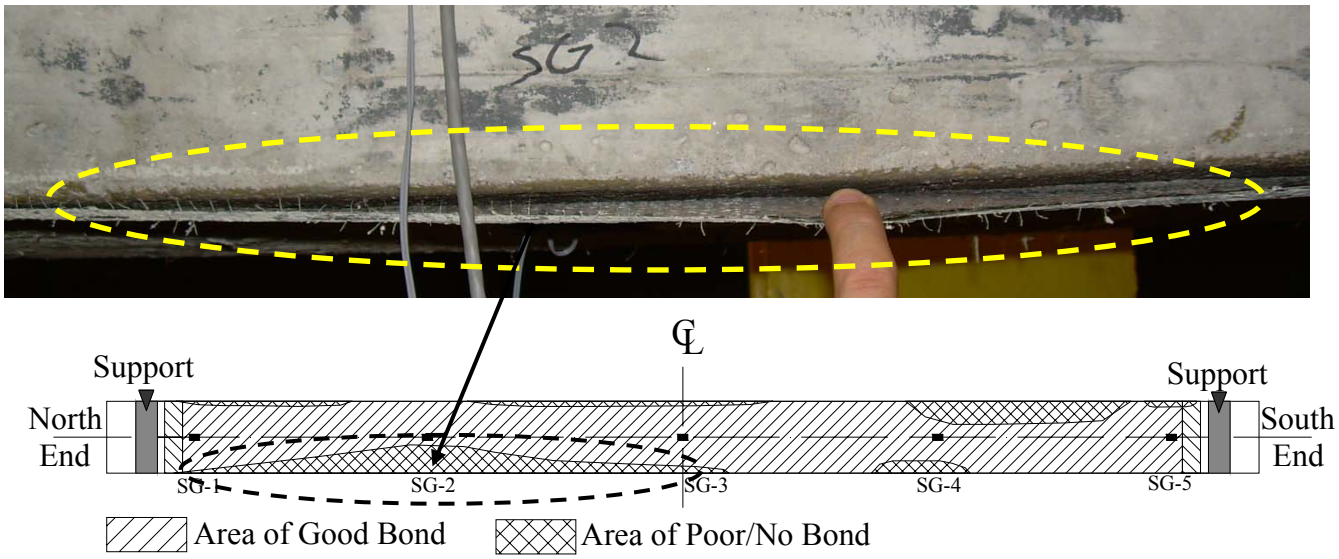

Figure 57: GE-F Post-fatigue Bond Inspection Result

Previous to conducting the ultimate load test, the CFRP-to-concrete bond was inspected. There was a significant amount of bond degradation that was found at numerous points along the specimen. The location west of SG2 was found to completely debonded from concrete. At this location the CFRP fabric could be pulled down to reveal the tension concrete surface (refer to Figure 57). A significant amount of soften was seen in this location in the fatigue results.

GE baseline specimen was tested on 5/30/2007. During the load testing, there were no observed problems with DAQ or the test set-up. Loading was paused at 25.5, 38.3, and 51.1 kips for cracks to be marked. Refer to Figure 58 and Figure 59 for the observed crack patterns at failure. The strain recorded at various percentages of the ultimate recorded load, during the test can be found in Figure 60.

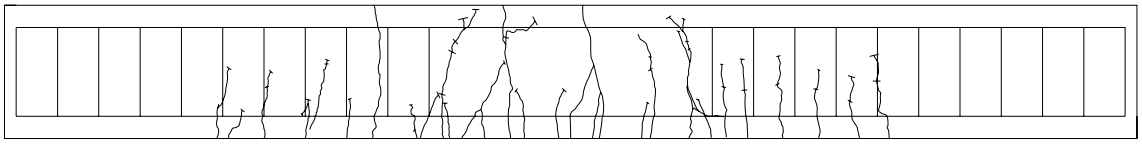

Figure 58: GE-F Eastern Face Crack Pattern

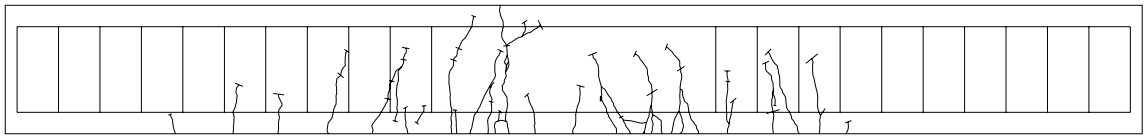

Figure 59: GE-F Western Face Crack Pattern

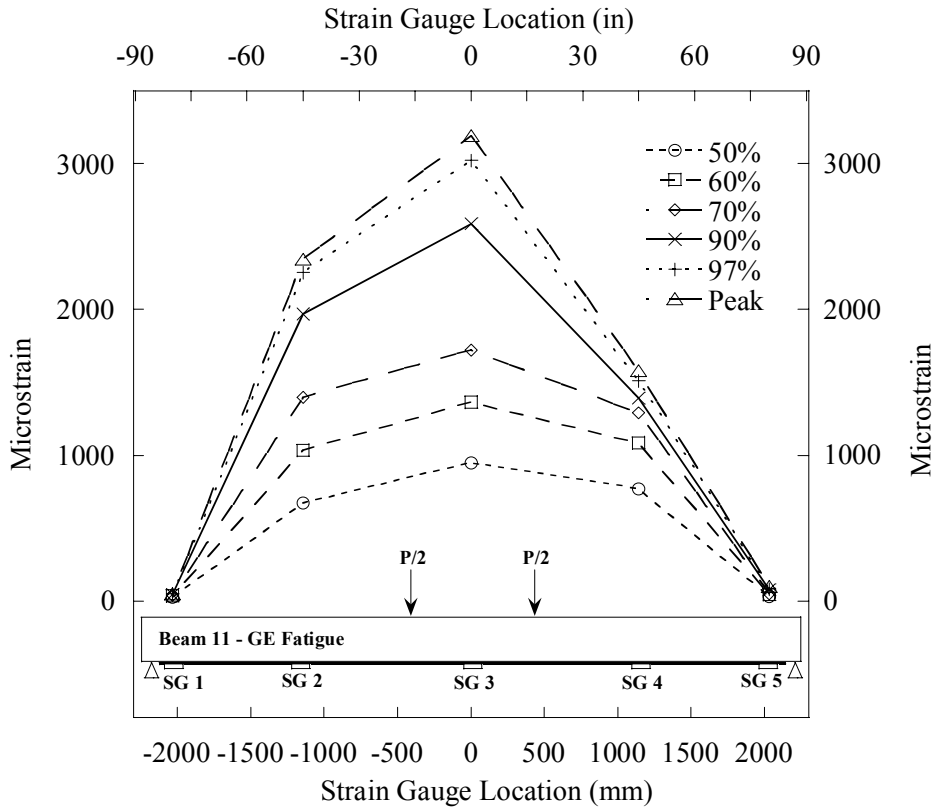

Figure 60: GE-F Strain Distribution

Failure occurred in specimen GE-F at a load of 60.3kip (Δ=0.81”). The dominate mode of failure was CFRP debonding (refer to Figure 61-a) at the north end of the specimen. Prior to failure, strain gauges 2 and 3 exhibit drastic increases in strain (Figure 62). Figure 61-b shows a picture of the debonded CFRP sheet. The same three distinct regions discussed in the results portion for the GE baseline specimen can be seen in Figure 61-b. This indicates non-uniformity in the bond.

(a) **(b)**

Figure 61: GE-F Specimen at Fail and Post-fail

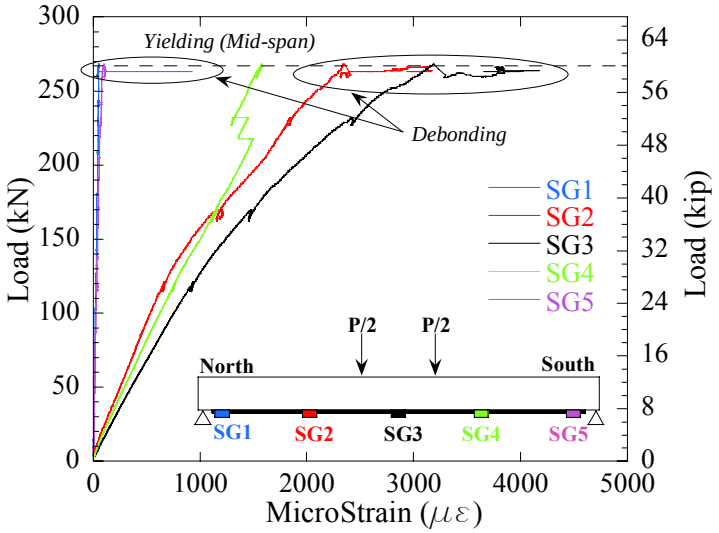

Figure 62: GE-F Load vs. Strain Plot

6.2.4 Fatigue Specimen Comparative Results

The following section compares the fatigue and ultimate load performance for the fatigued specimens. A plot of maximum and residual deflection vs. cycle number is shown in Figure 63. A significant amount of scatter can be seen in the measurement taken during the fatigue test for the PU-F specimen. This scatter was cause by sensor drift that occurred during the test. As mentioned in Chapter 5, the PU-F specimen was the only beam to be instrumented with laser displacement gauges. The deflection data acquired from the PU-F was found to be bad and therefore is not considered.

Both EP-F and GE-F specimens display a significant reduction in flexural stiffness between the 1st and 100,000th cycle. Furthermore, approximately 80% of maximum and residual member deflections accumulate within 300,000 cycles (Approximately 1 day of load cycling). Therefore it can be concluded that the majority of stiffness loss, during cyclic loading, was due to cracking/fatigue softening of concrete and bond degradation (evident from bond inspections). It can be assumed that no material softening occurs in CFRP over time to fatigue (Hollaway and Leeming 1999).

It took approximately 6.5 – 7.5 days to complete the fatigue cycling. Therefore, it can be assumed that a portion of the residual deflection was also caused by creep of concrete during the fatigue loading process. In order to make an approximate prediction of the creep induced deflection, Equations 9 and 10 were used as defined by ACI-318.

$$\Delta_{Creep} = \lambda \cdot \Delta_i \qquad \textbf{Equation 9}$$

Where

$$\lambda = \frac{\xi}{1+50\rho'} \qquad \textbf{Equation 10}$$

Two different values for the instantaneous deflection Δ_i were considered; one corresponding to the deflection at the mean fatigue load (9.6kip) and the other corresponding to the deflection at the maximum fatigue load (19.2kip). The ratio of the 7.5 day creep deflection to maximum residual deflection can be seen in Figure 64. It is can be observed that for the mean fatigue load, the approximate creep deflection is below that of the residual deflection for both the EP and GE specimens. This result would indicate that creep deflection was a contributing factor to the maximum and residual deflection accumulated during the fatigue loading process. Yet, given the measurements taken during the test, there is no way to determine the exact extent of deflections caused by creep of concrete.

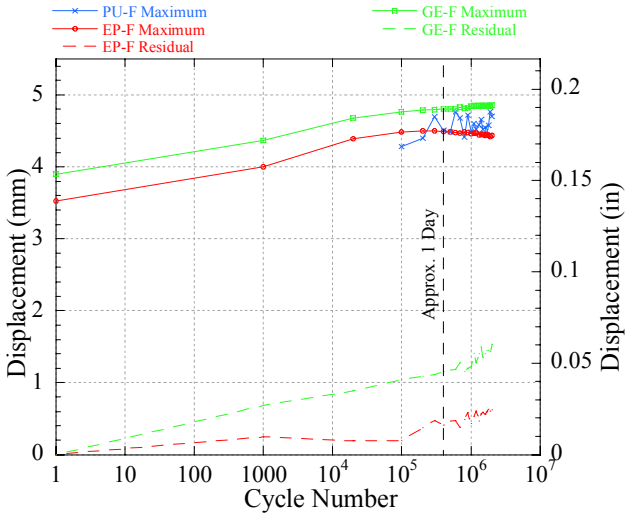

Figure 63: Deflection vs. Cycle-Fatigue Specimens

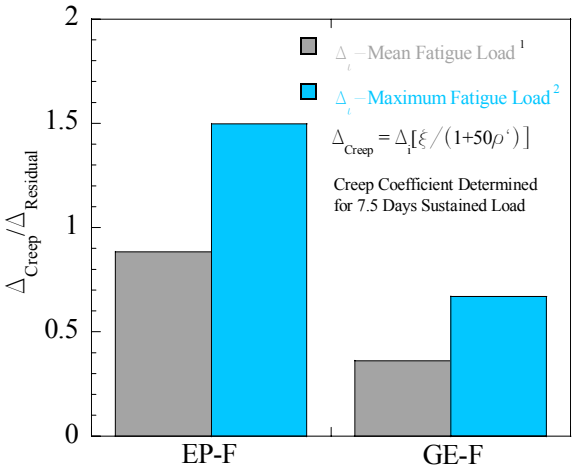

[1] Deflection determined via calculation with a cracked section
[2] Deflection determined via static measurements prior to fatigue testing

Figure 64: Effect of Creep on Residual Deflection

Although the load-bearing capacity for all three specimens increased, the EP-F and GE-F specimens displayed a considerable reduction in deflection capacity at failure (refer to Figure 65). Furthermore, both epoxy based specimens achieved yield as failure occurred (GE-F) or just previous to failure (EP-F). There was also a significant decrease in the maximum achieved strain in the CFRP laminate for the epoxy based systems (refer to Table 24). The decrease in maximum strain, at the time of failure, indicates inefficient use of the CFRP in term of strength.

Fatigue loading seemed to have little effect of the polyurethane based CFRP system. Compared to the urethane baseline specimen, exposure to fatigue only caused a 4.4% reduction in load bearing capacity and a 14.5% reduction in ultimate deflection.

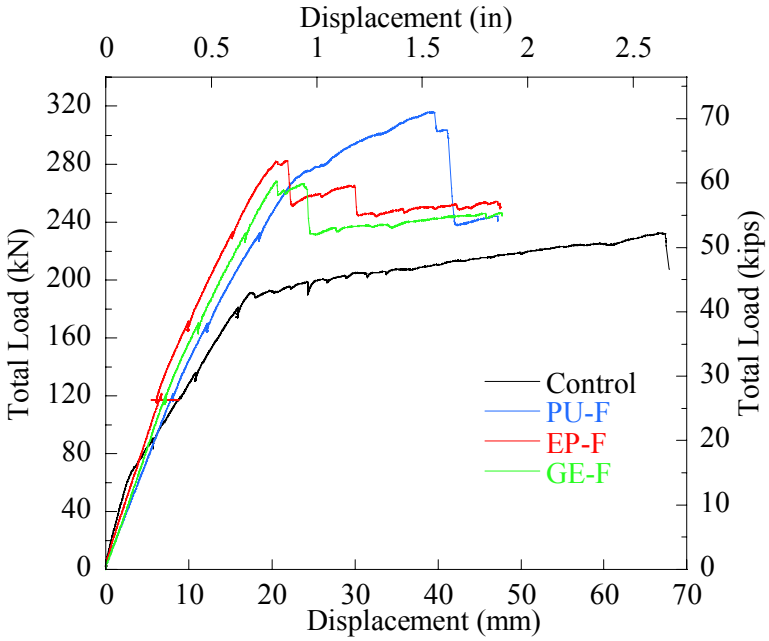

Figure 65: Fatigue Specimen Ultimate Load Test Result

Table 24: Fatigue Specimen Load, Deflection and Strain Results

Specimen ID	Beam No.	Yielding Load		Yielding Deflection		Ultimate Load		Ultimate Deflection		Maximum Strain (με)
		kN	*kip*	*mm*	*in*	*kN*	*kip*	*mm*	*in*	
Control	16	190.8	42.9	19.1	0.75	232.2	52.2	66.8	2.63	N/A
PU-F	2	270.4	60.8	4.0	0.9	315.8	71	39.6	1.56	5637
EP-F	6	275.8	62	3.4	0.77	282.4	63.5	21.8	0.86	3403
GE-F	11	267.8	60.2	3.6	0.8	268.2	60.3	20.6	0.81	3194

6.3 Thermal/Humidity Conditioning Results

The following section discusses the results from the T-type specimens. It was these specimen that underwent numerous cycles of heating/humidity and cooling for an extended period of time.

6.3.1 PU-T: Beam 3

As seen in Figure 66, the PU-T specimen did not show any locations of poor bond that may have resulted from environmental conditioning.

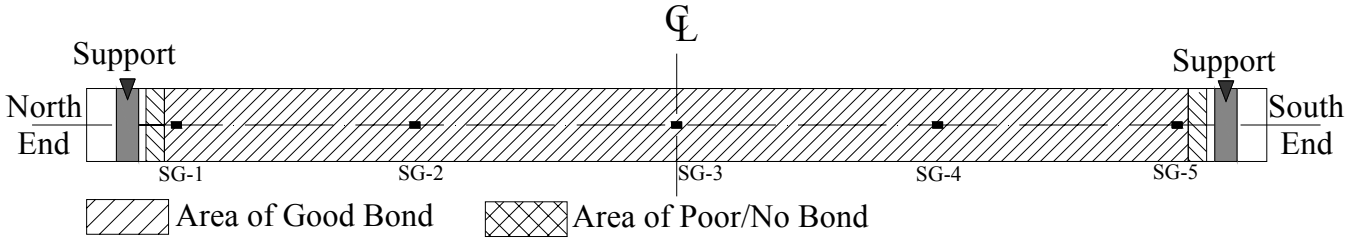

Figure 66: PU-T Post-Conditioning Bond Inspection Result

The PU-T specimen was tested to ultimate failure on 10/23/2008. During the load test there were a number of issues with the actuator cross-head rolling the spreader beam. When this rolling action was encountered, the load test was stopped and the beam unloaded. Reloading was started when the apparent problem was resolved. The following observations were taken:

Load Attempt 1: During the loading attempt the actuator kicked out at approximately 63 kips. At this load level, cracking of concrete had occurred and therefore would not be seen in future loading. The actuator was re-positioned and all DAQ measurements were reset before re-loading.

Load Attempt 2: Early in the loading procedure it was evident that the actuator cross-head was rolling slightly. It was decided to stop the test and change the load spreader and spreader bearing pads (neoprene). The spreader was replaced with a similar W-section and the bearing pads were replaced with wooden pads. DAQ was not re-set before the next test.

Load Attempt 3: Once again during the early stages of the loading procedure it was evident that the actuator cross-head was rolling. Therefore the test was stopped. The bearing pads at both the spreader and support positions were replaced with steel reinforced neoprene pads. DAQ was not re-set before the next test.

Load Attempt 4: The forth loading attempt to failure was successful with failure occurring at 74.3kips (Δ=1.74”).

At various points, during the numerous loading attempts, cracked were marked and the observed crack patterns can be seen in Figure 67 and Figure 68. The recorded strain, at various points during loading, can be seen in Figure 69.

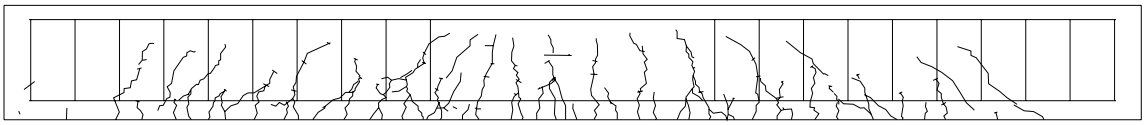

Figure 67:PU-T Eastern Face Crack Pattern

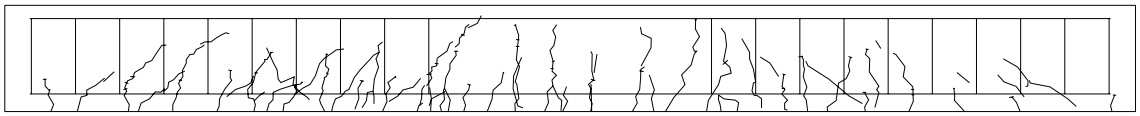

Figure 68: PU-T Western Face Crack Pattern

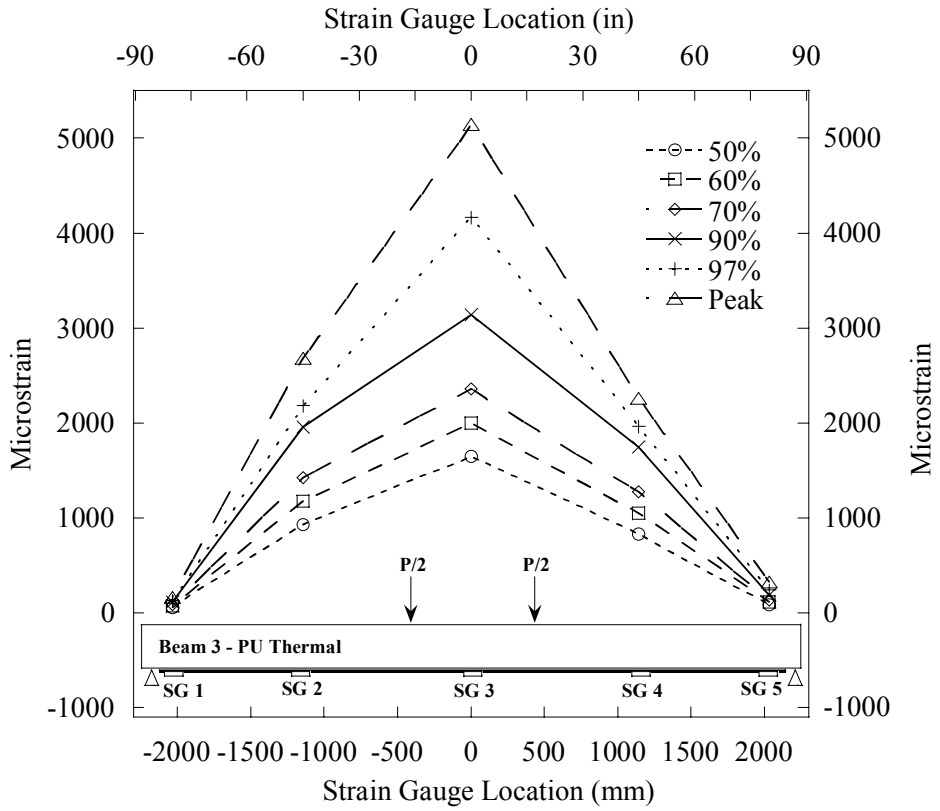

Figure 69: PU-T Strain Distribution

As mentioned above, failure of the PU-T specimen ultimately occurred at a load of 74.3kip. This failure was caused by FRP debonding near the north end of the beam (refer to Figure 70). Inspection of the CFRP debonding surface revealed that failure occurred within the urethane adhesive layer i.e. cohesive failure

(a) North End (b) South End

Figure 70: PU-T at Failure

6.3.2 EP-T: Beam 7

During the post-conditioning CFRP inspection of specimen EP-T there were a few locations found to have poor adhesion to concrete. The areas in Figure 71 shown in red could have possibly been due to environmental condition given the location of the void. The void shown in blue, near SG2, is more than likely a void that occurred during FRP application and/or curing.

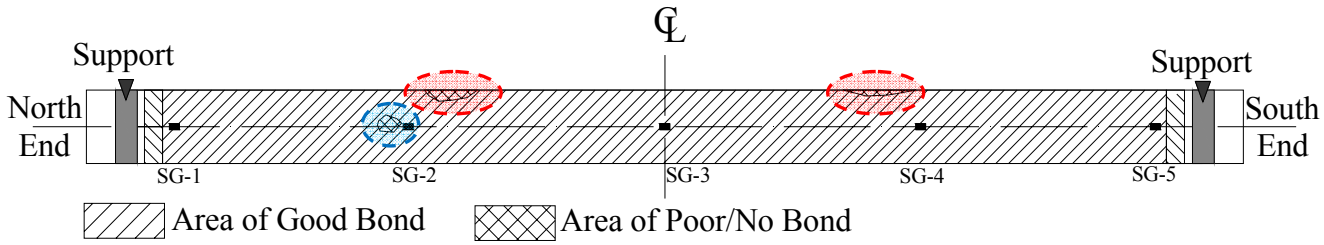

Figure 71: EP-T Post-conditioning Bond Inspection Result

The EP-T specimen was tested to ultimate failure on 10/22/2008. During testing, there were no errors in procedure or problems with the DAQ. The observed crack pattern (marked at 25.9 and 37 kips) at beam failure can be seen in Figure 72 and Figure 73. The recorded strain distribution, observed during testing, can be seen in Figure 74.

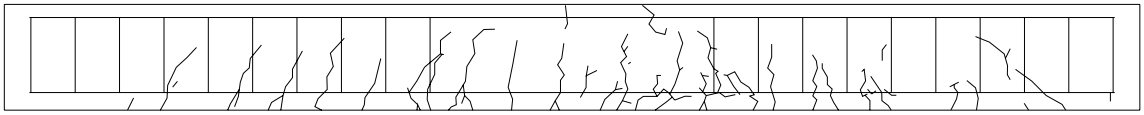

Figure 72: EP-T Eastern Face Crack Pattern

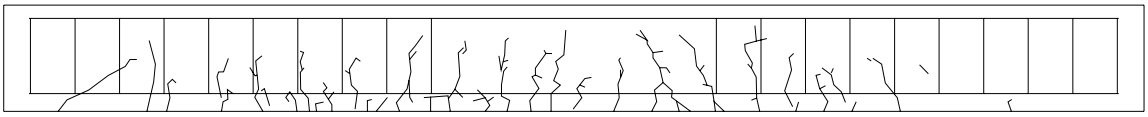

Figure 73: EP-T Western Face Crack Pattern

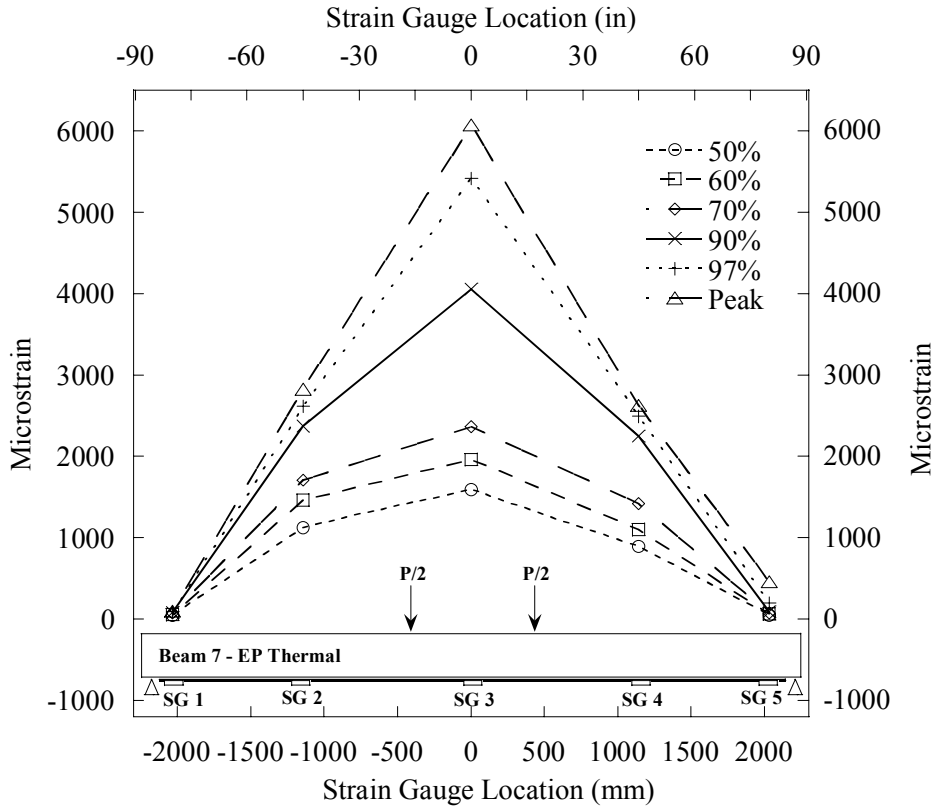

Figure 74: EP-T Strain Distribution

Ultimate failure of the EP-T specimen occurred at a load of 74.6kip (Δ=1.57”). Failure was caused by FRP debonding that originated from the north of the specimen. A significant amount of sudden softening occurred at the SG3 location (due to steel yielding) and at the SG2 location (CFRP debonding); this can be observed in the load vs. strain plot (Figure 76). After failure the specimen was inspected and following was observed:

- At mid-span, approximately at the point where FRP bonding resumed, it was found that concrete cover separation had occurred (refer to Figure 76).

- Upon inspecting the debonded surface of the CFRP, it was found that multi-layer debonding had occurred. That is, as described early in the failure of the GE baseline specimen (Figure 40) when rupture of the FRP-to-concrete interface occurs in more than single layer such as that adhesive or concrete substrate layer.

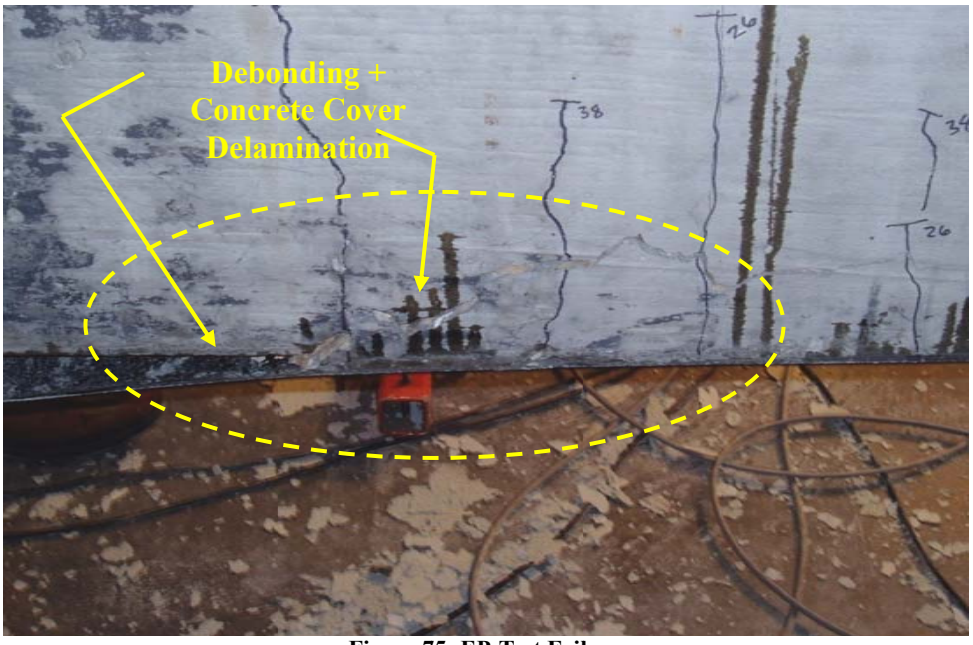

Figure 75: EP-T at Failure

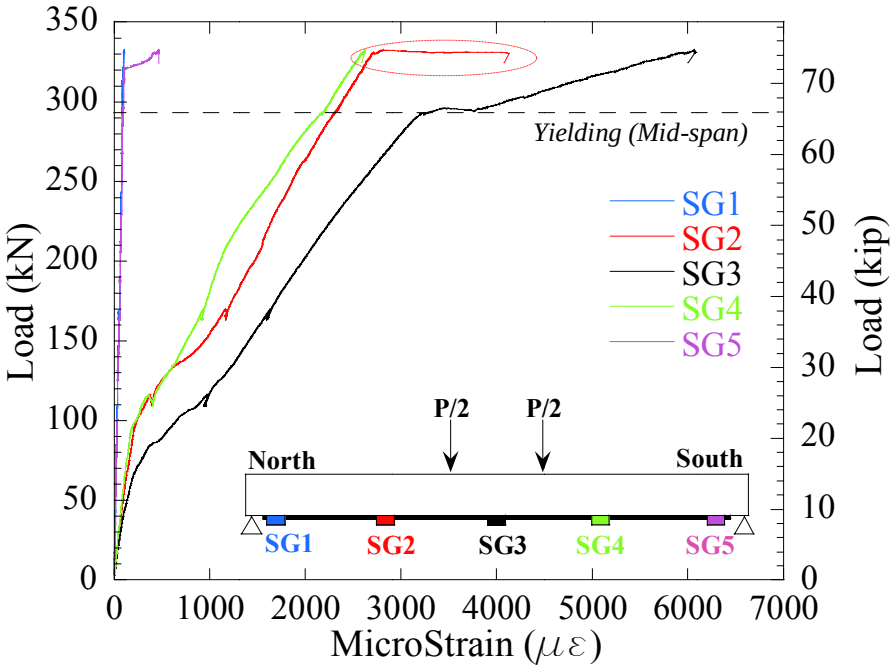

Figure 76: EP-T Load vs. Strain Plot

6.3.3 GE-T: Beam 15

Upon inspection of the GE-T specimen, it was determined that virtually no bond degradation occurred due to environmental conditioning (refer to Figure 77). It should be noted here that the GE-T specimen was the only GE-type specimen to exhibit, upon tap inspection, a sound and uniform bond.

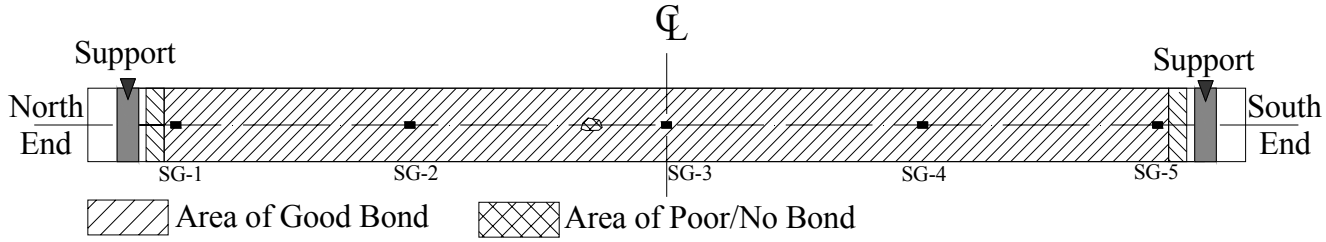

Figure 77: Post-Thermal Conditioning Bond Integrity

Ultimate testing of the GE-T specimen occurred on 10/23/2008. During the loading procedure there were no observed problems with loading or DAQ. Loading was paused at 28 and 39kips to mark cracks; crack patterns can be seen in Figure 78 and Figure 79. The observed strain profile during loading can be seen in Figure 80.

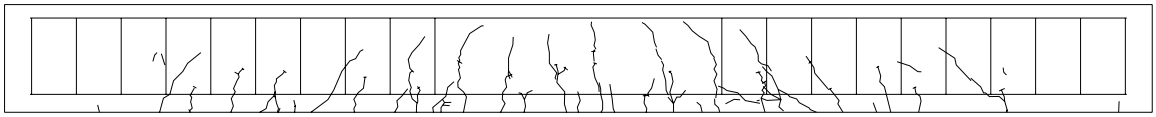

Figure 78: GE-T Eastern Face Crack Pattern

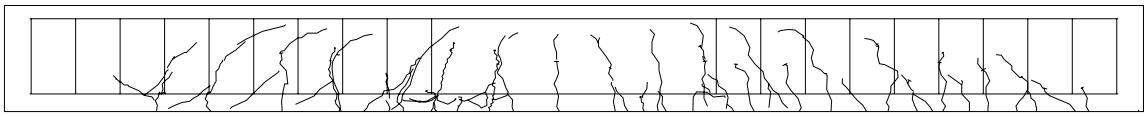

Figure 79: GE-T Western Face Crack Pattern

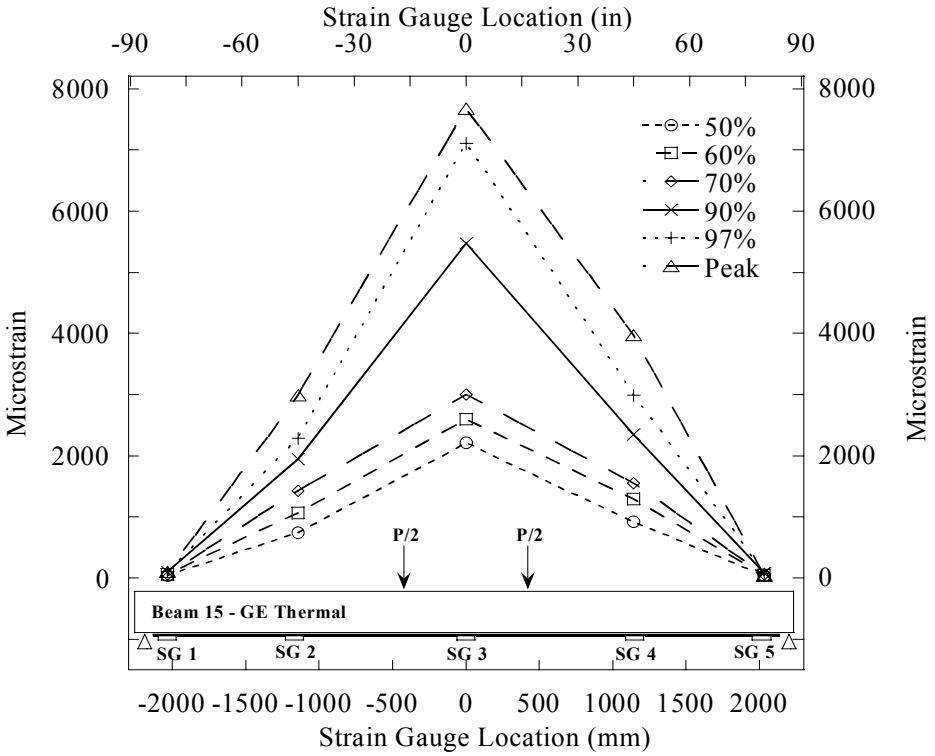

Figure 80: GE-T Strain Distribution

Failure occurred in the GE-T specimen at a load of 70.6kip (Δ=1.67”). Failure was ultimately caused by debonding (refer to Figure 81) and interlaminar shear rupture (refer to Figure 82-b) of CFRP that originated at the north end of the specimen. At a load of approximately 68kip, loss of CFRP/concrete composite action occurred at the SG2/4 locations (refer to Figure 83). The following observations were made during a post-failure inspection of the specimen:

- At mid-span, there was a large amount of concrete cover (approx. 12” - 14”) that separated from the internal reinforcing steel.

- There appeared to be a significant amount of inconsistency with the CFRP bond to concrete. Some locations exhibited excellent bond; while others showed poor or no bond at all.

- At the north end of the specimen, where debonding occurred, it can be observed that a small portion of the CFRP laminate seems to be under the support (refer to Figure 82-a). If this observation is correct, it would be the extra anchorage provided by this happening to induce the interlaminar failure seen.

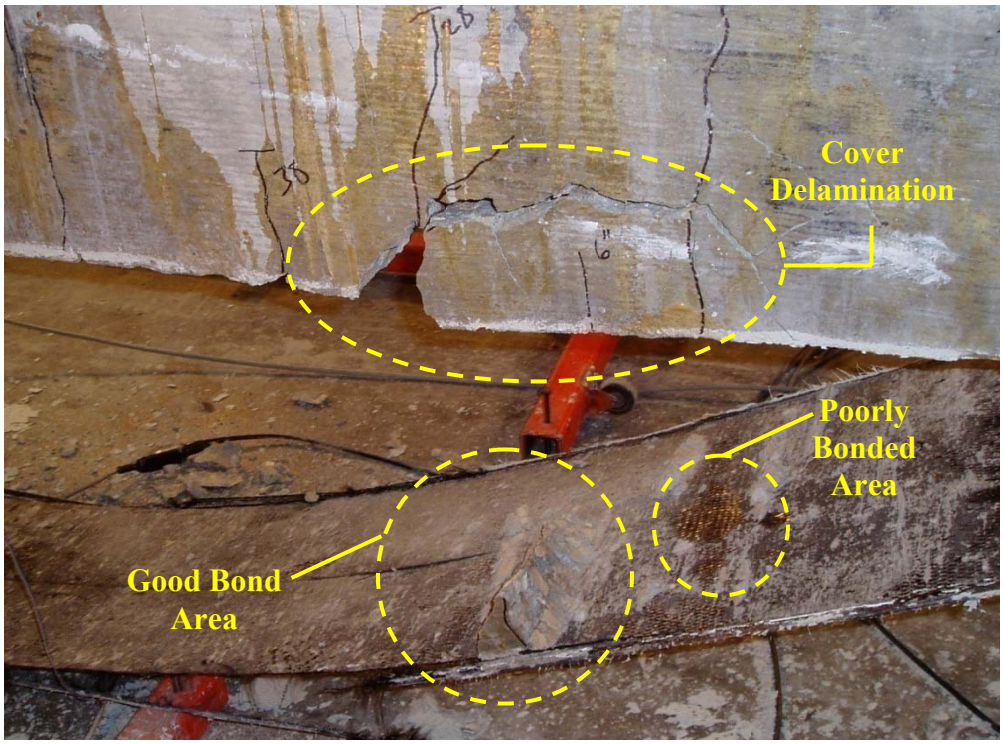

Figure 81: Debonding / Delamination Failure

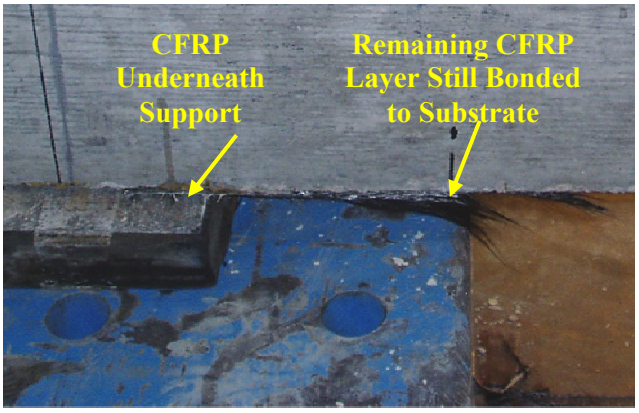

(a)

(b)

Figure 82: Interlaminar Shear Failure

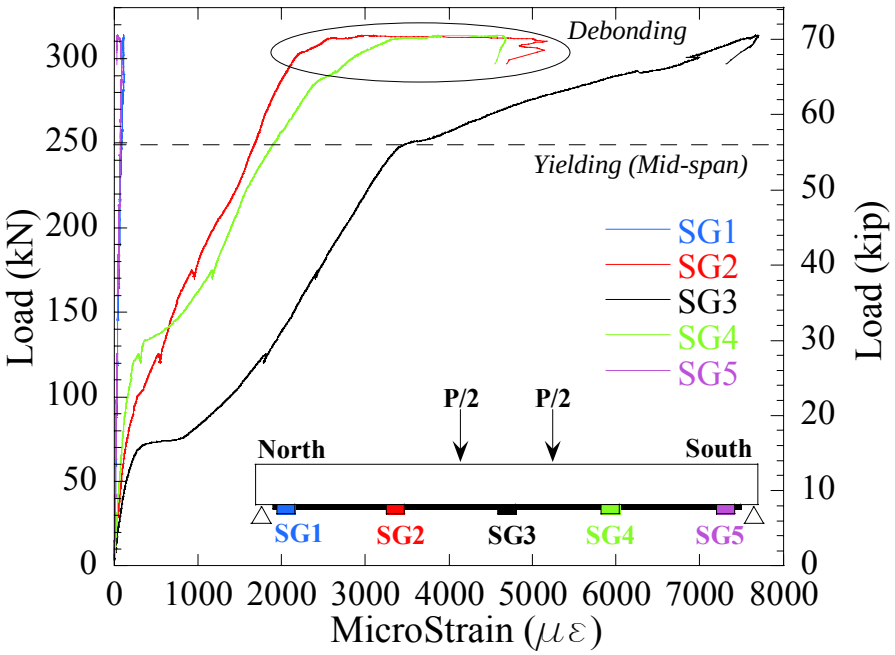

Figure 83: GE-T Load vs. Strain Plot

6.3.4 Thermal Specimen Comparative Results

There was not a considerable difference in the load-deflection behavior (Figure 84) between any of the specimens subjected to environmental conditioning. There was only a 11% difference between the ultimate deflections for the PU-T and GE-T specimens; these specimens had the lowest and highest ultimate deflections respectively. Furthermore, the difference between the minimum and maximum observed ultimate loads was found to be 5.9%. Therefore there was no one CFRP system that significantly outperformed any other in term of post-conditioning flexural performance. It should be noted that the GE system achieved a considerable level of mid-span strain failure. Moreover, all specimens performed comparably or out performed baseline ultimate load, deflection, and strain achieved at failure (refer to Table 25).

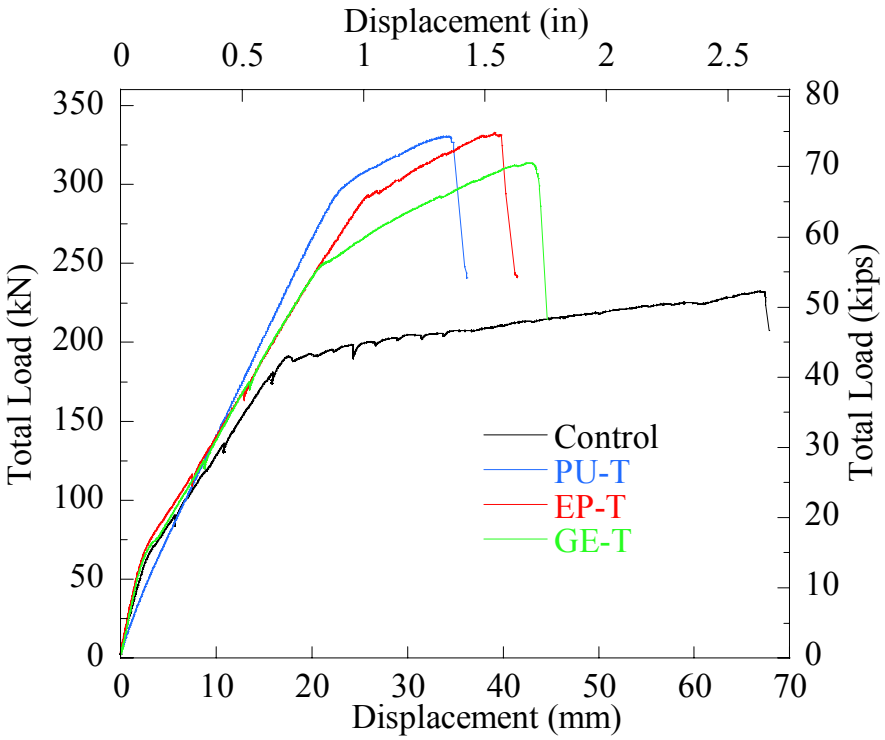

Figure 84: Load-Deflection Results for Thermally Conditioned Specimens

Table 25: Thermally Conditioning Load, Deflection, and Strain Results

Specimen ID	Beam No.	Yielding Load		Yielding Deflection		Ultimate Load		Ultimate Deflection		Maximum Strain (με)
		kN	*kip*	*mm*	*in*	*kN*	*kip*	*mm*	*in*	
Control	16	190.8	42.9	19.1	0.75	232.2	52.2	66.8	2.63	N/A
PU-T	3	294.9	66.3	4.0	0.89	330.5	74.3	44.2	1.74	5139
EP-T	7	295.8	66.5	4.6	1.04	332.7	74.8	39.9	1.57	6072
GE-T	15	249.5	56.1	3.7	0.83	314.0	70.6	42.4	1.67	7676

6.4 Fatigue/Thermal Results

The following section presents the results observed from specimens that received both 2 million fatigue cycles and thermal conditioning. Fatigue results for each specimen will be presented first followed by ultimate load test results.

6.4.1 PU-F-T: Beam 4

The PU-F-T displayed excellent fatigue performance in regard to CFRP bond to concrete. There was not substantial softening that occurred at any gauge position (refer to Figure 85). This would indicate little or no degradation in the CFRP-to-concrete interface. The calculated mean strain was found to be within reason to assume that no sensor drift occurred during the fatigue loading procedure.

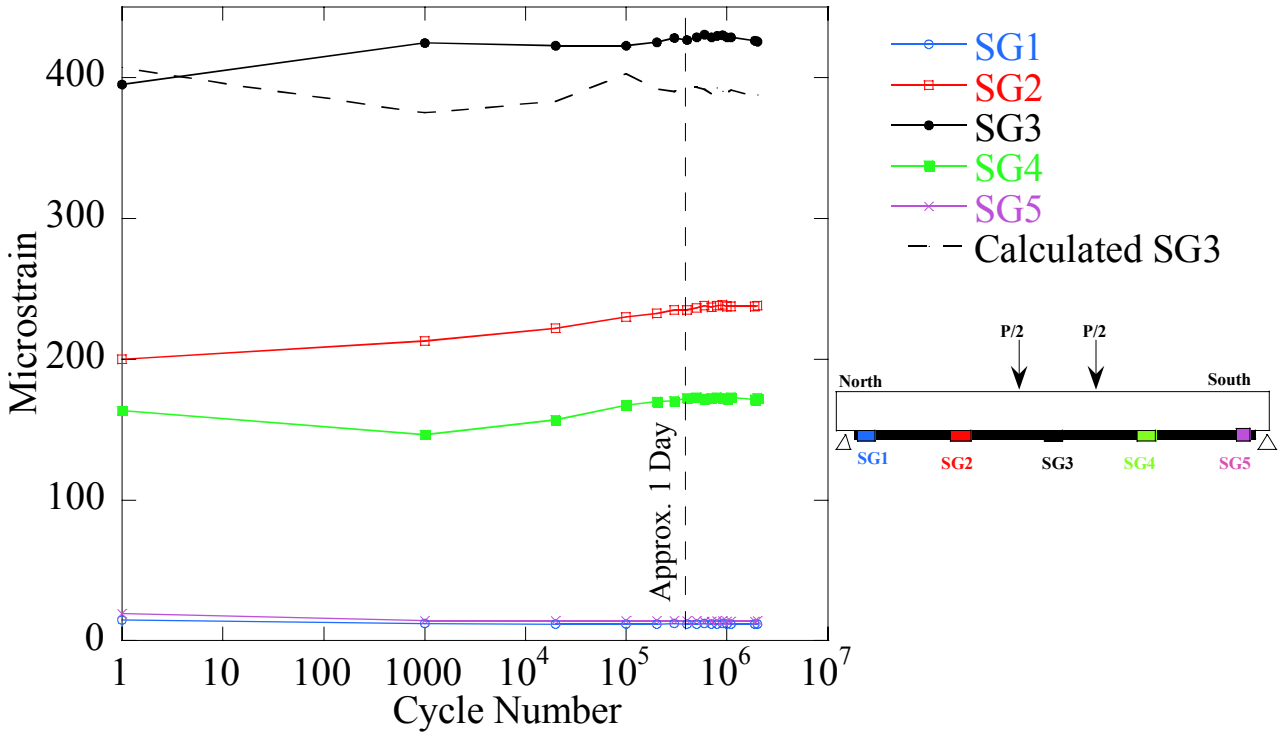

Figure 85: PU-F-T Mean Strain Fatigue Response

The post-fatigue/thermal conditioning bond inspection revealed that little detectable bond degradation occurred from conditioning (refer to Figure 86). The only flaw that was observed in the PU-F-T specimen was an area of chipped concrete on the east face near mid-span.

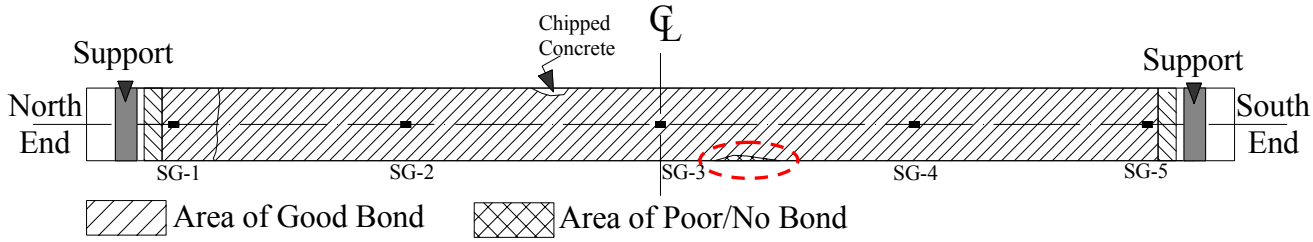

Figure 86: PU-F-T Post-conditioning Bond Integrity Results

The ultimate load testing of the PU-F-T specimen occurred on 10/22/2008. There were no problems observed during the load test. Pauses in loading occurred at 26, 37, and 53kips so that cracks could be marked; results can be seen in Figure 87 and Figure 88. The strain profile recorded during testing can be seen in Figure 89.

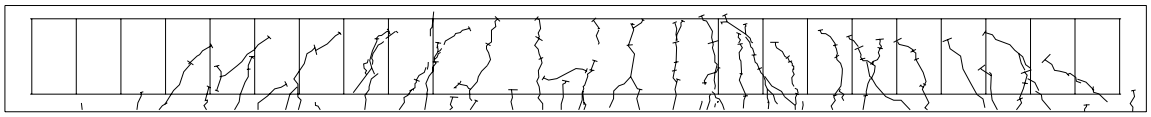

Figure 87: PU-F-T Eastern Face Cracking Pattern

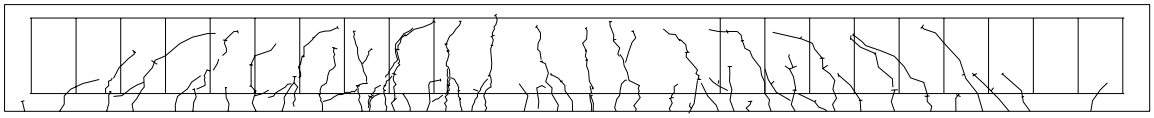

Figure 88: PU-F-T Western Face Crack Pattern

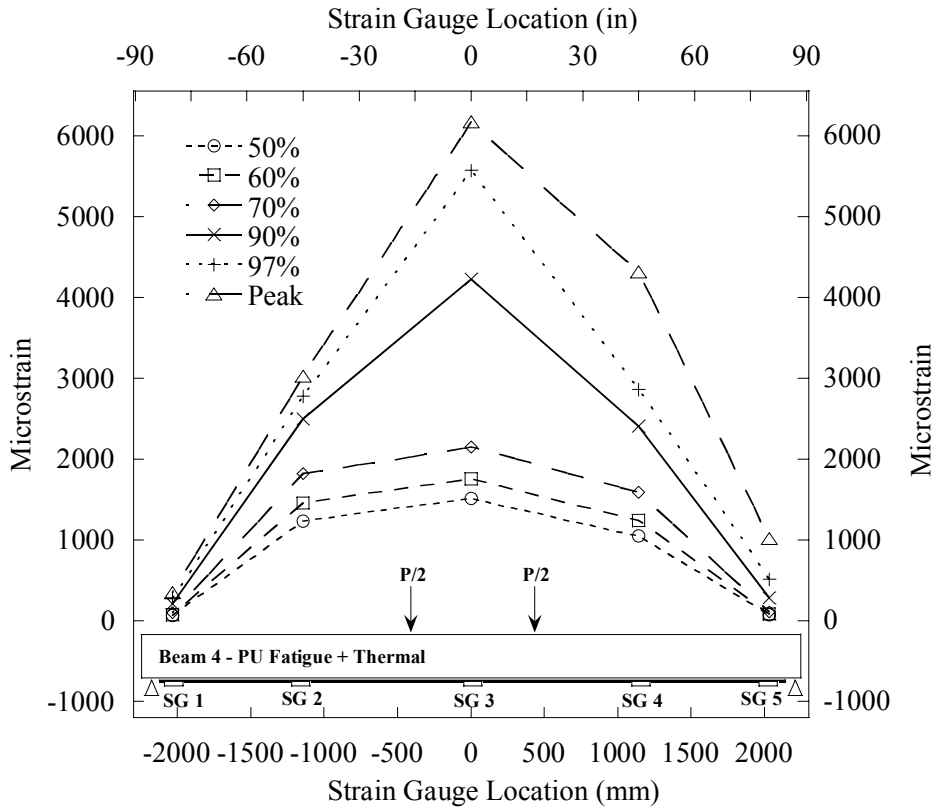

Figure 89: PU-F-T Strain Distribution

Failure of the PU-T-F specimen occurred at 73.9kip (Δ=1.76”). The dominate mode failure was observed to be debonding that originated at the south end of the specimen. This observation is verified by the load-strain plot in Figure 90. Strain gauges 4 and 5 displayed a short period (outlined in red) of considerable softening previous to failure. The increased strain values observed in SG3 can be accredited to yielding of tensile steel. After inspecting the post-fail CFRP laminate, it was determined that the debonding failure occurred in the urethane adhesive layer.

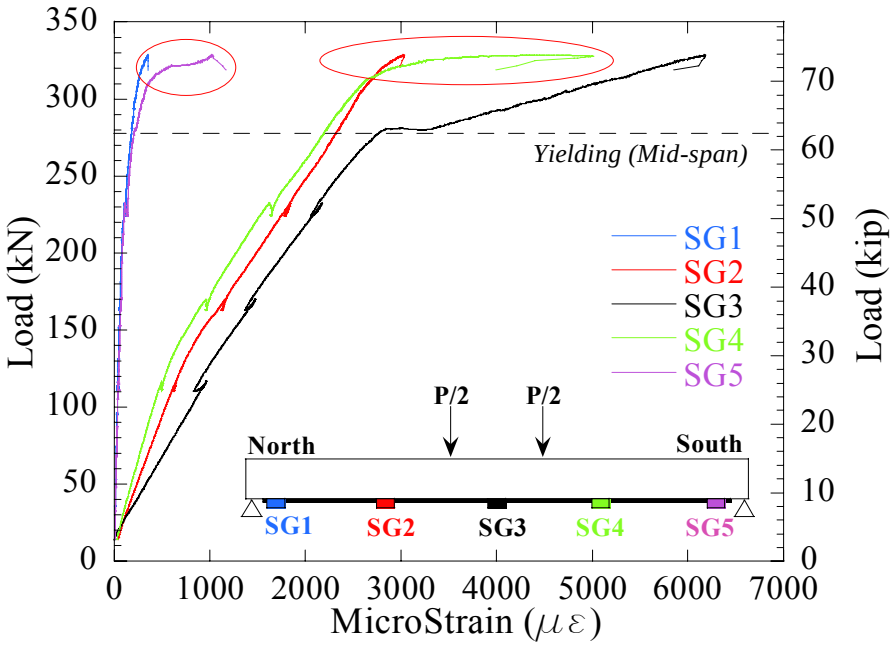

Figure 90: PU-F-T Load vs. Strain Plot

6.4.2 EP-F-T: Beam 8

The fatigue results for the EP-F-T specimen showed gradual softening in the mid-span mean strain (refer to Figure 91). It was also found that, during the 1000th and 10,000th fatigue cycle, a sudden jump in mean strain occurred in strain gauge 4. The ultimate load test, discuss below, will reveal that debonding failure occurs in the region of gauge 4. Beside these two observations, there was no other important result observed in the fatigue-strain results. It can be concluded that no sensor drift occurred based on the calculated strain results.

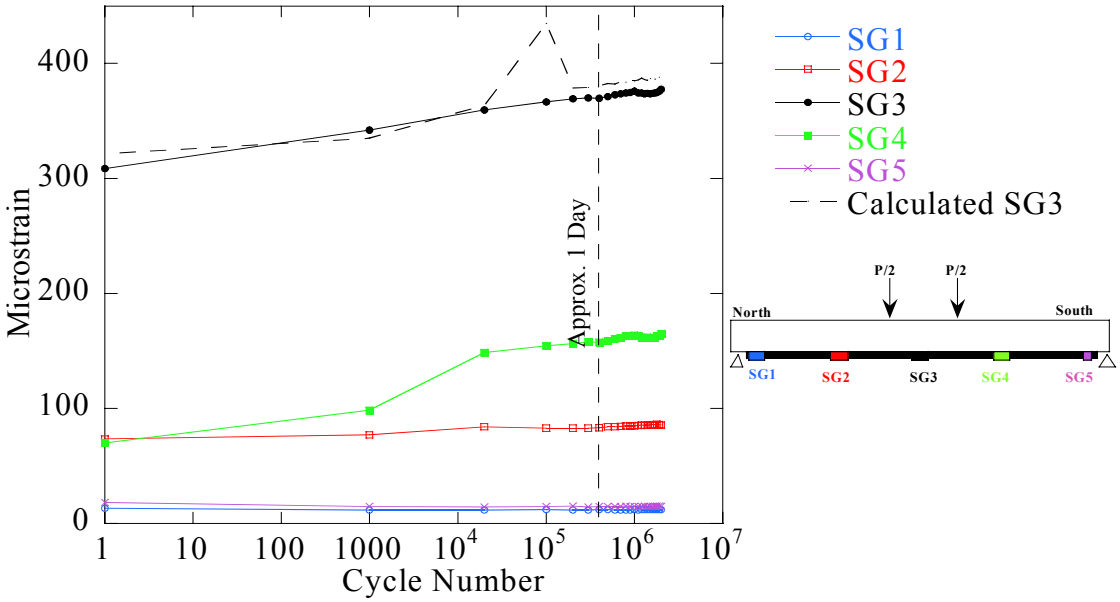

Figure 91: EP-F-T Mean Strain Fatigue Response

The post-fatigue/thermal conditioning bond inspection revealed that little detectable bond degradation occurred from conditioning (refer to Figure 92). The only flaws found on the specimen were 3 areas of chipped concrete on the west face near the south support.

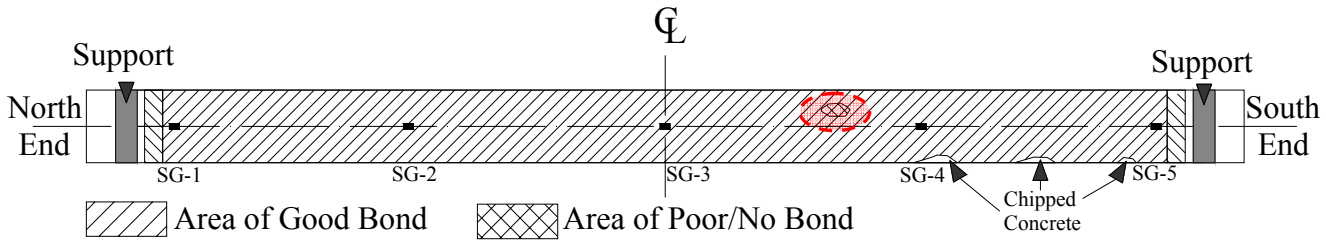

Figure 92: EP-F-T Post-conditioning Bond Integrity Result

The EP-F-T specimen was tested to ultimate failure on 10/22/2008. During the loading procedure it was observed, at the 54kip mark, that the actuator's cross head was rolling slightly out of plane. Due to this event, the specimen was unloaded and the actuator was re-positioned for a second loading attempt. During the second load attempt the specimen reached failure. It should be noted that DAQ was not zeroed previous to the second loading attempt. The crack patterns observed during testing can be found in Figure 93 and Figure 94

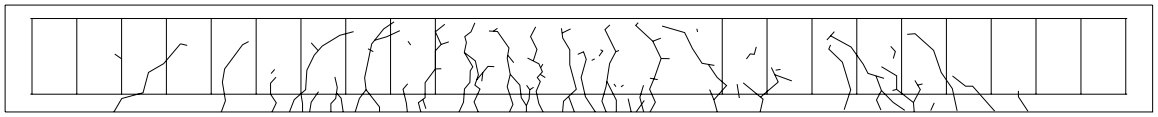

Figure 93: EP-F-T Eastern Face Crack Pattern

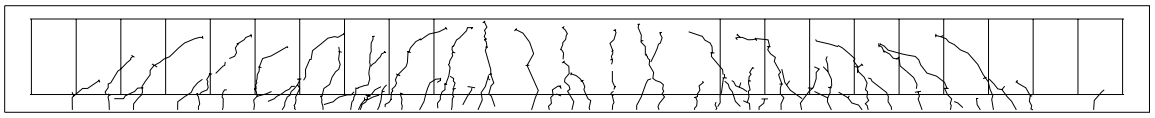

Figure 94: EP-F-T Western Face Crack Pattern

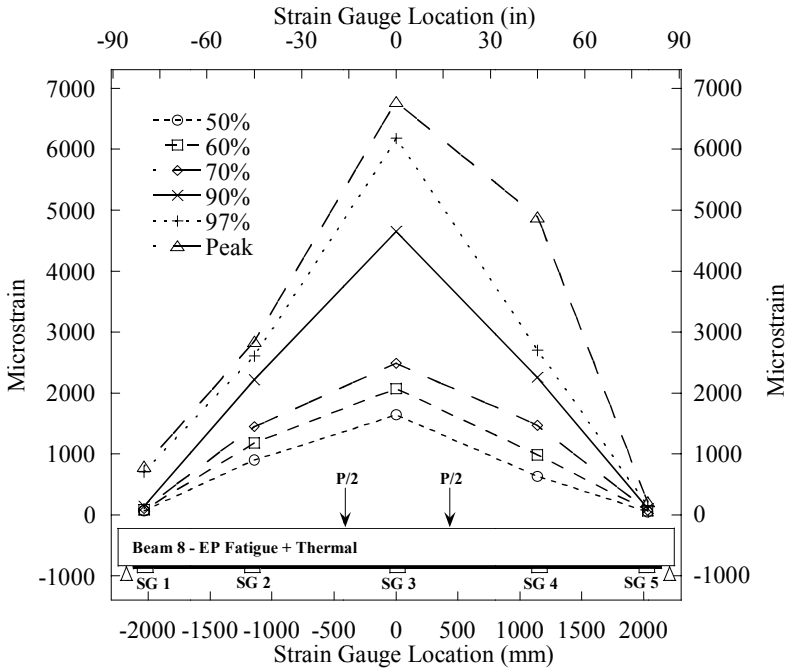

Figure 95: EP-F-T Strain Distribution

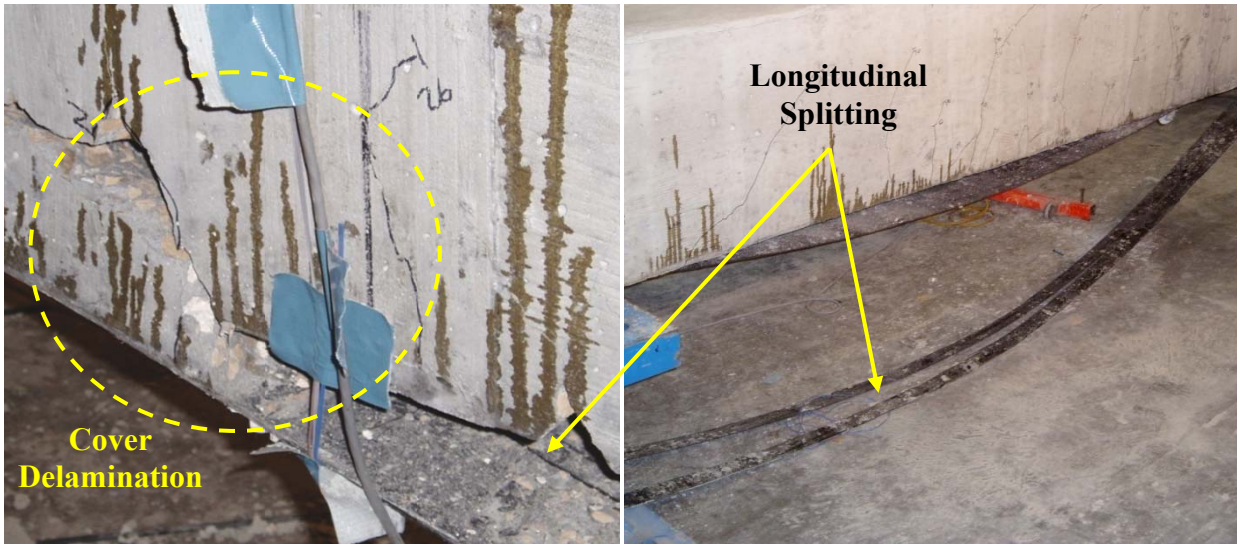

(a) Failure at Mid-span **(b) South End**

Figure 96: EP-F-T Failure Modes

Failure of the EP-F-T specimen occurred at a load of 76.5kip (Δ=1.69”). The dominating mode of failure was determined to be debonding that occurred at the south end of the specimen. This conclusion can be validated by the softening observed in Figure 97-b (Figure 97-a is from load attempt 1) at the SG4 position. Softening at the SG3 location is due to yielding of steel. During failure, a considerable amount of longitudinal splitting occurred in the CFRP composite plate (refer to Figure 96-b). Upon examining the specimen, it was observed that concrete cover separation (approximately a 24” portion in length) also occurred near mid-span. It was also observed that the debonding surface of the CFRP was inconsistent as seen in previous EP-type specimen.

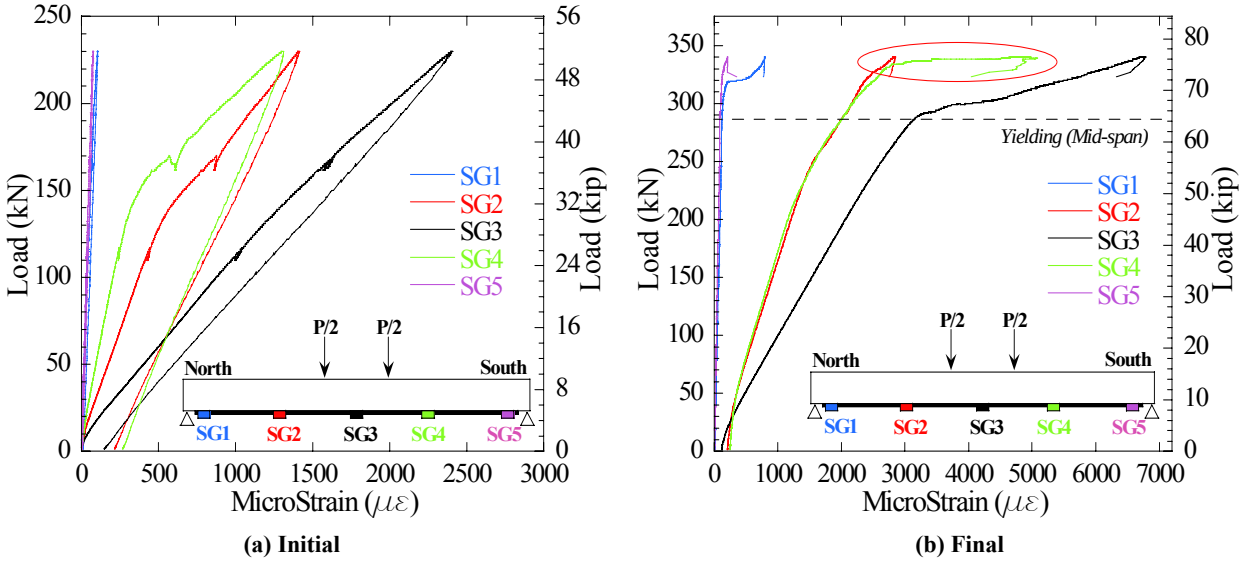

Figure 97: EP-F-T Load vs. Strain Plot

6.4.3 GE-F-T: Beam 12

The fatigue results from the GE-F-T specimen revealed that the mean strain at mid-span increased gradually (approx. by 100 microstrain) during the 2 million fatigue cycles (refer to Figure 98). The calculated result for mid-span strain shows good agreement with the values obtained experimentally; indicating that no considerable sensor drift occurred. It can also be observed that, at approximately 50,000 cycles, strain gauge 2 began to show signs of softening.

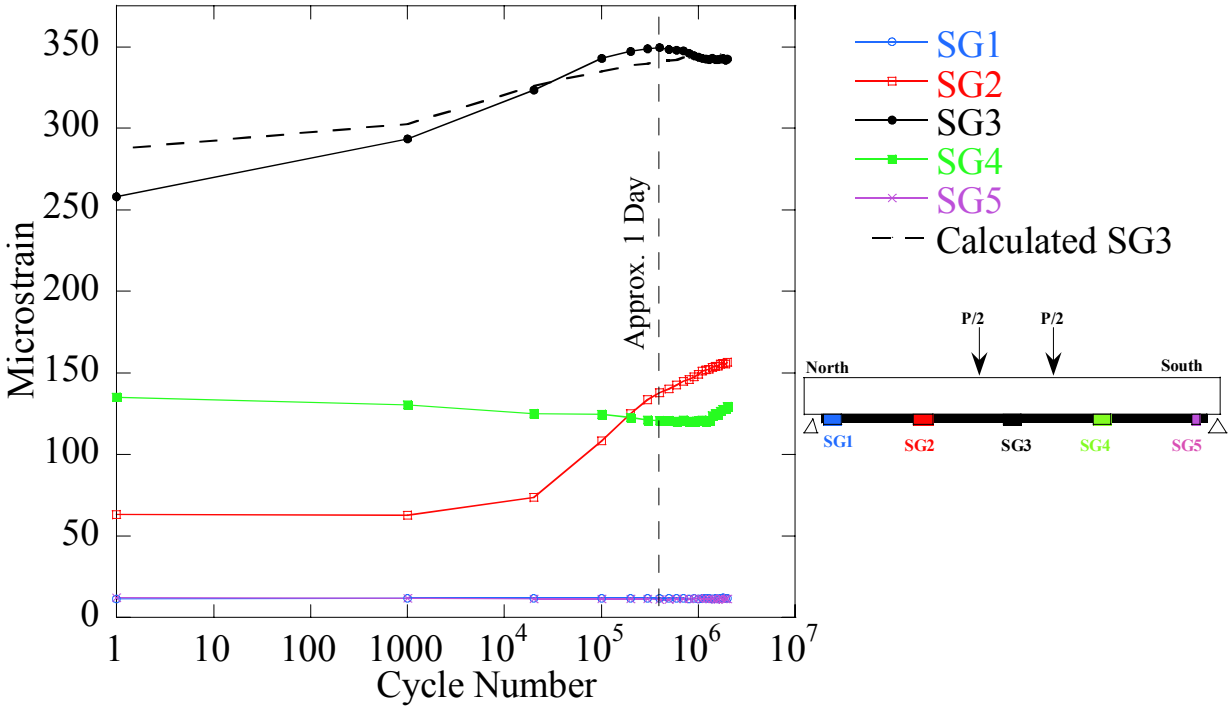

Figure 98: GE-F-T Mean Strain Fatigue Response

Upon inspecting the bonded CFRP plate, it was found that a substantial amount of bond loss occurred near strain gauge 2 and along the western face of the specimen near mid-span. As seen above in Figure 98, strain gauge 2 underwent softening during fatigue loading. Therefore this region of poor bond could be attributed to fatigue. There were also some other small regions located were bond was found to be poor (Figure 99).

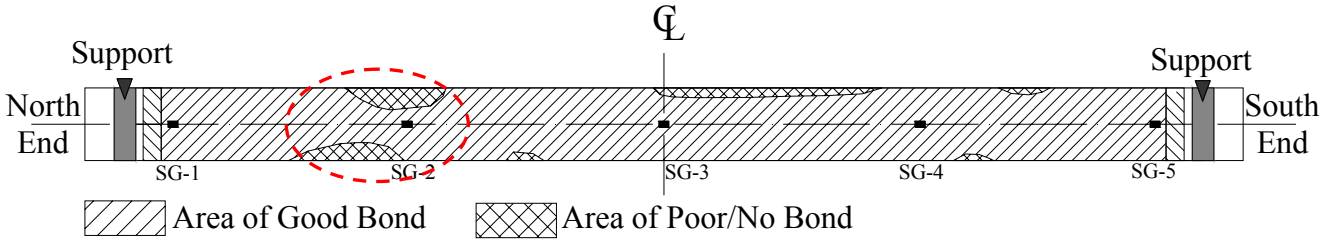

Figure 99: GE-F-T Post-conditioning Bond Integrity Result

The ultimate test for specimen GE-F-T was conducted on 10/22/2008. There were no apparent issues with loading or DAQ during the ultimate test. The observed crack patterns at failure can be seen in Figure 100 and Figure 101. At failure, there were not a significant number of cracks observed due to the low failure load of the specimen. The recorded strain profile can be seen in Figure 102.

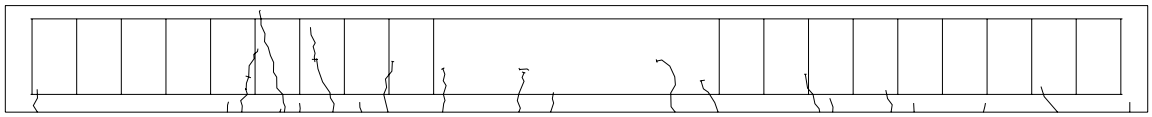

Figure 100: GE-F-T Eastern Face Crack Pattern

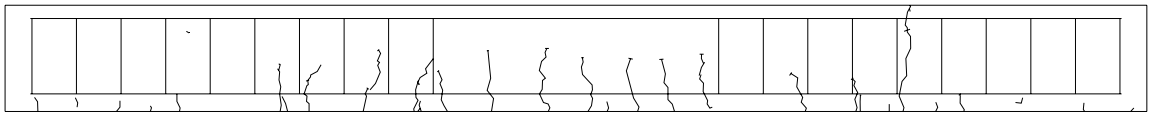

Figure 101: GE-F-T Western Face Crack Pattern

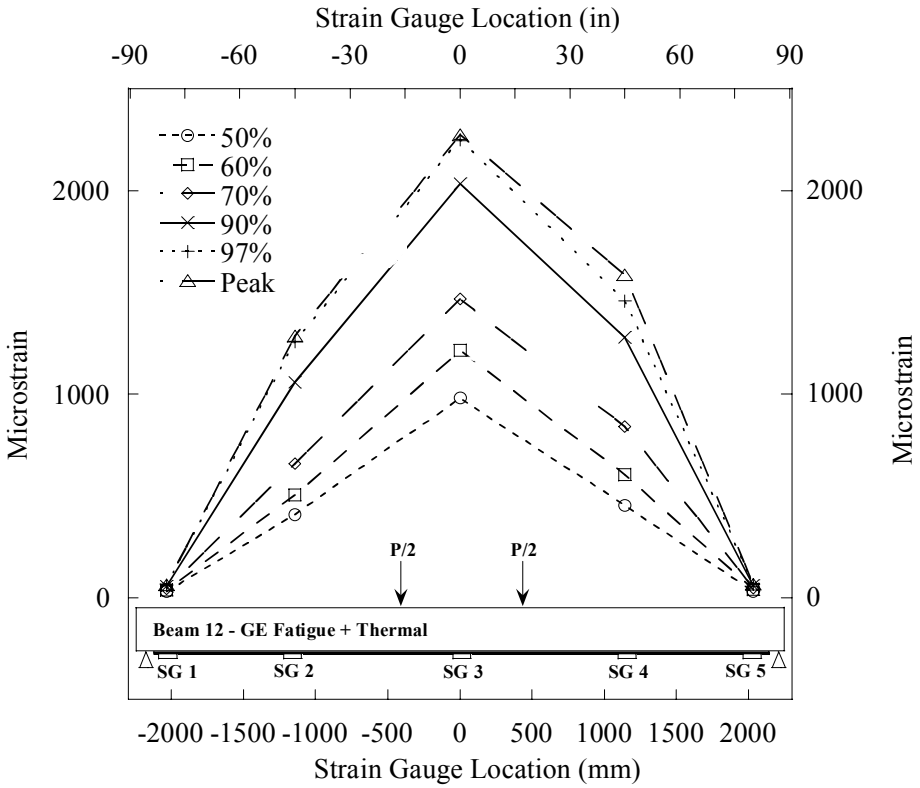

Figure 102: GE-F-T Strain Distribution

Failure of the GE-F-T specimen occurred at 53.1kip (Δ=0.71”). Failure was initiated by debonding at the south end of the specimen. This conclusion can be varied by the load-strain plot shown in Figure 103; abrupt increases in strain at the SG4 and SG5 would indicate this type of failure.

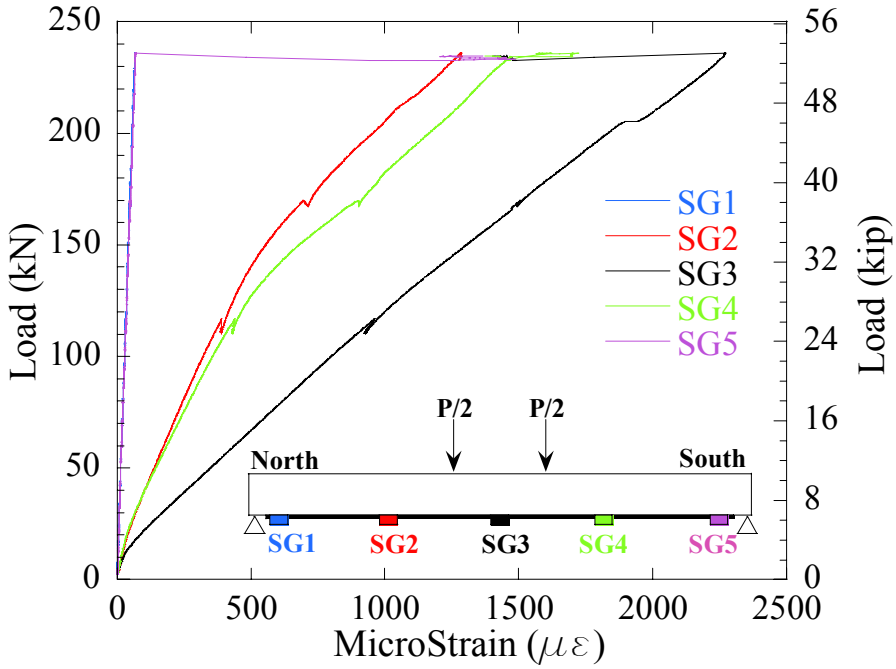

Figure 103: GE-F-T Load vs. Strain Plot

6.4.4 Fatigue/Thermal Specimen Comparative Results

It was observed that the EP-F and GE-F specimens underwent a significant reduction in flexural stiffness between the 1st and 100,000th cycle. Both specimens display similar Δ-*n* curves. Just as was observed in the EP-F and GE-F specimens, the EP-F-T and GE-F-T specimens accumulated 80% of their residual deflection prior to the 1-day mark (refer to Figure 104). Therefore it is concluded that the majority of stiffness loss is attributed to cracking/fatigue softening of concrete and fatigue induced bonded degradation (as seen in bond inspections). The total reduction in stiffness caused by debonding and concrete softening cannot be individually quantified with the measurements taken in this study.

As discuss in Section 6.2.4, the effect of creep on the residual deflection was also investigated for the F-T specimens. The ratio of the 7.5 day creep deflection to maximum residual deflection can be seen in Figure 105. The PU specimen indicates a ratio greater than 1 for both mean and maximum fatigue loads. It is believed that this is due to measurement scatter from the fatigue loading process. It is can be observed that for the mean and maximum fatigue load, the approximate creep deflection is below that of the residual deflection for both the EP and GE specimens. This result would indicate that creep deflection could be a contributing factor to the maximum and residual deflection accumulated during the fatigue loading process. Yet, given the measurements taken during the test, there is no way to determine the exact extent of deflections caused by creep of concrete.

It was suggested by Chami et al. (2009) that the application of externally bonded CFRP to RC beams does not improve the creep deflection behavior of RC beams.

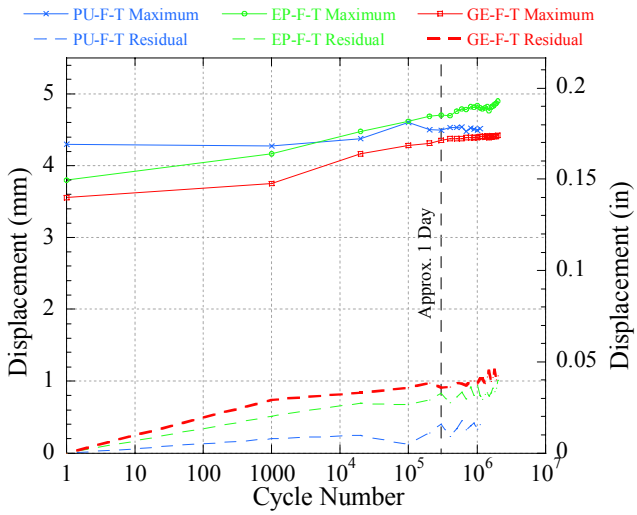

Figure 104: F-T Fatigue Loading Deflection Results

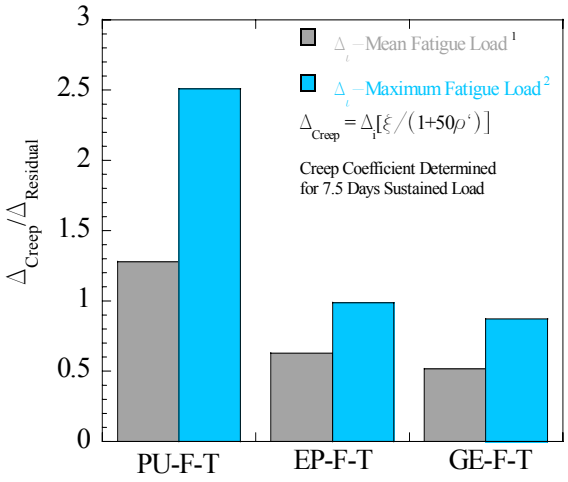

[1] Deflection determined via calculation with a cracked section
[2] Deflection determined via static measurements prior to fatigue testing

Figure 105: Effect of Creep on Residual Deflection (F-T)

It can be observed form load-deflection results (Figure 106) of the F-T specimen types that there is no significant difference between the PU and EP strengthened beams. Although, the GE-F-T specimen showed significant decreases in deflection, ultimate load, and mid-span strain achieved at failure (refer to values in Table 26).

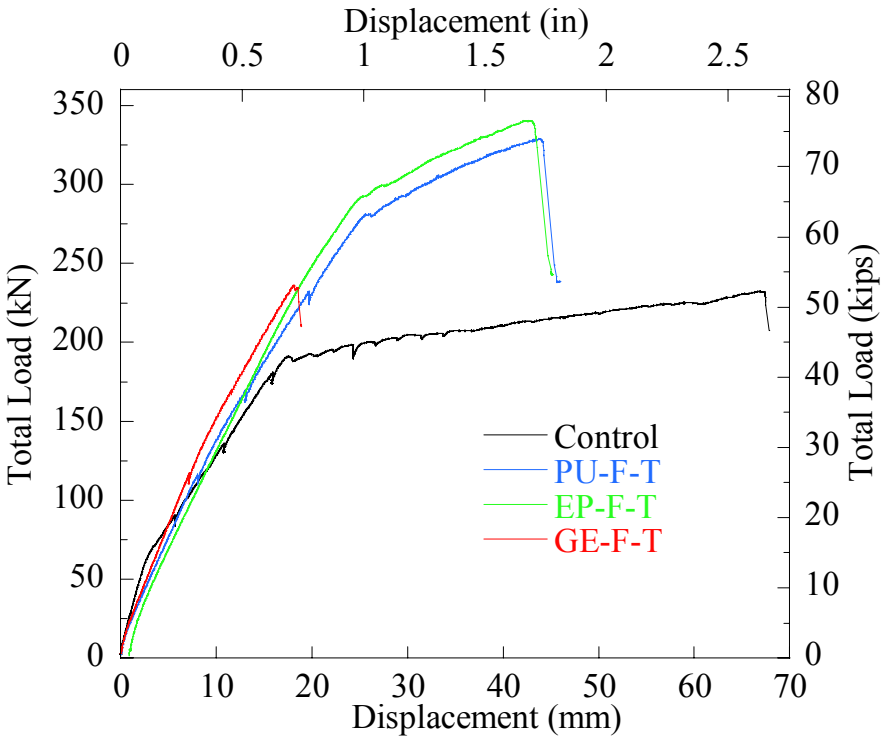

Figure 106: Fatigue + Thermal Load-Deflection Results

Table 26: Fatigue + Thermal Load, Deflection, and Strain Results

Specimen ID	Beam No.	Yielding Load		Yielding Deflection		Ultimate Load		Ultimate Deflection		Maximum Strain (με)
		kN	*kip*	*mm*	*in*	*kN*	*kip*	*mm*	*in*	
Control	16	190.8	42.9	19.1	0.75	232.2	52.2	66.8	2.63	N/A
PU-F-T	4	278.0	62.5	4.4	0.98	328.7	73.9	44.7	1.76	6174
EP-F-T	8	287.3	64.6	4.2	0.95	340.3	76.5	42.9	1.69	6785
GE-F-T	12	*		*		236.2	53.1	18.0	0.71	2273

*Specimen did not achieve yielding.

6.5 Bond Pull-off Results

One beam specimen (beam no. 9) was dedicated for the use of performing bond pull-off testing. Bond pull-off testing is used to assess the adhesion between two materials that have been connected via a bonded joint. A small 2-layer patch of CFRP laminate, one patch per CFRP system, was applied to beam 9 in the same manner as described in Chapter 5. Beam 9 was then conditioned in the ECC for the period of time as all other environmentally conditioned specimens.

Upon completion of the conditioning period, bond pull-off test locations were prepared and tested. Pull-off testing was performed using a James Instruments Inc. *007 James Bond Tester* fixture (2" pull-off test disc). This fixture conforms to the current ASTM standard for such a test. Measured pull-off force and failure location within the sample have been tabulated in Table 27.

Table 27: Bond Pull-off Results

Label	Matrix Type	Pull Off Force (lbf)	Sample Location	Failure Location
A1	GE	1800	side	Concrete
A2	GE	1200	side	Concrete
A3	GE	1700	side	Top Epoxy
B1	PU	650	bottom	Urethane
B2	PU	600	bottom	Urethane
B3	PU	600	bottom	Urethane
C1	EP	1400	bottom	Concrete
C2	EP	1550	bottom	Concrete
C3	EP	1800	bottom	Concrete

The dominate mode of failure observed, in the epoxy-based systems, was rupture of disc specimen within the concrete layer. This indicates a good bond between FRP and concrete, that is a sound FRP/concrete interface layer. Specimen A3 was observed to fail in the top epoxy layer of the pull-off specimen. This means that the testing disc was pulled from the CFRP substrate leaving the CFRP material remaining adhered to concrete. This indicates, based on the results from specimens A1 and A2, that the pull-off specimen was not prepared properly or that a poor bond existed between the test disc and the CFRP substrate.

All PU matrix specimens exhibited a cohesive failure mode occurring within the urethane adhesive layer. The pull-off force at failure, although low compared to the epoxy systems, and the failure surface for this matrix system was very consistent compared to the epoxy based systems. This can be seen in Figure 107.

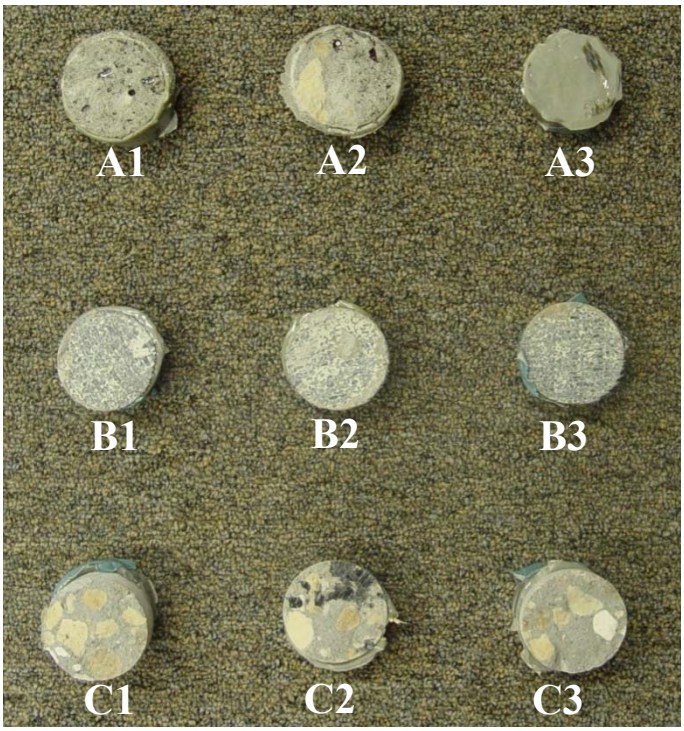

Figure 107: Bond Pull-off Specimens at Failure

6.6 Graphical Summary of Results

The purpose of the following section is to provide some general results, found in this study, in a quick reference format. Figure 108, Figure 109, and Figure 110 depict the retention of critical flexural parameters compared to the results found in baseline test. Values that exceed 100% indicate that the parameter increased compared to baseline testing. Figure 111 depicts the results from the bond pull-off tests in a graphical format.

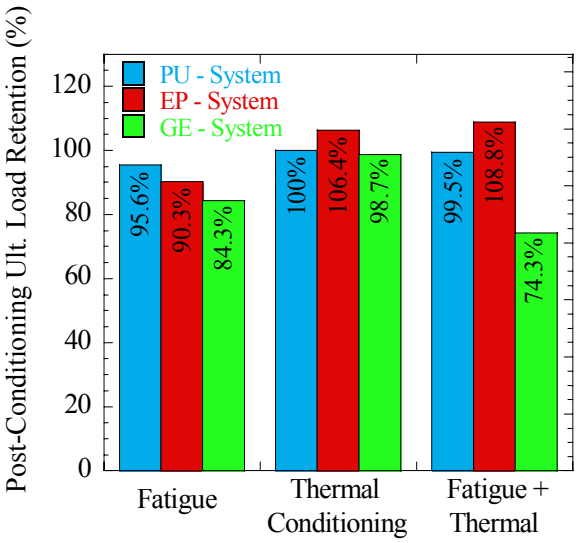

Figure 108: Ultimate Load Retention

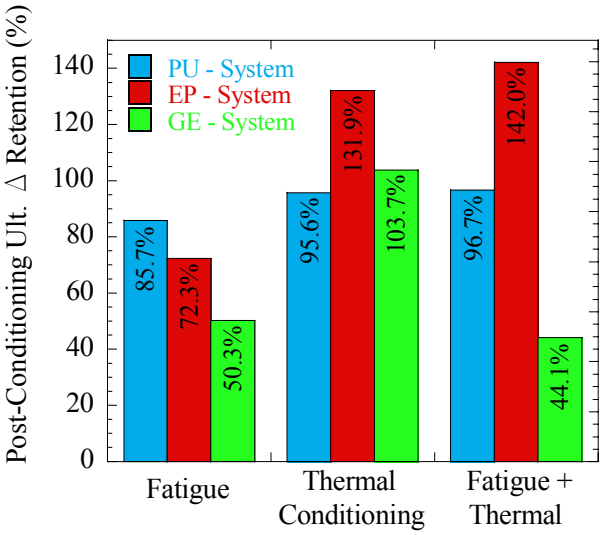

Figure 109: Ultimate Deflection Retention

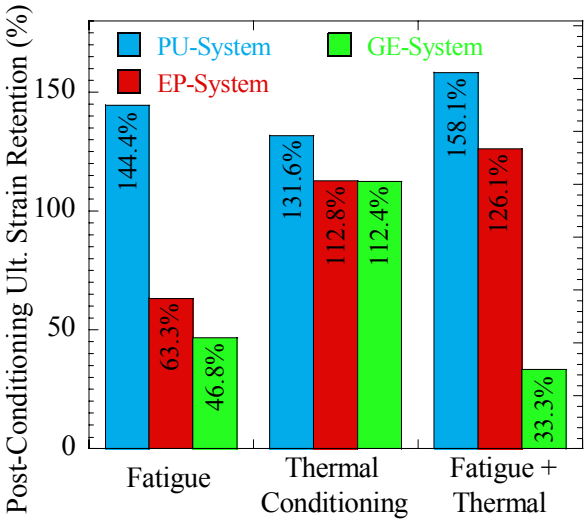

Figure 110: Max. Mid-span Strain Retention

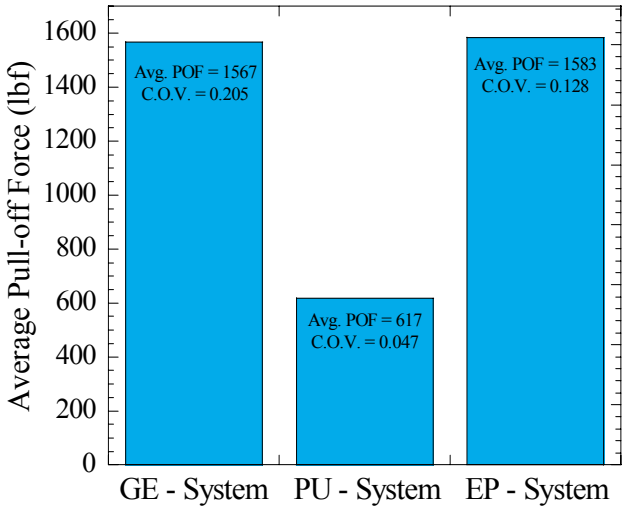

Figure 111: Bond Pull-off Result

Chapter 7: Conclusions & Recommendations

7.1 Conclusions

The work presented in this study is the result of an experimental investigation focused on evaluating the performance durability of reinforced concrete beam strengthened with externally bonded CFRP composite sheets. 12 RC beams were strengthened with externally bonded CFRP laminates. Beams were conditioned mechanically and/or environmentally to simulate long-term exposure to a Florida-like service environment. The other main objective of this study was to evaluate three different CFRP systems:

- *PU System*: A commercially available pre-impregnated and pre-packaged carbon/polyurethane composite system.

- *EP System*: A carbon/epoxy composite system previously investigated and currently used in the field by the FDOT

- *GE System*: A carbon/epoxy composite system employing a generic epoxy matrix (commercially available epoxy resin and hardener not marketed together).

Based on observations and results discussed, the following conclusions can be drawn:

- The application of externally bonded CFRP laminates can increase member flexural capacity 40+%. Yet, this increase in capacity comes at the price of a significant decrease in ductility (50+%).

- Epoxy based composite systems (EP and GE) displayed significant levels of interface softening and reduction of flexural stiffness during the first 10,000-100,000 cycles of fatigue. Therefore it can be concluded that the epoxy systems are sensitive to fatigue loading and susceptible to fatigue initiated interface degradation. However, degradation seems to stabilize after a large number of load cycles.

- Thermal conditioning did not have an adverse effect that could be deemed significant, on the post-conditioning flexural performance of all strengthened beams.

- Members strengthened with the PU composite system displayed a considerable level of consistency in the following areas:

    - Ductility (although reduced from the RC control)

    - Load bearing capacity at failure

    - Failure mode

- Post-conditioning bond integrity

- The consistency of results with the PU system indicates that both the fatigue loading and thermal conditioning had little or no adverse effect on the strengthening ability of this system.

- It is believed that creep of concrete caused a portion of member residual deflection accumulated during the fatigue loading process.

Based on results found, the use of externally bonded CFRPs are suitable for short-term rehabilitation efforts. No concrete conclusion can be made on the feasibility of externally bonded CFRP as a long-term or permanent strengthening option. Bond degradation appears to occur initially from fatigue but seems to stabilize over time.

7.2 Recommendations

Based on the conclusions discussed above, the following other recommendations can be made:

- The polyurethane (PU) composite system shows promise. Therefore it is recommended that further investigation be conduction on performance of this system.

- Future environmental conditioning studies should be conducted under higher levels of control throughout the duration of the study i.e. full control over specimen exposure to temperature and humidity.

- Future fatigue studies should incorporate greater control over loading frequency and more detailed sensor arrangements i.e. strain monitoring of concrete and reinforcing steel

- It is recommended that closer attention be paid to the surface preparation of concrete prior to applying FRP systems.

- It is highly advised that an untested matrix system not be used in field applications. This even refers to commercial resins and hardeners, if two portions have not been used in conjunction with one another.

- It is recommended that more detailed documentation be kept on the design, construction, and in-situ load testing of CFRP strengthened bridges in Florida.

7.3 Possible Areas of Future Research

This study did not incorporate a sufficient number of specimens nor was a sufficient quantity of data collected to develop a mechanics or chemistry-based model to describe the service life of concrete members strengthened with CFRP. The following areas are suggested for future study:

- Investigate service-level fatigue in existing FDOT retrofitted bridges via strain-based monitoring and weigh-in-motion (WIM).

- Development of an efficient and accurate methodology for field inspection and condition assessment of FRP strengthened bridge structures.

- Investigate the use of in-situ load testing to establish performance datums for FRP strengthened bridge structures.

References

ACI Committee 318 (2005). *Building Code Requirements for Structural Concrete (ACI 318-05) and Commentary (ACI 318R-05).* Detroit: American Concrete Institute.

ACI Committee 440 (2008). *Guide for the Design and Construction of Externally Bonded FRP Systems for Strengthening Concrete Structures.* American Concrete Institute.

Abanilla, M. A., Li, Y., & Karbhari, V. M. (2006). Durability characterization of wet layup graphite/epoxy composites used in external strengthening. *Journal of Composites: Part B , 37*, 200-212.

Aidoo, J., Harries, K. A., & Petrou, M. F. (2004). Fatigue Behavior of Carbon Fiber Reinforced Polymer-Strengthened Reinforced Concrete Bridge Girders. *Journal of Composites for Construction , 8* (6), 501-509.

Andreopoulos, A. G., Konstantinidou, A. V., & Petsalas, H. J. (1989). Elastomeric Polyurethanes Reinforced with Aramid Fibers. *Journal of Applied Polymer Science , 38*, 2073-2978.

Apicella, A., Migliaresi, C., Nicolais, L., & Roccotelli, S. (1983). The water aging of unsaturated polyester-based composites: Influence of resin chemical structure. *Composites , 14* (4), 387-392.

Barne, R. A., & Mays, G. C. (1999). Fatigue performance of concrete beams strengthened with CFRP plate. *Journal of Composites for Construction , 3* (2), 63-72.

Bazinet, S., Cereone, L., & Worth, F. (2003). Composite FRP moves into underwater repair applications. *SAMPE Journal , 39* (3), 8-16.

Bonacci, J. F., & Maalaj, M. (2001). Behavioraly Trends of RC Beams Strengthened with Externally Bonded FRP. *Journal of Composites for Construction , 5* (2).

Chami, G. A., Theriault, M., & Neale, K. W. (2009). Creep behaviour of CFRP-strengthened reinforced concrete beams. *Construction and Building Materials , 23*, 1640-1652.

Ferrier, E., Bigaud, D., Hamelin, P., Bizindavyi, L., & W., N. K. (2005). Fatigue of CFRP externally bonded to concrete. *Journal of Materials and Structures , 38*, 39-46.

Gamage, J., Al-Mahaidi, R., & Wong, M. B. (2006). Bond Characteristics of CFRP Plated Concrete Members Under Elevated Temperatures. *Composite Structures* (75), 199-205.

Gheorghiu, C., Labossiere, P., & and Proulx, J. (2006). Fatigue and monotonic strength of RC beams strengthened with CFRP's. *Journal of Composites: Part A , 37*, 1111-1118.

Grace, N. F., & Grace, M. (2005). Effcet of repeated loading and long term humidity exposure on flexural response of CFRP strengthened concrete beams. *Proceedings of Bond Behavior of FRP in Structures Conference.* Hong Kong.

Grace, N. F., & Singh, S. B. (2005). Durability evaluation of carbon fiber-reinforced polymer strengthened concrete beams: Experimental study and design. *ACI Structural Journal , 102* (1), 40-53.

Karbhari, V. M., & Engineer, M. (1996). Effect of environmental exposure on the external strengthening of concrete with composites – Short term bond durability. *Journal of Reinforced Plastics and Composites , 15*, 1194-1216.

Karbhari, V. M., Chin, J. W., Hunston, D., Benmokrane, B., Juska, T., Morgon, R., et al. (2003). Durability gap analysis for fiber-reinforced polymer composite in civil infrastructure. *Journal of Composites for Construction , 7* (3), 238-247.

Kutty, S. K., & Nando, G. B. (1991). Short Kevlar Fiber-Reinforced Thermoplastic Polyurethane Composite. *Journal of Applied Polymer Science , 43*, 1913-1923.

Kutty, S. K., & Nando, G. B. (1991). Stress Relaxation Behavior of Short Kevlar Fiber-Reinforced Thermoplastic Polyurethane. *Journal of Applied Polymer Science , 42*, 1835-1844.

Lu, X. Z., Teng, J. G., Ye, L. P., & Jiang, J. J. (2005). Bond-slip models for FRP sheets/plates bonded to concrete. *Engineering Structures , 27*, 920-937.

Mallick, P. K. (2008). *Fiber-Reinforced Composites.* Boca Raton: CRC Press.

Marom, G., & Broutman, L. J. (1981). Moisture penetration into composites under external stress. *Polymer Composites , 2* (3), 132-136.

Meier, U., & Kaiser, H. (1991). Strengthening of structures with CFRP laminates. *Proceedings Specialty Conference on Advanced Composites Material* (pp. 224-232). New York: ASCE.

Meier, U., Deuring, M., Meier, H., & Schwegler, G. (1992). Strengthening of structures with CFRP laminates: Research and applications in Switzerland. *Reprinted from Advanced Composite Materials in Bridges and Structures* .

Norris, T., Saadatmanesh, H., & Ehsani, M. (1997). Shear and flexural strengthening of R/C beams with carbon fiber sheets. *Journal of Construction Engineering , 123* (7), 903-911.

Olka, M. A. (2009). *Flexural mechanical durability of concrete beams strengthened by externally bonded carbon fiber reinforced polymer sheets.* University of Central Florida, MS Thesis, Orlando.

Ritchie, P. A., Thomas, D. A., Lu, L. W., & Connelly, G. M. (1991). External Reinforcement of Concrete Beams using Fiber Reinforced Plastics. *ACI Structural Journal , 88* (4), 490-500.

Schutte, C. L. (1994). Environmental durability of glass-fiber composites. *Material Science Eng., R. , 13* (7), 265-322.

Sen, R., & Mullins, G. (2007). Application of FRP composites for underwater pile repair. *Composites: Part B , 28*, 751-758.

Setiadi, Y., Jar, P.-Y. B., Kuboki, T., & Cheng, J.-J. R. (2005). Comparison of Damage Developmentin Random Fiber-reinforced Polymers (FRPs) under Cyclic Loading. *Journal of Composite Materials , 40* (1), 71-91.

Soudki, K., El-Salakawy, E., & Craig, B. (2007). Behavior of CFRP strengthened reinforced concrete beams in corrosive environment. *Journal of Composites for Construction , 11* (3).

Spadea, G., Bencardino, F., & Swamy, R. N. (1998). Structural behavior of composite RC beam with externally bonded CFRP. *Journal of Composites for Construction , 2* (3), 132-137.

Szycher, M. (1999). *Szycher's Handbook of Polyurethanes.* Boca Raton: CRC Press.

Tavakkolizadeh, M., & Saadatmanesh, H. (2001). Galvanic Corrosion of Carbon and Steel in Aggressive Environments. *Conposites for Construction , 5* (3), 200-210.

Toutanji, H., Zhao, L., Deng, Y., Zhang, Y., & and Balaguru, P. (2006). Cyclic behavior of RC beams strengthened with carbon fiber sheets bonded by inorganic Matrix. *Journal of Materials in Civil Engineering , 18* (1), 28-35.

Zheng, Q., & Morgan, R. J. (1993). Synergistic thermal moisture damage mechanisms of epoxies and there carbon fiber composites. *Journal of Composite Materials , 27* (15), 1465-1478.

Appendix A

(Moment-Curvature MathCAD Flow Chart)
Taken from Olka (2009)

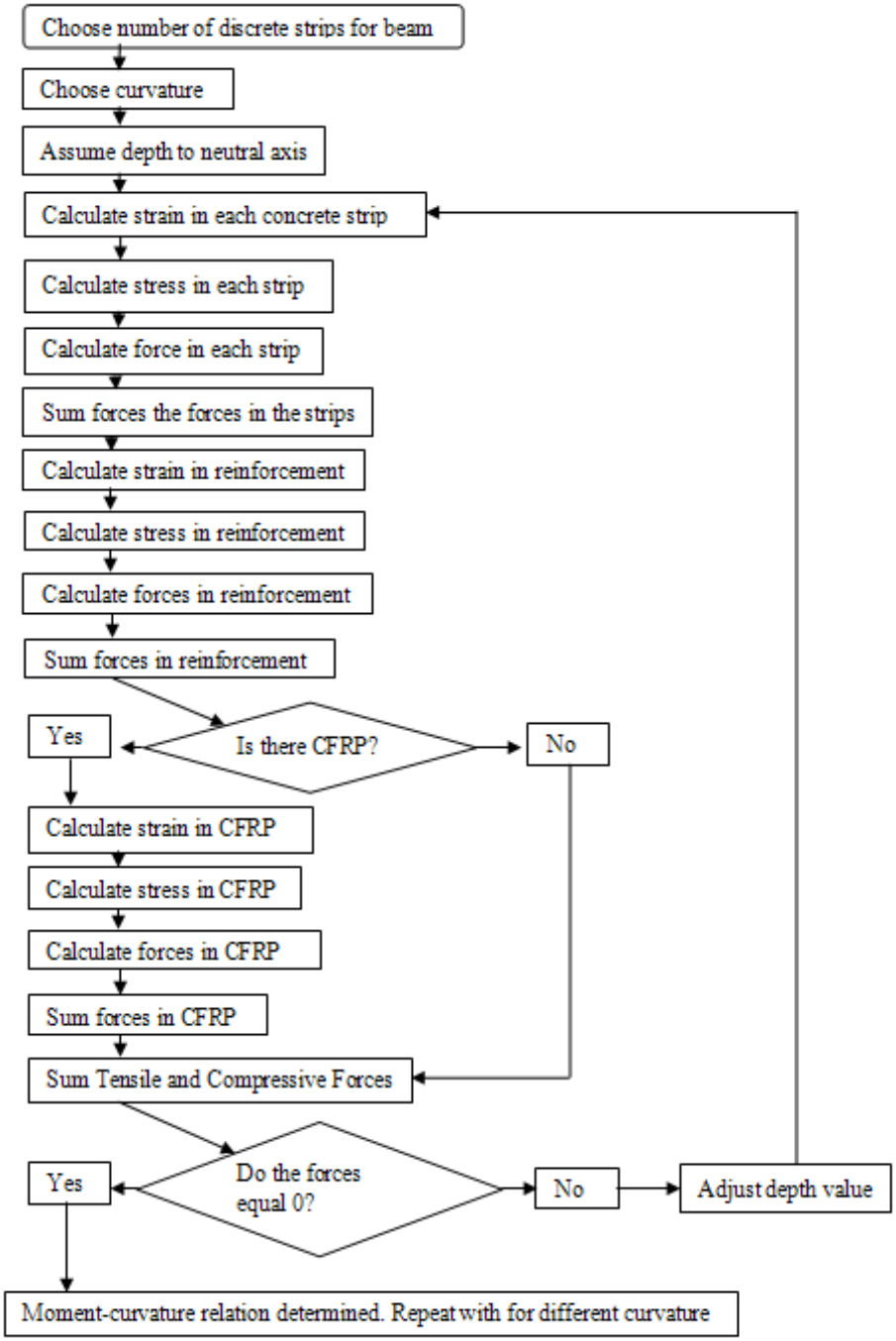
Choose number of discrete strips for beam
Choose curvature
Assume depth to neutral axis
Calculate strain in each concrete strip
Calculate stress in each strip
Calculate force in each strip
Sum forces the forces in the strips
Calculate strain in reinforcement
Calculate stress in reinforcement
Calculate forces in reinforcement
Sum forces in reinforcement
Is there CFRP?
Yes
No
Calculate strain in CFRP
Calculate stress in CFRP
Calculate forces in CFRP
Sum forces in CFRP
Sum Tensile and Compressive Forces
Do the forces equal 0?
Yes
No
Adjust depth value
Moment-curvature relation determined. Repeat with for different curvature

Appendix B

(Watlow Controller – Program Sheets)

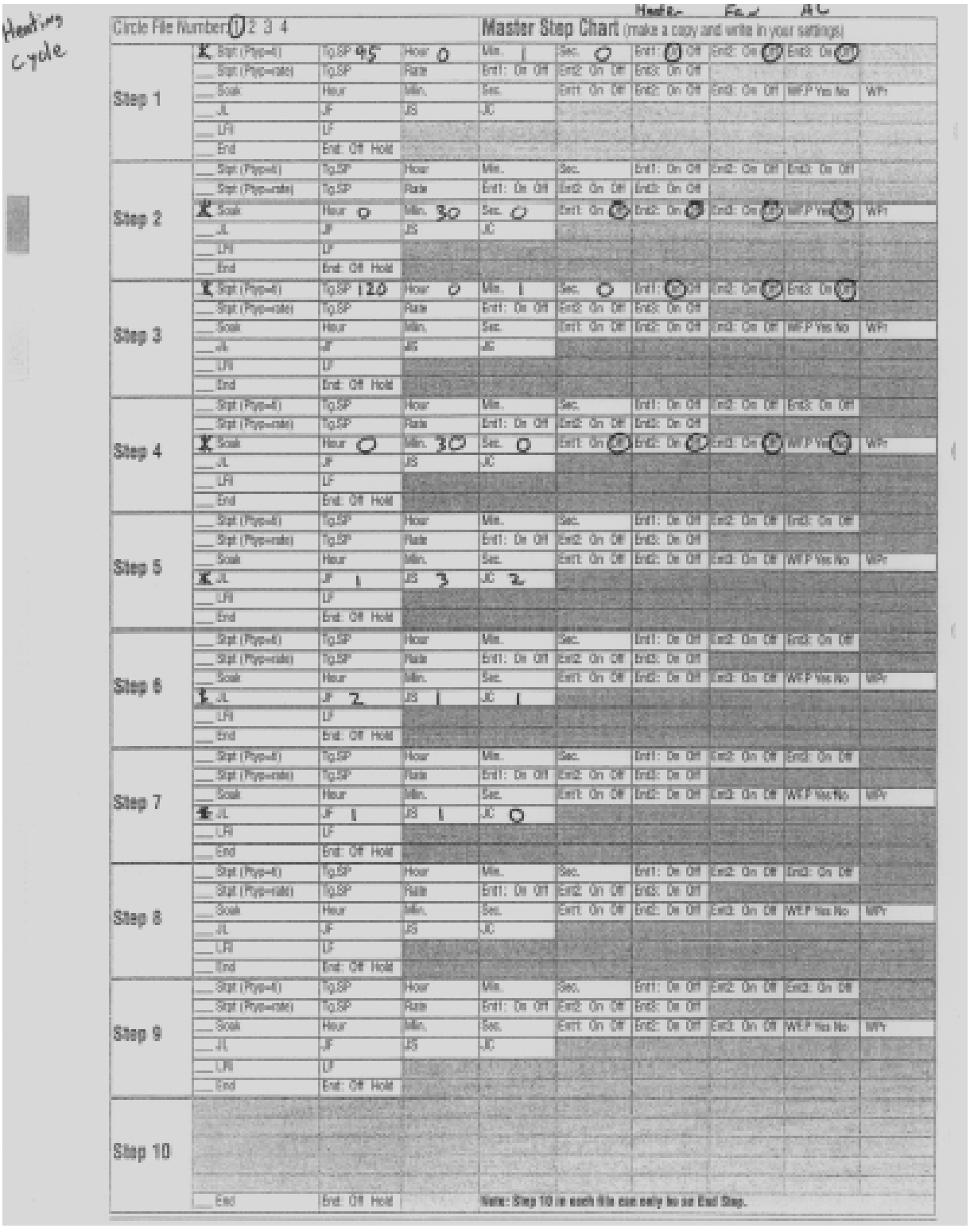

Circle File Number 1 2 3 4

Master Step Chart (make a copy and write in your settings)

Step 1	Stpt (Pyp=t)	TgSP 95	Hour 0	Min. 1	Sec. 0	Ent1: On (Off)	Ent2: On (Off)	Ent3: On (Off)	
	Stpt (Pyp=rate)	TgSP	Rate	Ent1: On Off	Ent2: On Off	Ent3: On Off			
	Soak	Hour	Min.	Sec.	Ent1: On Off	Ent2: On Off	Ent3: On Off	WFP Yes No	WPr
	JL	JF	JS	JC					
	LPI	LF							
	End	End: Off Hold							
Step 2	Stpt (Pyp=t)	TgSP	Hour	Min.	Sec.	Ent1: On Off	Ent2: On Off	Ent3: On Off	
	Stpt (Pyp=rate)	TgSP	Rate	Ent1: On Off	Ent2: On Off	Ent3: On Off			
	Soak	Hour 0	Min. 30	Sec. 0	Ent1: On (Off)	Ent2: On (Off)	Ent3: On (Off)	WFP Yes (No)	WPr
	JL	JF	JS	JC					
	LPI	LF							
	End	End: Off Hold							
Step 3	Stpt (Pyp=t)	TgSP 120	Hour 0	Min. 1	Sec. 0	Ent1: (On) Off	Ent2: On (Off)	Ent3: On (Off)	
	Stpt (Pyp=rate)	TgSP	Rate	Ent1: On Off	Ent2: On Off	Ent3: On Off			
	Soak	Hour	Min.	Sec.	Ent1: On Off	Ent2: On Off	Ent3: On Off	WFP Yes No	WPr
	JL	JF	JS	JC					
	LPI	LF							
	End	End: Off Hold							
Step 4	Stpt (Pyp=t)	TgSP	Hour	Min.	Sec.	Ent1: On Off	Ent2: On Off	Ent3: On Off	
	Stpt (Pyp=rate)	TgSP	Rate	Ent1: On Off	Ent2: On Off	Ent3: On Off			
	Soak	Hour 0	Min. 30	Sec. 0	Ent1: On (Off)	Ent2: On (Off)	Ent3: On (Off)	WFP Yes (No)	WPr
	JL	JF	JS	JC					
	LPI	LF							
	End	End: Off Hold							
Step 5	Stpt (Pyp=t)	TgSP	Hour	Min.	Sec.	Ent1: On Off	Ent2: On Off	Ent3: On Off	
	Stpt (Pyp=rate)	TgSP	Rate	Ent1: On Off	Ent2: On Off	Ent3: On Off			
	Soak	Hour	Min.	Sec.	Ent1: On Off	Ent2: On Off	Ent3: On Off	WFP Yes No	WPr
	JL	JF 1	JS 3	JC 2					
	LPI	LF							
	End	End: Off Hold							
Step 6	Stpt (Pyp=t)	TgSP	Hour	Min.	Sec.	Ent1: On Off	Ent2: On Off	Ent3: On Off	
	Stpt (Pyp=rate)	TgSP	Rate	Ent1: On Off	Ent2: On Off	Ent3: On Off			
	Soak	Hour	Min.	Sec.	Ent1: On Off	Ent2: On Off	Ent3: On Off	WFP Yes No	WPr
	JL	JF 2	JS 1	JC 1					
	LPI	LF							
	End	End: Off Hold							
Step 7	Stpt (Pyp=t)	TgSP	Hour	Min.	Sec.	Ent1: On Off	Ent2: On Off	Ent3: On Off	
	Stpt (Pyp=rate)	TgSP	Rate	Ent1: On Off	Ent2: On Off	Ent3: On Off			
	Soak	Hour	Min.	Sec.	Ent1: On Off	Ent2: On Off	Ent3: On Off	WFP Yes No	WPr
	JL	JF 1	JS 1	JC 0					
	LPI	LF							
	End	End: Off Hold							
Step 8	Stpt (Pyp=t)	TgSP	Hour	Min.	Sec.	Ent1: On Off	Ent2: On Off	Ent3: On Off	
	Stpt (Pyp=rate)	TgSP	Rate	Ent1: On Off	Ent2: On Off	Ent3: On Off			
	Soak	Hour	Min.	Sec.	Ent1: On Off	Ent2: On Off	Ent3: On Off	WFP Yes No	WPr
	JL	JF	JS	JC					
	LPI	LF							
	End	End: Off Hold							
Step 9	Stpt (Pyp=t)	TgSP	Hour	Min.	Sec.	Ent1: On Off	Ent2: On Off	Ent3: On Off	
	Stpt (Pyp=rate)	TgSP	Rate	Ent1: On Off	Ent2: On Off	Ent3: On Off			
	Soak	Hour	Min.	Sec.	Ent1: On Off	Ent2: On Off	Ent3: On Off	WFP Yes No	WPr
	JL	JF	JS	JC					
	LPI	LF							
	End	End: Off Hold							
Step 10									
	End	End: Off Hold		Note: Step 10 is each file can only be an End Step.					

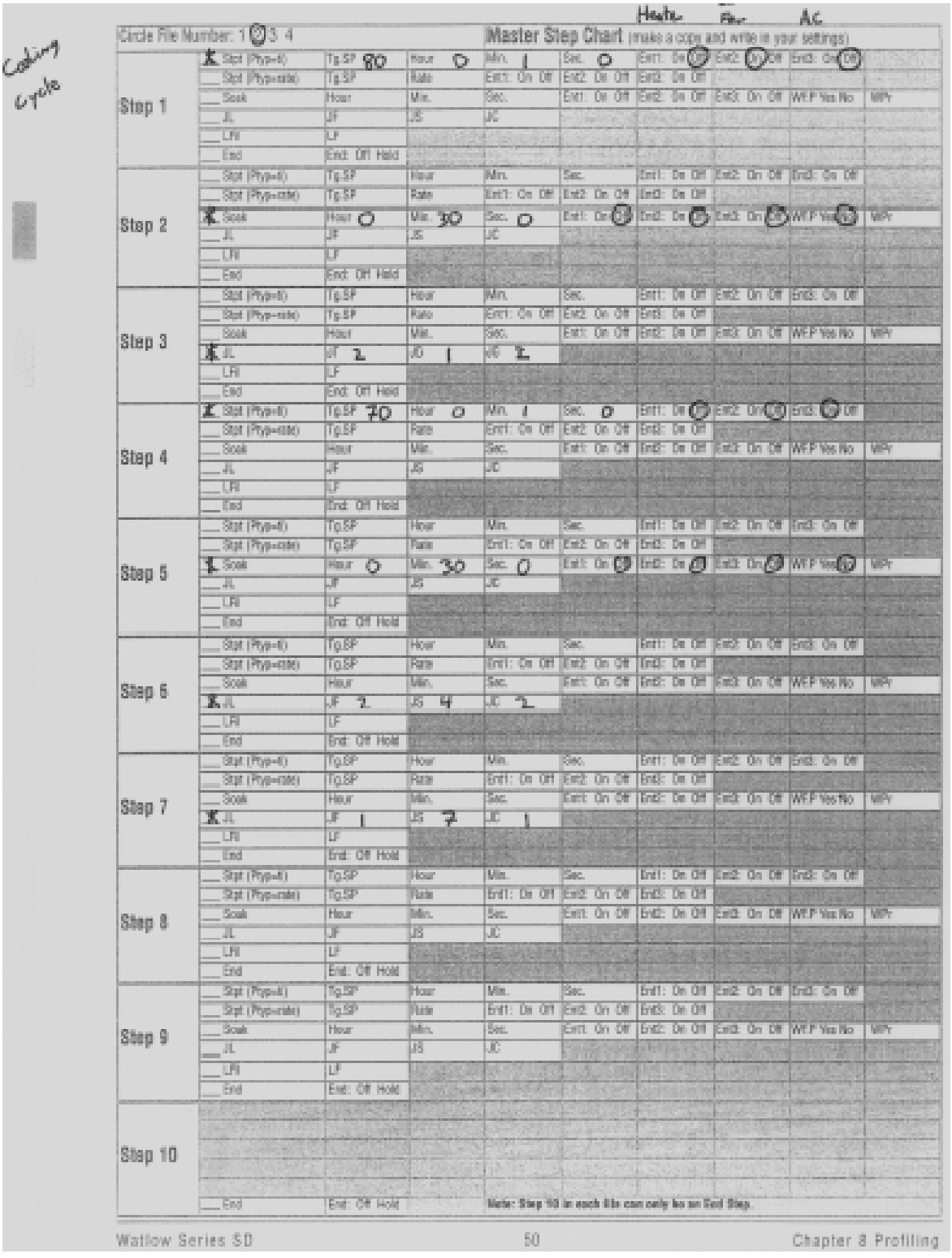

Heate Pur AC

Cooling cycle

Circle File Number: 1 2 3 4

Master Step Chart (make a copy and write in your settings)

Step 1	X Stpt (Pvp=#)	Tg.SP 80	Hour 0	Min. 1	Sec. 0	Ent1: On Off	Ent2: On Off	Ent3: On Off		
	Stpt (Pvp=rate)	Tg.SP	Rate	Ent1: On Off	Ent2: On Off	Ent3: On Off				
	Soak	Hour	Min.	Sec.	Ent1: On Off	Ent2: On Off	Ent3: On Off	W.F.P Yes No	WPr	
	JL	JF	JS	JC						
	LN	LF								
	End	End: Off Hold								
Step 2	Stpt (Pvp=#)	Tg.SP	Hour	Min.	Sec.	Ent1: On Off	Ent2: On Off	Ent3: On Off		
	Stpt (Pvp=rate)	Tg.SP	Rate	Ent1: On Off	Ent2: On Off	Ent3: On Off				
	X Soak	Hour 0	Min. 30	Sec. 0	Ent1: On Off	Ent2: On Off	Ent3: On Off	W.F.P Yes No	WPr	
	JL	JF	JS	JC						
	LN	LF								
	End	End: Off Hold								
Step 3	Stpt (Pvp=#)	Tg.SP	Hour	Min.	Sec.	Ent1: On Off	Ent2: On Off	Ent3: On Off		
	Stpt (Pvp=rate)	Tg.SP	Rate	Ent1: On Off	Ent2: On Off	Ent3: On Off				
	Soak	Hour	Min.	Sec.	Ent1: On Off	Ent2: On Off	Ent3: On Off	W.F.P Yes No	WPr	
	X JL	JF 2	JS 1	JC 2						
	LN	LF								
	End	End: Off Hold								
Step 4	X Stpt (Pvp=#)	Tg.SP 70	Hour 0	Min. 1	Sec. 0	Ent1: On Off	Ent2: On Off	Ent3: On Off		
	Stpt (Pvp=rate)	Tg.SP	Rate	Ent1: On Off	Ent2: On Off	Ent3: On Off				
	Soak	Hour	Min.	Sec.	Ent1: On Off	Ent2: On Off	Ent3: On Off	W.F.P Yes No	WPr	
	JL	JF	JS	JC						
	LN	LF								
	End	End: Off Hold								
Step 5	Stpt (Pvp=#)	Tg.SP	Hour	Min.	Sec.	Ent1: On Off	Ent2: On Off	Ent3: On Off		
	Stpt (Pvp=rate)	Tg.SP	Rate	Ent1: On Off	Ent2: On Off	Ent3: On Off				
	X Soak	Hour 0	Min. 30	Sec. 0	Ent1: On Off	Ent2: On Off	Ent3: On Off	W.F.P Yes No	WPr	
	JL	JF	JS	JC						
	LN	LF								
	End	End: Off Hold								
Step 6	Stpt (Pvp=#)	Tg.SP	Hour	Min.	Sec.	Ent1: On Off	Ent2: On Off	Ent3: On Off		
	Stpt (Pvp=rate)	Tg.SP	Rate	Ent1: On Off	Ent2: On Off	Ent3: On Off				
	Soak	Hour	Min.	Sec.	Ent1: On Off	Ent2: On Off	Ent3: On Off	W.F.P Yes No	WPr	
	X JL	JF 2	JS 4	JC 2						
	LN	LF								
	End	End: Off Hold								
Step 7	Stpt (Pvp=#)	Tg.SP	Hour	Min.	Sec.	Ent1: On Off	Ent2: On Off	Ent3: On Off		
	Stpt (Pvp=rate)	Tg.SP	Rate	Ent1: On Off	Ent2: On Off	Ent3: On Off				
	Soak	Hour	Min.	Sec.	Ent1: On Off	Ent2: On Off	Ent3: On Off	W.F.P Yes No	WPr	
	X JL	JF 1	JS 7	JC 1						
	LN	LF								
	End	End: Off Hold								
Step 8	Stpt (Pvp=#)	Tg.SP	Hour	Min.	Sec.	Ent1: On Off	Ent2: On Off	Ent3: On Off		
	Stpt (Pvp=rate)	Tg.SP	Rate	Ent1: On Off	Ent2: On Off	Ent3: On Off				
	Soak	Hour	Min.	Sec.	Ent1: On Off	Ent2: On Off	Ent3: On Off	W.F.P Yes No	WPr	
	JL	JF	JS	JC						
	LN	LF								
	End	End: Off Hold								
Step 9	Stpt (Pvp=#)	Tg.SP	Hour	Min.	Sec.	Ent1: On Off	Ent2: On Off	Ent3: On Off		
	Stpt (Pvp=rate)	Tg.SP	Rate	Ent1: On Off	Ent2: On Off	Ent3: On Off				
	Soak	Hour	Min.	Sec.	Ent1: On Off	Ent2: On Off	Ent3: On Off	W.F.P Yes No	WPr	
	JL	JF	JS	JC						
	LN	LF								
	End	End: Off Hold								
Step 10										
	End	End: Off Hold		Note: Step 10 in each file can only be an End Step.						

Watlow Series SD 50 Chapter 8 Profiling

Appendix C

(Environmental Condition Chamber Service Notes)
Documented by Steve Eudy – FDOT Structures Research Center

Date	*Note*
3/05/08	Stopped test due to heat/cool system failure
3/18/08	Troubleshot system and found that the blower motor was not starting. Called service technician out and he determined the blower motor to be faulty. He was able to replace the motor under warranty. Started system back up in heat mode and started logging.
3/28/08	Came in the morning and checked on the system to find that the laptop had gone into a sleep state and the Excel humidity logger had stopped recording the humidity at 1:54PM on 3/27. All data in between 3/27 (1:54PM) and 3/28 (6:11AM) is missing.
4/02/08	System ran all weekend and I came in on Wednesday to find the system had iced over the coils and had frozen up. I shut down the unit and let it thaw out and then proceeded to start it back up in heat mode. I will observe it and see if the system freezes up again. If it does, I will call a tech out to look at the refrigerant charge and troubleshoot problem further. Heat cycle started up at 12:15pm. **Note: System time has been 2 hours behind Eastern Standard time since the daylight savings time change and it was 1 hour behind before the time change.**
4/07/08	Humidity logger was down for several days while I was out, so I re-connected using a cable instead of trying to depend on the wireless setup we are using. Restarted logging at 2:58PM.
4/14/08	Stopped the system because of the coils freezing up (7:28am).Called technician out. Technician came out and found that the insulation was blocking airflow to the coils, causing them to freeze up. He thawed the system, added a correct p-trap to the drain, and I started the system back up into the heat cycle at 11:00am.
4/24/08	Shut off AC unit at 8:50am, unit froze up. The system is not triggering to change cycles. Technician came out and fixed the problem. Placed pressure sensor. System was started back up.
5/05/08	Stopped the system (10:07am). System is not cooling off. Changed the set points to: Heat=100 Cool=65 to see if this keeps the system from freezing up. Since we are beginning to see an increase in ambient, heating will be easier to achieve.

Date	*Note*
5/27/08	Noticed that system was taking a really long time to cool. Went outside and noticed that the system was struggling with no exhaust fan. Stopped the system at 9:26AM and I guess we need to call yet another technician out. The system stayed off all day.
5/28/08	Turned system on just to check if it just needed to rest. Started it up in heat mode. We will keep an eye on it to see if it short cycles again. If so, then I'll call in the technicians.
6/02/08	System seemed to run fine on Friday (5/29). Cooling cycle working like it should. However, I came in this morning to find the system not doing so well. I'm calling the technicians again. System was shutdown at 7:20AM.
6/04/08	Technician came out and looked at the system and found the exhaust fan cycle switch was bad. He replaced the switch and also put a line temperature switch to shutdown the compressor when the system starts freezing up. The unit was restarted in the cool process at 12:13PM.
6/26/08	Checked the OCTTEMP thermocouple logger and uploaded the data. The logger status is "running", however, the onboard file seems to indicate that the logging stopped on 6/1/08.It looks like the logger stopped or ran out of batteries. The HVAC has not failed since the 6/4 visit, so we will have to just add the number of thermal cycles completed during this timeframe and live without the data. I am going to have to restart the logger. Restarted logger.
6/27/08	The logger was only able to record two random values overnight. I changed the battery and everything is working fine now. Battery life is a little disappointing. Restarted the logger to the 1 log an hour. Looks good so far. We basically achieved 25days/1.5cycles per day = 16 cycles from 6/1 to 6/26. This brings the total to 63 up until now.
8/07/08	Power surge at 2:40pm or so caused system to lock up. I had to power the system down. We lost data from 8/6 at 12:19 pm to 8/7 at 2:40PM.
9/08/08	Power must have surged or gone out over the weekend. Restarted the temperature controller.